Time Domain Simulation of Optical Amplifiers Incorporating ASE Noise Effect in WDM Photonic Systems

By

CHEUK CHI (ANTONY) LIU, B. ENG

A Thesis

Submitted to the School of Graduate Studies

in Partial Fulfillment of the Requirements

for the Degree

Master of Applied Science

McMaster University

MASTER OF APPLIED SCIENCE (2004) McMaster University
(Electrical and Computer Engineering) Hamilton, Ontario

TITLE: Time-Domain Simulation of Optical Amplifiers incorporating ASE Noise Effect in WDM Photonic Systems

AUTHOR: Cheuk Chi (Antony) Liu,
B.ENG (McMaster University)

SUPERVISOR: Dr. Xun Li

NUMBER OF PAGES: vii, 120

Abstract

To overcome optical signal attenuation in fiber-optic transmission system, amplifiers must be used in the optical link. However, the accompanying amplified spontaneous emission (ASE) noise in optical amplifiers becomes the major factor that impairs the amplified optical signal, thereby degrade the system performance especially in a cascaded amplifier system. This thesis aims at providing a numerical tool that simulates the noise effects when applying optical amplifiers in high-speed long haul transmission systems. A time domain model for Erbium-doped fiber amplifier (EDFA) and semiconductor optical amplifier (SOA), which is capable of handling the locally generated broadband ASE noise and multichannel signals, is developed with affordable computational complexity. Not only the averaged ASE noise contribution to gain saturation has been included in this model, but also the random nature of the ASE noise in optical amplifiers is incorporated through appropriate statistics. Other effects such as the nonuniform spatial distribution of carriers and frequency chirping are also considered in this model. This model is implemented numerically in order to examine the static and dynamic behaviors of the optical amplifiers. Various effects arising from the ASE noise are shown in signal waveforms picked up at any point along the optical link. Furthermore, the newly developed optical amplifier simulator is integrated with an existing time-domain simulation platform that has many other optical components assembled and is capable of handling point-to-point multichannel fiber-optic transmission system in arbitrary configuration. Consequently, the influence of the ASE noise on power booster, in-line

amplifier, preamplifier, and the combination of them has been studied thoroughly in both single-channel and WDM fiber-optic transmission systems.

Acknowledgements

I would like to gratefully acknowledge the enthusiastic supervision of my supervisor, Professor Xun Li, during the whole process of this work.

I would specially like to thank my girlfriend Janette Wong for her willingness and assistance to discuss ideas and her constant support throughout my study period. I am grateful to all members from the Photonics Research Group, McMaster University, for being the surrogate family during the years I stayed there and for their continued moral support there after.

Finally, I am forever indebted to my family for their unconditional love, endless patience and encouragement when it was most required.

Contents

Chapter 1

Introduction

1.1 Background

The field of optical fiber communications, which makes use of the low-loss, broadband characteristics of optical fibers and the advantages of having light as the carrier, is progressing at a tremendous speed [1]. Invention of the optical amplifiers and wavelength-division multiplexing (WDM) technology enabled very high capacity fiber-optic transmission links that run for thousands of kilometers without any electronic repeaters, but many design challenges were brought at the same time. As electronic amplifiers do, optical amplifiers add noise to the signal they amplify. Therefore, in the design of a fiber-optic communication link, it is essential to be able to predict the deterioration that the information signals experience due to the gain saturation caused by amplified spontaneous emission (ASE) noise in the optical amplifiers.

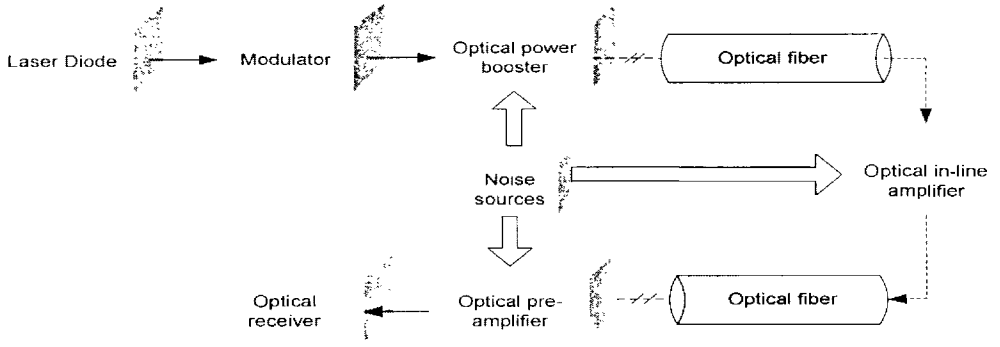

Figure 1.1: Major elements of a fiber-optic transmission link. The basic components are the laser diode, the optical modulator, the optical fiber, the optical amplifier, and the photodetecting receiver.

Generally, a basic fiber-optic transmission system comprises the elements shown in Figure 1.1. In WDM transmission systems, information bits are used to modulate the carriers from the laser diode at a number of wavelengths, which are then transmitted through the optical fiber. The attenuation of optical signal level due to the loss from the fiber needs to be restored by the optical amplifiers. In the meantime, the optical amplifiers add noise to the signal and thus hamper the performance of data recovery at the receiver.

The main source of noise in an optical amplifier is the spontaneous emission of photons. In the spontaneous emission process, there is non-zero probability per unit time that a conduction band (CB) electron (excited ion) will spontaneously recombine with a valence band (VB) hole (ground ion) to emit a photon with random phase and direction. These spontaneously emitted photons cover a wide range of frequencies, and also take part in reducing the population available for optical gain [2]. The photons generated at the front section of the active medium travel along with the signals and get amplified accordingly; it is so-called the amplified spontaneous emission (ASE) noise. On the basis of the optical signal is not converted back to the electrical domain until the end of the chain, the ASE noise continues to grow and accumulates over many amplifiers in a cascade amplifiers system. As a result, the signal level drops and the ASE level increases along the transmission line, and thereby degrade the signal-to-noise ratio (SNR) considerably at the receiver. Hence, depending on the amount of accumulation, ASE at the output of one amplifier stage could influence the operation conditions of the next stage and result in severe system performance degradation [3].

1.2 Motivation

The goal of this project is to develop a numerical tool that simulates the noise effects when applying optical amplifiers in high-speed long haul transmission systems. The model of both semiconductor optical amplifier (SOA) and Erbium-doped fiber amplifier (EDFA) is implemented. Making use of the time domain simulation, the noise behavior of optical amplifiers can be predicted and evaluated. Other than that, special attention should be paid to the noise effects when the amplifiers are cascaded in an optical link, so that this numerical solver will be integrated with our existing system platform to form a whole fiber-optic communication system in order to study this circumstance. In fact, with the increased complexity of optical links and networks nowadays, computer-based simulation and modeling tools can make the design process more efficient, cheaper, and faster.

1.3 Thesis Organization

The following six chapters describe the thesis work carried out, and their contents are briefly outlined here. In chapter 2, we describe the basic principles of operation and the characteristics of two different types of optical amplifier. In addition, their applications are discussed and compared with respect to each other. In chapter 3, a detailed model for both SOA and EDFA based on sets of rate equations is established. As well as, the noise characteristics are described with appropriate statistical properties. In chapter 4, we explain how to implement our model based on numerical methods in detail. All of the time domain simulation results are shown and analyzed and the noise and cross gain saturation effect during multichannel signal amplification are also examined in chapter 5. In chapter 6, the amplifier module is incorporated into our system platform to form a fiber-optic transmission system, so the ASE noise effect in single channel and WDM fiber-optic transmission system for

different applications can be studied. Finally, we summarize the main results of the preceding chapters in chapter 7.

Chapter 2

Principles of Optical Amplifiers

In this chapter, first looks at the basic usage of optical amplifiers and classifies the two fundamental amplifier types: semiconductor optical amplifiers (SOAs) and Erbium-doped fiber amplifiers (EDFAs). Secondly, the operational principles of optical amplifiers are explained, and their basic properties, such as gain and saturation will be discussed. We then turn to noise characteristics, which are of great significance when amplifiers are applied to transmission systems.

2.1 Basic Usage of Optical amplifier

Optical amplifiers are used in the optical transmission link, in order to compensate for signal attenuation during transmission due to fiber loss. They operate solely in the optical domain with no inter-conversion of photons to electrons. Therefore, instead of using regenerative repeaters, which require optoelectronic devices for source and detector, together with electronic circuitry for reamplifying, retiming and reshaping, optical amplifiers can be placed at intervals along a fiber link to provide linear amplification of the transmitted optical signal. The optical amplifier, in principle, provides a much simpler solution in that it is a single in-line component which can be used for any kind of modulation at any transmission rate. Moreover, if such device is sufficiently linear it may allow multiplex operation of several signals at different optical wavelengths (i.e. wavelength division multiplexing - WDM).

2.2 Principles of Operation

The two main optical amplifier types can be classified as semiconductor optical amplifiers (SOAs) and doped-fiber amplifiers (DFAs). Optical amplification is produced by the process of stimulated emission induced by a population inversion in a lasing medium. It applies to semiconductor optical amplifiers or erbium doped fiber amplifiers. All optical amplifiers increase the power level of incident light through a stimulated emission process. The mechanism to create the population inversion that is needed for stimulated emission to occur is the same as is used in laser diodes [4]. Although the structure of an optical amplifier is similar to that of a laser, it does not have the optical feedback mechanism that is necessary for lasing to take place. Thus, an optical amplifier can boost incoming signal levels, but it cannot generate a coherent optical output by itself. The basic operation is shown in Fig.2.1. Here, the device absorbs energy supplied from an external source called the pump. The pump supplies energy to electrons in an active medium, which raises them to higher energy levels to produce a population inversion. An incoming signal photon will trigger these excited electrons to drop to lower levels through a stimulated emission process, thereby producing an amplified signal [4]. Beside, an incoming photon can stimulate an electron from lower to upper level. This is a stimulated absorption process as the incoming photon is extinguished.

In general, the optical gain depends not only on the wavelength of the incident signal, but also on the local power at any point in the amplifier [5]. As the signal power increases, the population inversion in the active region is greatly depleted leading to a decrease in the amplifier gain. Signal distortion can be caused by such gain saturation. Moreover, it can also further limit the gain achievable when optical amplifiers are used as multichannel amplifiers.

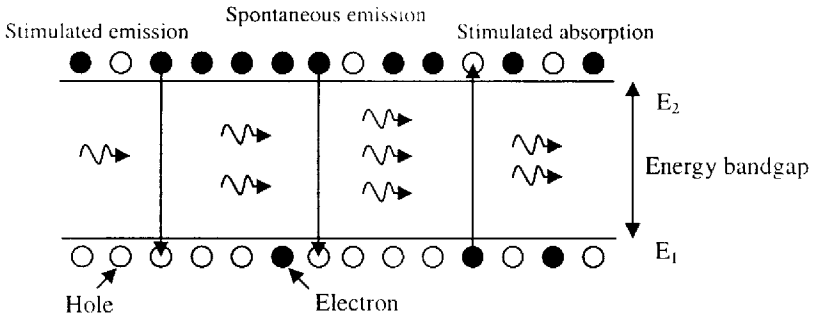

Figure 2.1: Schematic diagram of two-level system with spontaneous and stimulated processes.

On the other hand, optical output from optical amplifiers is composed of an amplified optical signal and an amplified spontaneous emission (ASE) of a broad spectral width [1]. The spontaneous emission noise is the dominate source of noise in optical amplifiers and it is a random process, which is statistically stationary and will cause fluctuations in both amplitude and phase of optical signal. In addition, photons of the spontaneous emission can interact directly with the signal. Moreover, interference is created between ASE components and the light signal. So, several types of noises (the shot noise of the signal and spontaneous emissions, beat noise between signal and spontaneous emissions, and beat noise between spontaneous emission components) can be observed, when the output photons are detected by a photodetector.

2.3 Characteristics of Different Types of Optical Amplifier

The two major types of SOAs are the resonant, Fabry-Perot amplifier (FPA) and the non-resonant, traveling-wave amplifier (TWA). In an FPA, the two cleaved facets of a semiconductor crystal act as partially reflective end mirrors that form a Fabry-Perot cavity. When an optical signal enters the FPA, it gets amplified as it

reflects back and forth between the mirrors until it is emitted at a higher intensity. The structure of a traveling-wave amplifier is the same as that of an FPA except that the end facets are antireflection-coated, so that internal reflection does not take place. Thus, the input light gets amplified only once during a single pass through the TWA. These devices have been used more widely than FPAs because they have a large optical bandwidth, high saturation power, and low polarization sensitivity. For most cases, recent literature on optical fiber systems uses the term "SOA" without qualification, for traveling-wave semiconductor optical amplifiers [4]. In this thesis, we will concentrate on TWAs only.

The active medium in an Erbium-doped fiber amplifier consists of a nominally 10 to 100-m length of optical fiber that has been lightly doped with rare-earth element – erbium (Er). Whereas semiconductor optical amplifiers use external current injection to excite electrons to higher energy levels, optical fiber amplifiers use optical pumping. In this process, one uses photons to directly raise electrons into excited states. The optical pumping process requires the use of three energy levels. The top energy level to which the electron is elevated must lie energetically above the desired lasing level. After reaching its excited state, the electron must release some of its energy and drop to the desired lasing level. From this level, a signal photon can then trigger it into stimulated emission, whereby it releases its remaining energy in the form of a new photon with a wavelength identical to that of the signal photon. Since the pump photon must have a higher energy than the signal photon, the pump wavelength is shorter than the signal wavelength [4].

2.4 System Applications

Three main applications of optical amplifiers in optical transmission system are power booster to increase transmitter laser power and compensate for the splitting

losses in optical distribution network; in-line amplifier to compensate the fiber loss; and preamplifier to improve receiver sensitivity. The optical fiber amplifier has tended to be dominating conventional system applications as it possesses higher gain, low noise figure, and negligible nonlinearities. However, the SOA can still be used as basic amplifiers because of its compact size and low cost, and it is easily integrated with other optical devices and circuits. In addition, the SOA is showing a great promise using in many functional applications, such as optical switch, wavelength converter, and other optical signal processing device, all of those cannot be performed by fiber amplifiers [2].

Chapter 3
Optical Amplifier Modeling

Models of optical amplifier steady-state and dynamic behavior are important tools that allow optical amplifier designer to develop optimized devices. They also allow us to predict how an SOA and EDFA or cascade of them respectively behaves in a particular application. In this chapter we concentrate on specific models and use them to focus on the main characteristics of SOAs and EDFAs.

Different from the laser diodes (LDs) which operate in a narrow spectral range, the optical amplifiers have to be described in a broad wavelength spectrum as the multichannel signals may spread over the entire gain spectrum where spontaneous emission noise is also emitted and coupled into the signal wavelength [6]. In our model, the spontaneous emission noise is generated by random number sources over the entire wavelength spectrum and is coupled to the signal channels in a self-consistent manner.

Firstly, the time-domain traveling wave model developed on the photon number (photon power) rate equations and the phase rate equations will be established for the simulation of both SOAs and EDFAs, where the optical power and phase driven by the locally generated noise source is described. In the spatial domain, such devices exhibit non-uniform population and photon distributions along the propagation direction. Therefore, the governing equations have to be discretized along the active medium to treat these variations. As stated before, it is necessary that the governing

equations are also solved in a broad spectral range, so the broad-band spontaneous emission noise and the multichannel optical signals can be considered. Last of all, the photon number (or photon power) rate equation and the phase rate equation are coupled to the carrier density (or population density) rate equation for the variation of gain and spontaneous emission noise.

3.1 Semiconductor Optical Amplifier

At present, there are numerous techniques for simulating semiconductor optical amplifier numerically. However, we use a more detailed model to take into account the longitudinal spatial nonuniformity of the carrier density and the locally generated broadband ASE noise. In opposite to [7], our aim is to provide the models of both SOA and EDFA to be adaptable with various bit rates of input signals for flexibility when they are assembled in the communication system platform. Therefore, we provide a set of coupled rate equations including t and z dependence to describe the amplification process in SOA, and in EDFA later. Originally, the time-dependent coupled wave equations for simulating the active devices can be derived from Maxwell's equations as follows:

$$\frac{1}{v_g}\frac{dE_{k\pm}(t,z)}{dt} \pm \frac{dE_{k\pm}(t,z)}{dz} = \left[-j\beta + \frac{1}{2}\left(\Gamma g_m(\nu_k, N(t,z)) - \alpha(N(t,z))\right)\right] E_{k\pm}(t,z) + E_N(t,z) \tag{3.1.1}$$

where $E_{k+}(t,z)$ and $E_{k-}(t,z)$ are the slowly varying forward and backward complex optical field respectively, k represents the corresponding wavelength located at the center of the segments that cover the entire spontaneous emission spectrum with N_k indicating the total number of the wavelength segments. On the other hand, v_g (m/s) is the group velocity, α (m^{-1}) is the material loss coefficient, and Γ is the confinement

factor. g_m (m^{-1}) is the material gain that depends on the position in the cavity and the carrier density $N(t,z)$ (m^{-3}), which turns to depend on the spatial position and time. Finally, $E_N(t,z)$ represents the spontaneous emission noise, which operates as the driving sources for oscillation.

It is convenient to introduce normalized complex field amplitude $E(t,z)$, so that the absolute square of this field amplitude corresponds to the photon number rate $S(t,z)$ (1/s) inside the amplifier cavity

$$S(t,z) = |E(t,z)|^2$$

or $$E(t,z) = \sqrt{S(t,z)}e^{j\phi(t,z)}$$

where $\phi(t,z)$ represents the phase of the optical field.

We can obtain the photon number rate equations from (3.1.1) as follows:

$$\frac{1}{v_g}\frac{dS_{k\pm}(t,z)}{dt} \pm \frac{dS_{k\pm}(t,z)}{dz} = \left(\Gamma g_m(v_k, N(t,z)) - \alpha(N(t,z))\right)S_{k\pm}(t,z) + R_{sp}(v_k, N(t,z)) + F_S(t,z) \tag{3.1.2}$$

where $S_{k+}(t,z)$ and $S_{k-}(t,z)$ represent the forward and backward signal or amplified spontaneous emission noise (ASE) photon rates at the k-th wavelength segment (N_k is total number of wavelength segments), respectively.

$$S_k(t,z) = |E_k(t,z)|^2 = \frac{P_k(t,z)}{hv_k}$$

$R_{sp}(v_k, N(t,z))$ is the mean value of the spontaneous emission rate.

The material loss coefficient and the spontaneous emission rate are defined as (3.1.3) and (3.1.4) respectively:

$$\alpha(N(t,z)) = K_0 + \Gamma K_1 N(t,z) \quad (1/m) \tag{3.1.3}$$

$$R_{sp}(v_k, N(t,z)) = \Gamma g_m(v_k, N(t,z)) n_{sp} \Delta v_k \quad (1/ms) \tag{3.1.4}$$

Here K_0 is the carrier-independent loss coefficient; K_1 is the carrier-dependent loss coefficient, and n_{sp} is the population inversion factor.

For the SOA gain model, a good approximation given by equation (3.1.5) presented in [8],[9] was used. There are two gain expressions since we considered two commonly used SOA materials, which are the Bulk and Multi-Quantum Well (MQW).

When a phenomenological gain model is used, the optical gain is given by

$$g_m(v_k, N(t,z))) = \frac{g_N[(N(t,z) - N_{tr})]}{[1 + \varepsilon\ S_k(t,z))]} D(v_k) \qquad (Bulk)$$

$$g_m(v_k, N(t,z)) = \frac{g_N \ln[N(t,z)/N_{tr}]}{[1 + \varepsilon\ S_k(t,z))]} D(v_k) \qquad (MQW)$$

where (3.1.5)

$$D(v) = \left[1 - \left(\frac{v - v_p}{v_{wl}}\right)^2\right] \qquad v > v_p$$

$$D(v) = \left[1 - \left(\frac{v - v_p}{v_{wr}}\right)^2\right] \qquad v < v_p$$

Here, g_N is the differential gain, the unit of it is (m^2) for bulk and (m^{-1}) for MQW, N_{tr} is the transparent carrier density, ε is the gain saturation factor, and $D(v)$ is the detuning factor at the corresponding frequency. The detuning factor is used to adjust the gain profile of SOA, where v_p is the frequency of the peak of gain, v_{wl} and v_{wr} are the left and right position on the gain spectrum at FWHM frequency width respectively.

In our model, the SOA is divided into M longitudinal sections of equal length, and a uniform carrier and averaged photon rates are used for each section. Fig. 3.1 illustrates the SOA sectioning. The ith section has a uniform carrier density N_i, an averaged signal photon rate $S_{sig,i}$, and an averaged ASE spectral photon rate $S_{ASE,i}$. The total current injected into the active region I is supposed to be equally

distributed among the sections, hence $I_i = I/M$. On the other hand, the photon number rate equations at different wavelengths in (3.1.2) are coupled through the carrier population sharing, governed by the carrier rate equation

$$\frac{dN^i(t)}{dt} = \frac{I_i}{edLW} - \frac{\Gamma}{dW}\left\{\sum_{k=1}^{N_s} g_m(\nu_k, N^i(t))[(S^i_{k+}(t) + S^i_{k-}(t))]\right\} - R_R(N^i(t)) \qquad (3.1.6)$$

where I_i is the amplifier bias current. In (3.1.6) all of the bias current is assumed to pass through the active region only, no current leakage is considered. The first term on the right hand side (RHS) of (3.1.6) represents the addition of carriers to the active region from the bias current. These injected carriers are then depleted by various mechanisms occurring within the amplifier. The second term represents radiative recombination of carriers due to the amplified signal and amplified spontaneous emission (ASE). The last term represents the radiative and nonradiative recombination mechanisms given by

$$R_R(N^i) = A_{nrad}N^i + B_{rad}N^{i2} + C_{aug}N^{i3} \qquad (3.1.7)$$

where A_{nrad} is a linear nonradiative recombination coefficient, B_{rad} is bimolecular radiative coefficient, and C_{aug} is the Auger recombination coefficient.

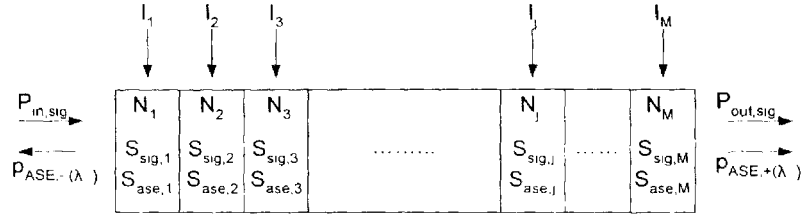

Figure 3.1: The SOA is divided into M sections of equal length.

In the model N_s signals are injected into the amplifier with optical frequencies $\nu_j (j = 1....N_s)$ and power P_{in,sig_j} before coupling loss. The signals travel through the amplifier cavity, and exit at the opposite facet. The SOA model is based on a set of

coupled differential equations that describe the interaction between the internal variables of the amplifier, i.e. the photon rate and carrier density. The solution of these equations enables external parameters such as signal fiber-to-fiber gain to be predicted. In the following analysis it is assumed that traverse variations (i.e. normal to the propagation direction) in the photon rates and carrier density are negligible. This is valid assumption because most SOAs have a narrow active region [10]. In the model, the left (input) and right (output) facets have power reflectivity R_1 and R_2, respectively. (3.1.8) is subjected to boundary conditions for the traveling signal photon rates and spontaneous emission photon rates

$$\left.\begin{aligned} S_+(t,0,\lambda_j) &= R_1 S_-(t,0,\lambda_j) + (1-R_1)S_{in}(t,0,\lambda_j) \\ S_+(t,0,\lambda_k) &= R_1 S_-(t,0,\lambda_k) \end{aligned}\right\} \text{ Left facet}$$

$$\left.\begin{aligned} S_-(t,L,\lambda_j) &= R_2 S_+(t,L,\lambda_j) \\ S_-(t,L,\lambda_k) &= R_2 S_+(t,L,\lambda_k) \end{aligned}\right\} \text{ Right facet} \qquad (3.1.8)$$

The input signal photon rate from the optical fiber is given as

$$S_{in,sig\_j}(t,0) = \frac{\eta_{in} P_{in,sig\_j}(t)}{h\nu_j} \qquad (3.1.9)$$

where η_{in} is the input coupling efficiency from the fiber to the device waveguide, and P_{in,sig_j} is the input power at the jth channel. The output power of the jth channel from the SOA can be expressed as

$$P_{out,sig\_j}(t) = h\nu_j \eta_{out}(1-R_2)S_{j+}(t,L) \qquad (3.1.10)$$

where η_{out} is the output coupling efficiency from the device waveguide to the fiber.

3.2 Erbium-Doped Fiber Amplifier

A method for describing the model of EDFA is similar with that we did for SOA before. The EDFA can be modeled by a two-level and homogeneously broadened atomic model [12],[13]. This is true for 1480-nm pump wavelength, where only upper level $I_{13/2}$ and bottom level $I_{15/2}$ are involved, as shown in Fig. 3.2. For 980-nm pumps, erbium ions are more accurately described by a three level model [14]-[16]. However a two-level model is still a good approximation since the number of atoms on the pump level $I_{11/2}$ is small due to its short lifetime. We choose the model used in [17]-[19], and start with a set of coupled rate equations to describe the steady state and transient dynamic of EDFA with random amplified spontaneous emission (ASE) noise incorporated.

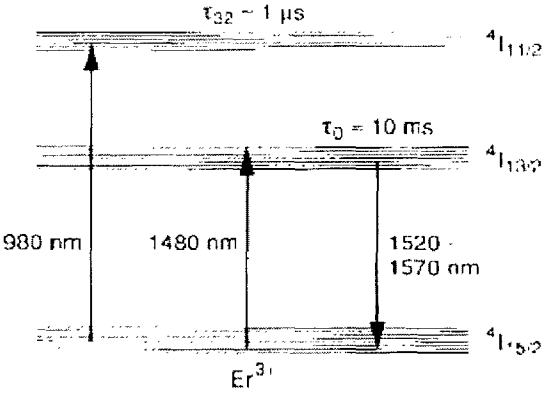

Figure 3.2: Energy level structure of Erbium ions in glass fiber host. EDFA can be pumped either at 980nm or 1480nm.

The photon power rate equations describing the propagation in forward and backward directions of the signals and ASE noise over the entire wavelength spectrum is as follows:

$$\frac{1}{v_g}\frac{dP_{k\pm}(t,z)}{dt} \pm \frac{dP_{k\pm}(t,z)}{dz} = \Gamma_s\left(\sigma_{es}(\lambda_k)N_2(t,z) - \sigma_{as}(\lambda_k)N_1(t,z)\right)P_{k\pm}(t,z) + R_{sp}(\nu_k, N_2(t,z)) + F_S(t,z) \tag{3.2.1}$$

As well as, the evolution of the pump light power through the longitudinal coordinate z can be described by the pump power propagation equation

$$\frac{1}{v_g}\frac{dP_{p\pm}(t,z)}{dt} \pm \frac{dP_{p\pm}(t,z)}{dz} = \Gamma_p\left(\sigma_{ep}N_2(t,z) - \sigma_{ps}N_1(t,z)\right)P_{p\pm}(t,z) \tag{3.2.2}$$

Here $P_{k+}(t,z)$ and $P_{k-}(t,z)$ are the forward and backward signal or amplified spontaneous emission noise photon powers at *kth* wavelength segment, whereas $P_{p+}(t,z)$ and $P_{p-}(t,z)$ represent the forward and backward propagation of the pump powers. v_g is group velocity of light in the fiber, and is assumed identical for signal and pump. Γ_s and Γ_p correspond to overlap factors between the pump and signal modes and the doped fiber core. The absorption (a) and emission (e) cross sections of the pump (p) and signal (s) are $\sigma_{p,s;a,e}$. The total population is given by $N_T = N_1 + N_2$, where N_1 and N_2 are the population densities of the ground level and metastable level respectively. The mean value of the spontaneous emission noise power is given by $R_{sp}(\nu_k, N_2(t,z)) = 2\Gamma_S\sigma_{es}N_2(t,z)h\nu_k\Delta\nu_k$. The random amplified spontaneous emission noise power is given in term of a Langevin force function $F_N(t,z)$, which will be discussed in detail later in this chapter.

For the sake of simplicity, the optical gain of EDFA is represented by a set of analytical data, which is curve-fitted by a well-known Levenberg Marquardt method.

The analytical gain expression of EDFA can be written in the form of rational function which depends on the carrier density and the wavelength, is given as follows [7]

$$g(\lambda, N) = \frac{a_0 + a_1\lambda + a_2\lambda^2 + a_3\lambda^3 + ...}{1 + b_1\lambda + b_2\lambda^2 + b_3\lambda^3 + ...} \qquad (3.2.3)$$

where each coefficient is a function of N,

such as : $a_0 = a_0^{'} + a_0^{''}N$, *and* $b_0 = b_0^{'} + b_0^{''}N$

After testing by trial and error procedure, a combination of 20 and 30 coefficients on the numerator and denominator respectively was chosen with a great balance between the efficiency and accuracy.

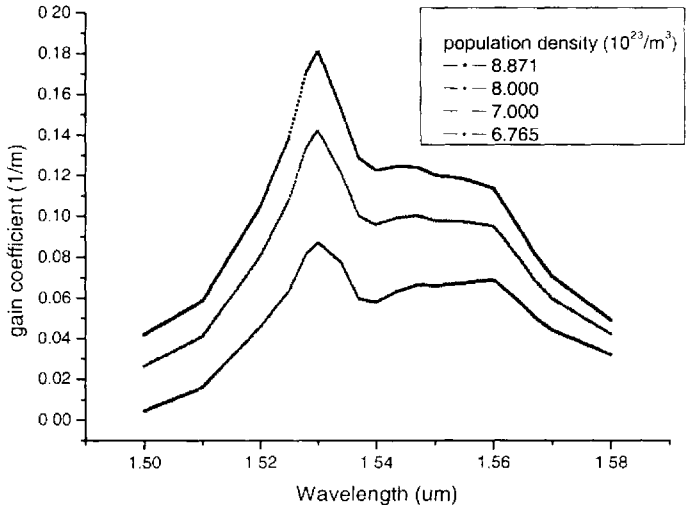

(a)

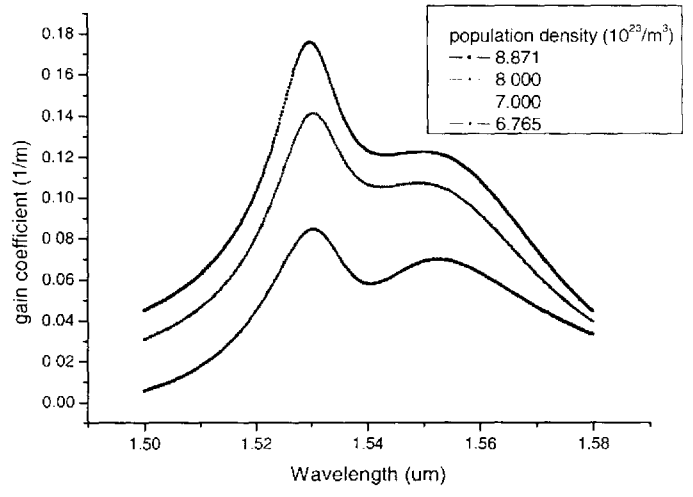

(b)

Figure 3.3: Analytical gain spectrum for EDFA a) without curve-fitting b) with Levenberg Marquardt curve-fitting.

Originally, the rate equation which governs the population density on the metastable level is

$$\frac{\partial N_2(z,t)}{\partial t} = \sum_k \frac{P_k \Gamma_k \sigma_{as}}{h\nu_k A} N_1(z,t) - \sum_k \frac{P_k \Gamma_k \sigma_{es}}{h\nu_k A} N_2(z,t) + \frac{P_p \Gamma_p \sigma_{ap}}{h\nu_p A} N_1(z,t) - \frac{P_p \Gamma_p \sigma_{ep}}{h\nu_p A} N_2(z,t) - \frac{N_2(z,t)}{\tau} \tag{3.2.4}$$

where A is the uniformly doped fiber core area, and τ is the spontaneous emission lifetime of the metastable level. Further reduction in (3.2.1) and (3.2.2), it gives

$$\frac{\partial N_2(z,t)}{\partial t} = -\sum_k \frac{P_k \Gamma_k}{h\nu_k A}\left[\sigma_{es} N_2(z,t) - \sigma_{as} N_1(z,t)\right] - \frac{P_p \Gamma_p}{h\nu_p A}\left[\sigma_{ep} N_2(z,t) - \sigma_{ap} N_1(z,t)\right] - \frac{N_2(z,t)}{\tau} \tag{3.2.5}$$

From (3.2.1), we note that (3.2.5) can be expressed as

$$\frac{\partial N_2(z,t)}{\partial t} = -\sum_k \frac{1}{h\nu_k A}\frac{\partial P_k(t,z)}{\partial z} - \frac{1}{h\nu_p A}\frac{\partial P_p(t,z)}{\partial z} - \frac{N_2(z,t)}{\tau} \tag{3.2.6}$$

Then, we define the average population density over each subsection as $N_2^i(t) = \frac{1}{l}\int_0^l N_2(t,z)dz$ which is kept as constant at i-th section and can vary in different subsections. l is the length of one subsection.

Finally, (3.2.6) can be rewritten including backward photon powers as follows:

$$\frac{\partial N_2{}^i(t)}{\partial t} = \sum_{k\pm}^{N_k} \frac{P_{k\pm}{}^i(t)}{h\nu_k V}\left(1 - G_{k\pm}{}^i(N_2{}^i(t))\right) + \sum_{\pm} \frac{P_{p\pm}{}^i(t)}{h\nu_p V}\left(1 - G_{p\pm}{}^i(N_2{}^i(t))\right) - \frac{N_2{}^i(t)}{\tau} \tag{3.2.7}$$

where $G_{k\pm}{}^i$ is the forward and backward sectional optical gain for pump and signal at the corresponding section of the doped fiber, and V is uniformly doped fiber core volume.

In the EDFA model, there are no reflectivities at both ends as it uses an optical fiber as gain medium. (3.2.8) is subjected to boundary conditions for the traveling

signal photon powers, spontaneous emission photon powers, and pump photon power

$$P_+(t,0,\lambda_j) = P_{in}(t,0,\lambda_j)$$

$$P_-(t,L,\lambda_k) = P_+(t,0,\lambda_k) = 0 \qquad \text{where } k = 1,\ldots,N_k \text{ and } j = 1,\ldots,N_s$$

$$P_+(t,0,\lambda_p) = P^+$$

$$P_-(t,L,\lambda_p) = P^- \tag{3.2.8}$$

The output power of the j th channel from the EDFA can be expressed as

$$P_{out,sig\_j}(t) = P_{j+}(t,L) \tag{3.2.9}$$

3.3 Frequency Chirp Computation

Frequency chirping is an important phenomenon that is known to limit the performance of lightwave systems. Optical pulses with time-dependent phase shift are called chirped. In consequence of the frequency chirp imposed on an optical pulse, its spectrum is considerably broadened. Such spectral broadening affects the pulse shape at the fiber output because of fiber dispersion and degrades system performance [5].

The optical gain in the active region will change due to the carrier fluctuation when the signal propagating through the amplifier. In the meanwhile, the material refractive index change is induced from the gain change. It is normally computed by the Kramers-Kronig transform as long as the optical gain profile is obtained [21].

$$\Delta n(\lambda_k, N^i) = \frac{\lambda_k^2}{2\pi^2} P\int_0^\infty \frac{g_m(\lambda_k', N^i)}{\lambda_k'^2 - \lambda_k^2} d\lambda_k' \tag{3.3.1}$$

Performing the Kramers-Kronig transformation to obtain the refractive index change at each section once the change of gain has been computed. Finally, the phase change can be computed straightforwardly by adding up each refractive index change of

section.

The total phase change is given by:

$$\Delta\phi(t) = \frac{\Delta z}{L}\sum_{i}(\frac{2\pi}{\lambda_s}\Delta n(\lambda_k, N'))\Delta z + F_\phi(t)\Delta z \tag{3.3.2}$$

Consequently, the frequency chirping Δf of the output signal is defined by differentiating its phase ϕ with respect to time:

$$\Delta f(t) = -\frac{1}{2\pi}\frac{\Delta\phi(t)}{\Delta t} = -\frac{v_g}{2\pi}\left(\frac{1}{L}\sum_{i}(\frac{2\pi}{\lambda_s}\Delta n_i)\Delta z + F_\phi(t)\right) \tag{3.3.3}$$

The output field can be determined for both SOA and EDFA after obtaining the output power and the output phase change:

$$E_{out,j}(t) = \sqrt{P_{out,j}(t)}e^{j(\phi_{in,j}(t)+\Delta\varphi_j(t))} \tag{3.3.4}$$

3.4 Noise Characteristics

The spontaneous emission noise brings in fluctuations on both of the photon power and the frequency, known as the intensity noise and the phase noise. In order to include the intensity and phase noise from spontaneous emission, the photon power rate equation (3.1.2) & (3.2.1) and the phase equation (3.3.2) have been transformed into stochastic equations by adding $F_S(t,z)$ and $F_\phi(t)$ respectively, which are random Langevin noise sources. For optical amplifiers, the most important signal degradation in optical communication system comes from the spontaneous emission noise.

In many cases of interest, it is sufficient to assume that the events of spontaneous emission at different times and different locations along the amplifier are statistically independent, and due to large numbers of photons it is possible to treat the noise in an

amplifier using Gaussian statistics. The complex amplitude $E_N(t,z)$ for the noise is written as $E_N(t,z)=\sqrt{S_N(t,z)}e^{j\phi_N(t)}$, where $S_N(t,z)$ follows an approximately Gaussian statistic around its mean value $\langle S_N \rangle$, while the phase ϕ_N may have any value $0 \le \phi_N < 2\pi$ with equal probability.

The amplified spontaneous emission (ASE) noise is assumed as a stationary, uncorrelated zero-mean Gaussian white noise with an autocorrelation function [22],[23].

$$\langle E_N(t,z)E_N^*(t',z')\rangle = R_{sp}\delta(t'-t)\delta(z'-z) \tag{3.4.1}$$

A stationary random signal is one whose characteristics do not depend upon the time origin, which implies that the mean values are independent of time whereas the autocorrelation function are functions of time difference only.

Since the slowly varying complex field $E_{k\pm}(t,z)=\sqrt{P_{k\pm}(t,z)}\exp(j\phi_{k\pm}(t))$ can be separated into the photon power P and the phase ϕ.

So, the Langevin noise power term in (3.1.2) and (3.2.1) can be expressed as

$$F_S(t,z) \approx 2\,\mathrm{Re}\left(E_k^*(t,z)E_N(t,z)\right) = 2\sqrt{\langle P_k(t,z)\rangle}\,\mathrm{Re}\left(E_N(t,z)\exp(-j\phi_k(t))\right) \tag{3.4.2}$$

The spontaneous emission contribution to the photon power is generated from a Gaussian distributed random number generator that satisfies the mean and autocorrelation:

$$\langle F_S(t,z)\rangle = \langle F_S(t',z')\rangle = 0$$

$$\text{(SOA)}\quad \langle F_S(t,z)F_S(t',z')\rangle = \frac{2S_k(t,z)R_{sp}(\nu_k,N(t,z))}{\Delta z}\delta(t'-t)\delta(z'-z)$$

$$\text{(EDFA)}\quad \langle F_S(t,z)F_S(t',z')\rangle = \frac{2P_k(t,z)R_{sp}(\nu_k,N_2(t,z))}{\Delta z}\delta(t'-t)\delta(z'-z) \tag{3.4.3}$$

Likewise, the Langevin noise phase term in (3.3.2) can be expressed as

$$F_\phi(t) \approx \frac{1}{P_k(t)} \mathrm{Im}\left(E_k^*(t) E_N(t)\right) = \frac{1}{\sqrt{P_k(t)}} \mathrm{Im}\left(E_N(t) \exp(-j\phi_k(t))\right) \tag{3.4.4}$$

The spontaneous emission contribution to the phase is generated from a Gaussian distributed random number generator that satisfies the mean and autocorrelation:

$$\left\langle F_\phi(t) \right\rangle = \left\langle F_\phi(t') \right\rangle = 0$$

$$\text{(SOA)} \quad \left\langle F_\phi(t) F_\phi(t') \right\rangle = \frac{R_{sp}(\nu, N(t))}{2S_k(t)L} \delta(t'-t)$$

$$\text{(EDFA)} \quad \left\langle F_\phi(t) F_\phi(t') \right\rangle = \frac{R_{sp}(\nu, N_2(t))}{2P_k(t)L} \delta(t'-t) \tag{3.4.5}$$

It can be noted that the autocorrelation of both noise sources are photon power dependent.

Chapter 4

Model Implementation

In order to obtain the optical amplifier performance, the set of coupled differential equations must be solved. Since the optical amplifiers model equations cannot be solved analytically, a numerical solution must be required. The methods for solving the SOA and EDFA model are based on the similar manner, except we used photon power in EDFA model instead of photon number rate used in SOA's. So, both of photon power and photon number rate are used interchangeably throughout this thesis. As well as, we only need to input and select a different set of parameters and constants for corresponding type of amplifiers. Moreover, the models of both SOA and EDFA we used are adaptable with various bit rates of input signals for generalization and flexibility when they are assembled in the communication system platform.

4.1 Steady-state Model

In this section, we use a steady state model to explore the main characteristics of various types of optical amplifiers. Firstly, in steady state conditions, the time derivative terms in all of the coupled differential equations stated in Chapter 3 are set to zero ($\frac{\partial}{\partial t} = 0$), since all parameters are independent with respect to time by now. We then apply a shooting method to solve the following set of equations for the carrier densities according to both signal and noise photon rate at each section

interfaces. The following carrier rate equation of SOA and population density equation of EDFA should be satisfied:

$$\frac{I_i}{edLW} = \frac{\Gamma}{dW}\left\{\sum_{k=1}^{N_k} g_m(\nu_k, N')[S_{k+}^i + S_{k-}^i]\right\} + R_R(N') \tag{4.1.1a}$$

and

$$0 = \sum_{k\pm} \frac{P_{k\pm}^{\ i}}{h\nu_k V}\left(1 - G_{k\pm}{}^i(N_2{}^i)\right) + \sum_{\pm} \frac{P_{p\pm}^{\ i}}{h\nu_p V}\left(1 - G_{p\pm}{}^i(N_2{}^i)\right) - \frac{N_2{}^i}{\tau} \tag{4.1.1b}$$

whereas the photon rate equation of SOA can be written as

$$\pm \frac{dS_{k\pm}(z)}{dz} = \left(\Gamma g_m(\nu_k, N(z)) - \alpha(N(z))\right)S_{k\pm}(z) + R_{sp}(\nu_k, N(z)) \tag{4.1.2a}$$

and the photon power and pump power equations of EDFA can also be written as

$$\pm \frac{dP_{k\pm}(z)}{dz} = \Gamma_s\left((\sigma_{es}(\lambda_k) + \sigma_{as}(\lambda_k))N_2(z) - \sigma_{as}(\lambda_k)N_T\right)P_{k\pm}(z) + R_{sp}(\nu_k, N_2(z)) \tag{4.1.2b}$$

$$\pm \frac{dP_{p\pm}(z)}{dz} = \Gamma_p\left((\sigma_{ep} + \sigma_{ps})N_2(z) - \sigma_{ps}N_T\right)P_{p\pm}(z) \tag{4.1.2c}$$

In the numerical simulation, the amplifier is split into a number of sections labeled i= 1 to M. The signal and spontaneous emission noise photon rates are computed at the section interfaces. It is assumed that the injection current is uniform in each section and the ith section has a uniform carrier density N'. The ASE spectrum is divided into a number of intervals labeled $k = 1$ to N_k with a uniform frequency ν_k in the $k-$th interval. The first step in the algorithm is to initialize the signal and spontaneous emission photon rates to zero, in order to obtain the initial carrier density in the first section from (4.1.1). The iteration then begins. Using Newton's Method section by section can solve the carrier density rate equation. With the known carrier density value, the coefficients of the photon rate equation in the corresponding section can be calculated, as well as the photon rate of its next section

can be computed by using the general solution of differential equation.

(SOA) $S_{k\pm}^{i\pm1} = S_{k\pm}^{i} G_{k\pm}^{i}(N^{i}) + n_{sp}\Delta\nu_{k}\left[G_{k\pm}^{i}(N^{i}) - 1\right]$

(EDFA) $P_{k\pm}^{i\pm1} = P_{k\pm}^{i} G_{k\pm}^{i}(N_{2}^{i}) + 2n_{sp}(N_{2}^{i})h\nu_{k}\Delta\nu_{k}\left[G_{k\pm}^{i}(N_{2}^{i}) - 1\right]$

$$P_{p\pm}^{i\pm1} = P_{p\pm}^{i}(t) G_{p\pm}^{i}(N_{2}^{i}) \tag{4.1.3}$$

where $G_{k\pm}^{i}$ is the sectional gain at corresponding section and wavelength segment.

(SOA) $G_{k\pm}^{i}(N^{i}) = e^{\pm\left(\Gamma g_{m}(\nu_{k},N^{i}) - \alpha(N^{i})\right)\Delta Z}$

(EDFA) $G_{k\pm}^{i}(N_{2}^{i}) = e^{\pm\Gamma_{k}\left((\sigma_{ek}(\lambda_{k}) + \sigma_{ak}(\lambda_{k}))N_{2}^{i} - \sigma_{ak}(\lambda_{k})N_{T}\right)\Delta Z}$ for signal power

$G_{p\pm}^{i}(N_{2}^{i}) = e^{\pm\Gamma_{p}\left((\sigma_{ep} + \sigma_{ap})N_{2}^{i} - \sigma_{ap}N_{T}\right)\Delta Z}$ for pump power (4.1.4)

and the excited ion density dependent population inversion factor n_{sp} is given as follows: $n_{sp}(N_{2}^{i}) = \dfrac{\sigma_{ek}N_{2}^{i}}{(\sigma_{ek} + \sigma_{ak})N_{2}^{i} - \sigma_{ak}N_{T}}$

We deal with both forward and backward computation for the forward and backward photon rate with obeying the boundary conditions at both facet ends. So, we have to compare those two carrier density values, which are computed from the forward and backward computation. If they do not agree with each other in a desired tolerance, the iteration continues with newly initial values every time until the percentage change is less than the desired tolerance. This process enables convergence toward the correct value of carrier density for each section, and its algorithm shows stability over a wide range of operating conditions.

Below shows the block diagram of implementation of both SOA and EDFA steady state model.

4.2 Block Diagram of Steady State model implementation

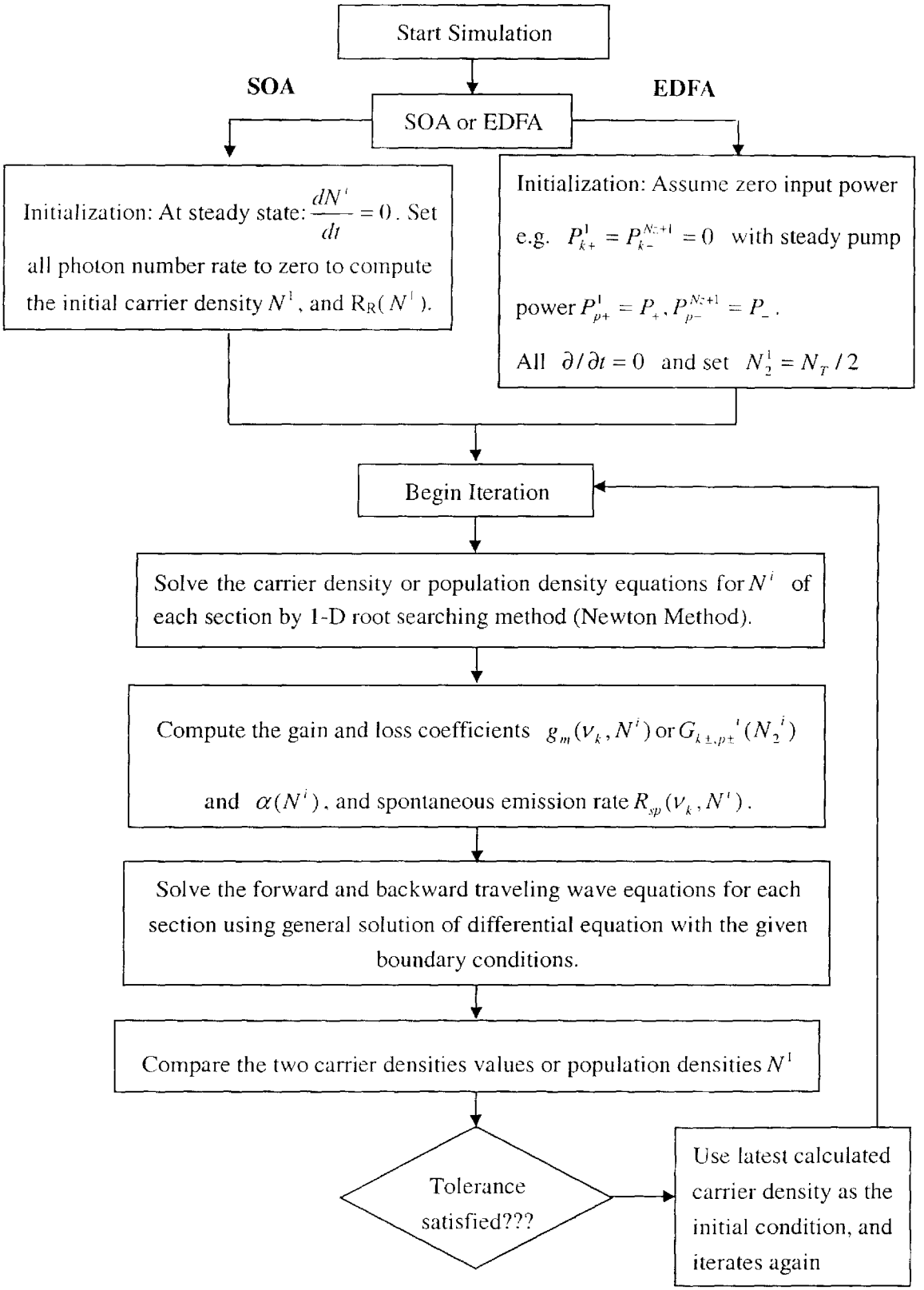

4.3 Large Signal Dynamic Model

As optical amplifiers are used to amplify modulated light, it is of interest to model the large signal dynamic performance of the amplifiers. Dynamic SOA and EDFA models can be used to predict pattern effects where amplified optical bits affect the following bits, signal distortion due to the amplified spontaneous emission (ASE) noise and gain saturation, and channel crosstalk that occurs when multiple signals are amplified in WDM system [2]. Moreover, the system performance of using SOA and EDFA can be distinguished due to they possess different properties and characteristics.

The first step in the algorithm is to initialize the carrier densities, signal photon and spontaneous emission noise rates, and the coefficients of the photon rate equation using the steady state algorithm described in previous section at the beginning of time $(t = 0)$. The time iteration now begins. We then start to switch on the time varying input signal powers and compute the photon rate at the first section with the boundary conditions. As well as, we use two independent random number generators to generate both Langevin noise sources in the photon rate equations and phase equations with Gaussian distribution and the given variances from (3.4.3) and (3.4.5). The time-dependent photon rate equations can be transformed into a time-stepped solution in [9], [25] by dividing the device into a number of subsections with the relation $\Delta z = v_g \Delta t$ utilized, as shown in Fig.4.3.1.

(SOA)

$$S_{k\pm}^{i\pm1}(t+\Delta t) = S_{k\pm}^{i}(t)e^{(\Gamma g_m(\nu_k,N^i(t))-\alpha(N^i(t)))\Delta z} + R_{sp}(\nu_k,N^i(t))\Delta z + \Delta z\sqrt{\frac{2S_k^i(t)R_{sp}(\nu_k,N^i(t))}{\Delta z}}x_{ek}$$

(EDFA)

$$P_{k\pm}^{i\pm1}(t+\Delta t) = P_{k\pm}^{i}(t)e^{\Gamma_k[(\sigma_e(\lambda_k)+\sigma_m(\lambda_k))N_2^i(t)-\sigma_m(\lambda_k)N_t]\Delta z} + R_{sp}(\nu_k,N_2^i(t))\Delta z + \Delta z\sqrt{\frac{2P_k^i(t)R_{sp}(\nu_k,N_2^i(t))}{\Delta z}}x_{ek}$$

(for signal power) (4.3.1)

$$P_{p\pm}^{(t\pm1)}(t+\Delta t) = P_{p\pm}^{t}(t)e^{\Gamma_p\left[(\sigma_p(\lambda_k)+\sigma_{ap}(\lambda_k))N_2^i(t)-\sigma_{ap}(\lambda_k)N_t\right]\Delta Z} \quad \text{(for pump power)} \quad (4.3.2)$$

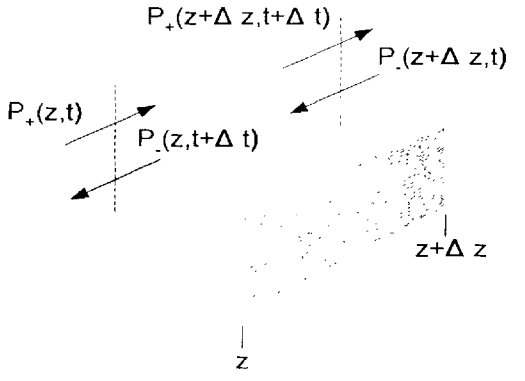

Figure 4.3.1: Schematic view of a section with two input powers at time t and two output powers at time t+Δt are updated.

The next step is to solve the carrier density (population density) rate equation by using Fourth-order Runge Kutta method [26], which is well-known method to solve ordinary differential equation, is accurate enough with the principle of simplicity and efficiency. On the other hand, we need to perform Kramers-Kronig transformation to evaluate the refractive index change in each subsection for computing the phase change and frequency chirp using the analytical equations (3.3.1)-(3.3.3).

$$\text{(SOA)} \quad \Delta\phi(t) = \frac{\Delta z}{L}\sum_i\left(\frac{2\pi}{\lambda_s}\Delta n(\lambda_k, N^i)\right)\Delta z + \Delta z\sqrt{\frac{R_{sp}(\nu_k, N\ (t))}{2S_k(t)L}}x_\phi$$

$$\text{(EDFA)} \quad \Delta\phi(t) = \frac{\Delta z}{L}\sum_i\left(\frac{2\pi}{\lambda_s}\Delta n(\lambda_k, N_2^i)\right)\Delta z + \Delta z\sqrt{\frac{R_{sp}(\nu_k, N_2(t))}{2P_k(t)L}}x_\phi \quad (4.3.3)$$

where x_{ck} and x_ϕ in (4.3.1) and (4.3.3) respectively, are independent Gaussian random variables with zero mean and with variance equal to 1.

If the simulation time limit is reached the algorithm stops. The output signal powers with intensity noise and the frequency chirping with phase noise in time domain can be obtained and the performance of the device can be analyzed. After the noise has been normalized, the noise power spectrum can also be calculated.

4.4 Block Diagram of Large signal dynamics model implementation:

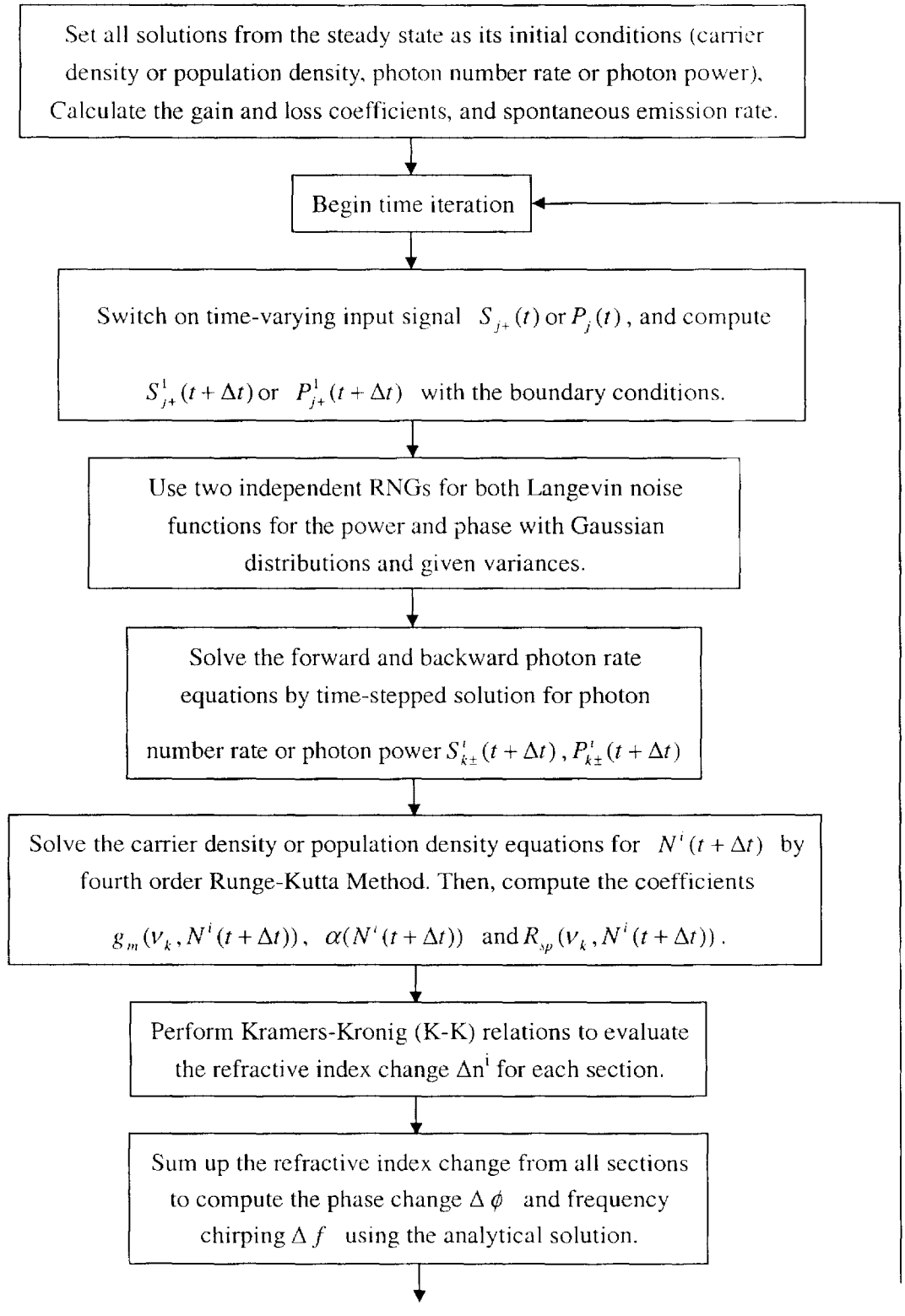

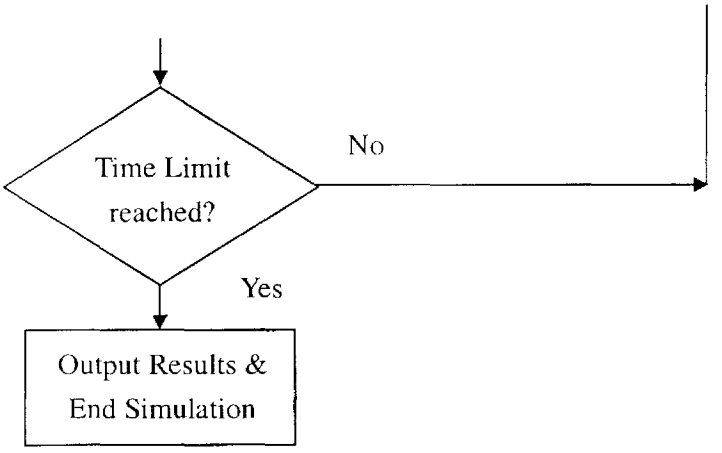
Time Limit reached?
No
Yes
Output Results & End Simulation

Chapter 5

Simulation results

The steady state and large signal dynamics simulation results for both semiconductor optical amplifier (SOA) and erbium-doped fiber amplifier (EDFA) are shown and analyzed. The noise and cross gain saturation effects during multichannel signal amplification in optical amplifier will also be examined. Finally, the frequency spectra of ASE noise are calculated with help of the fast Fourier transform.

5.1 Steady state simulation results

The longitudinal structure of the SOA is sufficiently divided into M=20 subsections with a uniform carrier density in each subsection, as we found that further increases in the subsection number gives a little improvement in the accuracy. Whereas the ASE spectrum is divided into $N_k = 390$ intervals with wavelength interval $\Delta\lambda = 0.30848$ nm [7]. Other material and structure parameters for the device under consideration are listed in Table 5.1.1.

Symbol	Parameter	Bulk active region	MQW active region
L	Active region length	400 μm	400 μm
W	Active region width	1.5 μm	1.5 μm
d	Active region thickness	0.1μm	0.06 μm
Γ	Optical confinement factor	0.4	0.05

n_1	Effective refractive index	3.22	3.22
R_1, R_2	Input & output facet reflectivity	5×10^{-5}	5×10^{-5}
η_{in}, η_{out}	Input & output coupling loss	0.5012	0.5012
I	Bias current	130 mA	130 mA
g_m	Differential gain	4×10^{-20} m^2	2×10^5 m^{-1}
N_{tr}	Transparency carrier density	5×10^{23} m^{-3}	5×10^{23} m^{-3}
ε	Nonlinear gain saturation coefficient	3.0×10^{-23} m^3	3.0×10^{-23} m^3
A_{nrad}	Linear nonradiative coefficient	1×10^9 s^{-1}	0.5×10^9 s^{-1}
B_{rad}	Bimolecular coefficient	6.8×10^{-16} s^{-1}m^3	6.8×10^{-16} s^{-1}m^3
C_{aug}	Auger coefficient	3.0×10^{-41} s^{-1}m^6	3.0×10^{-41} s^{-1}m^6
n_{sp}	Population inversion factor	1.7	2.0

Table 5.1.1 Parameters used for the simulations of both Bulk and MQW SOAs

As for the structure of EDFA, it is divided into M=10 subsections; the ASE spectrum is divided into $N_k = 400$ intervals with wavelength interval $\Delta\lambda = 0.2$ nm [7]. Other pertinent simulation parameters for the EDFA are given in Table 5.1.2.

Symbol	Parameter	Value
L	EDFA length	100 m
Γ_k	Overlap factor (signal or noise)	0.505
Γ_p	Overlap factor (pump)	0.505
A	Effective cross-section	3.456×10^{-12} m^2
λ_p	Pump wavelength	1480 nm

τ	$I_{13/2}$ ion lifetime	12 ms
P_p	Pump power (forward)	36 mW
N_T	Total erbium-ion concentration	9.28×10^{23} m^{-3}

Table 5.1.2 Parameters used for the simulation of EDFA

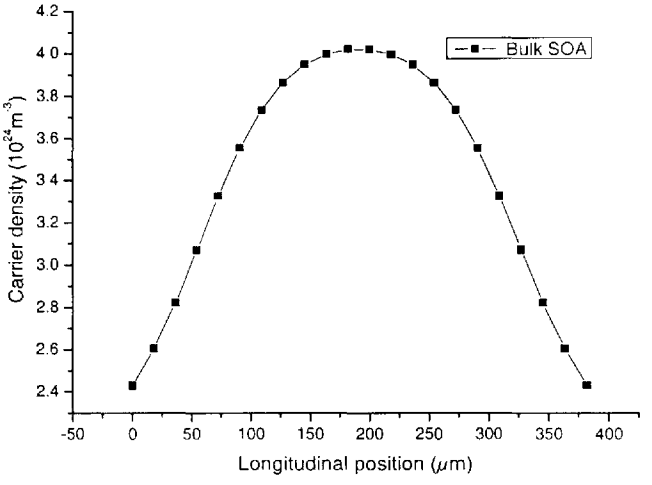

(a)

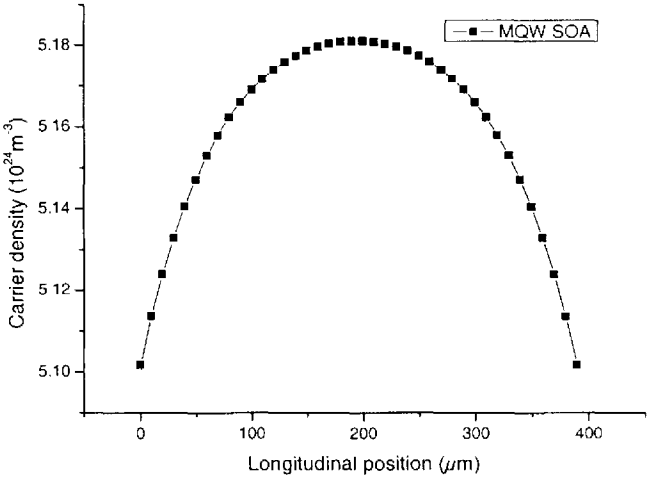

(b)

Figure 5.1.1 Longitudinal carrier density profiles in a SOA with an absence of input signal (0 W). (a) Bulk material (b) MQW material.

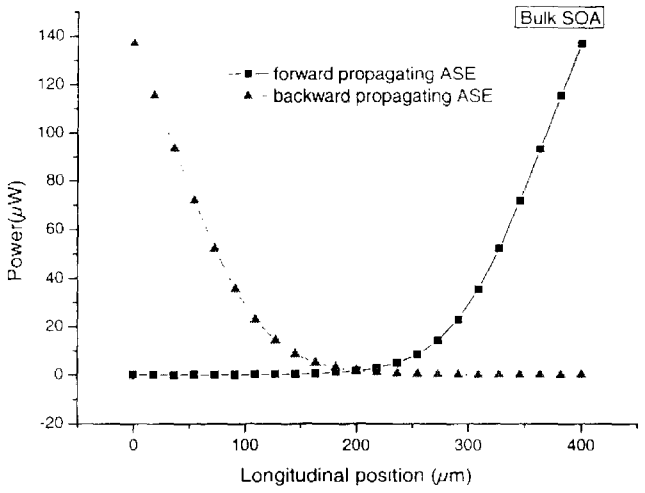

(a)

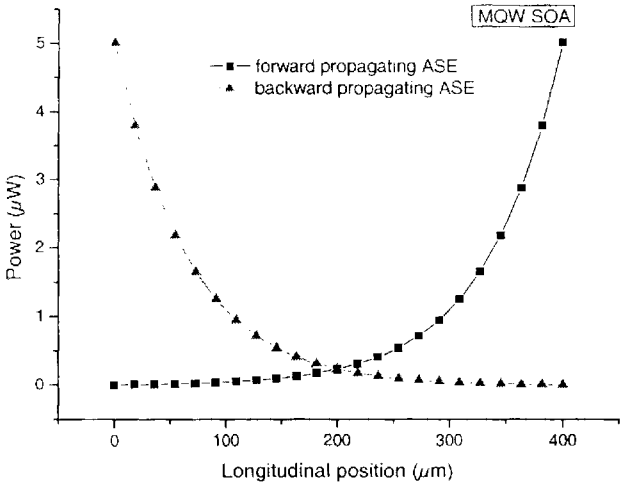

(b)

Figure 5.1.2 SOA forward and backward propagating ASE photon powers spatial distribution with zero input power. (a) Bulk SOA (b) Multi quantum-well SOA.

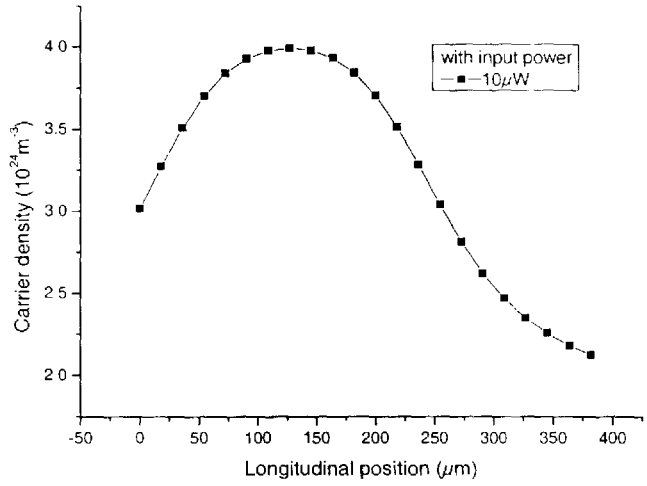

(a)

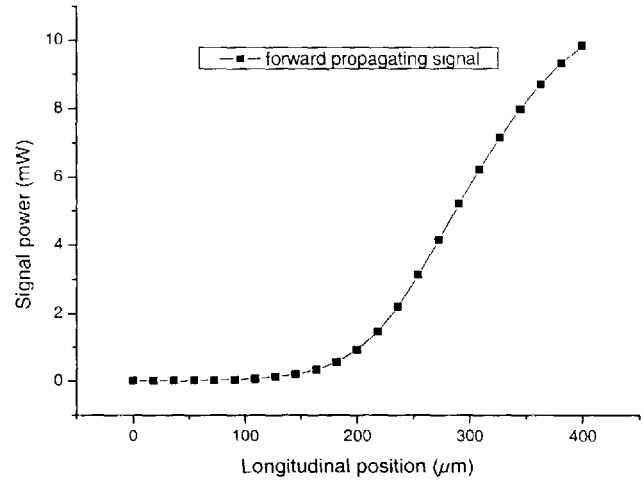

(b)

Figure 5.1.3 Bulk SOA (a) carrier density, (b) forward propagating signal photon power spatial distributions with the input signal power is 10 μW (-20 dBm). Signal wavelength is 1550.12 nm.

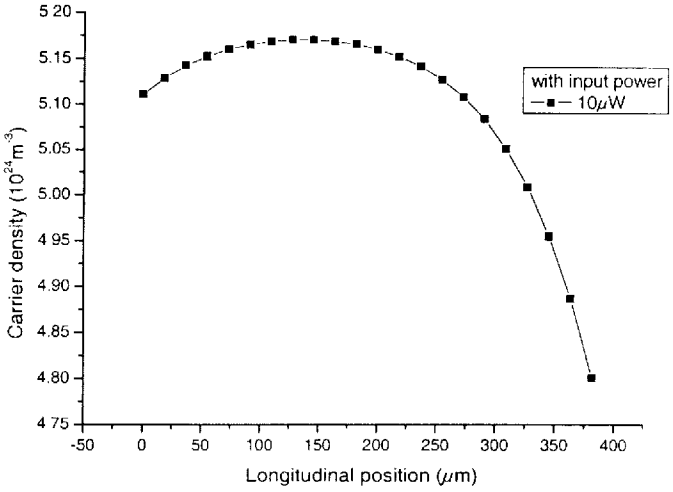

(a)

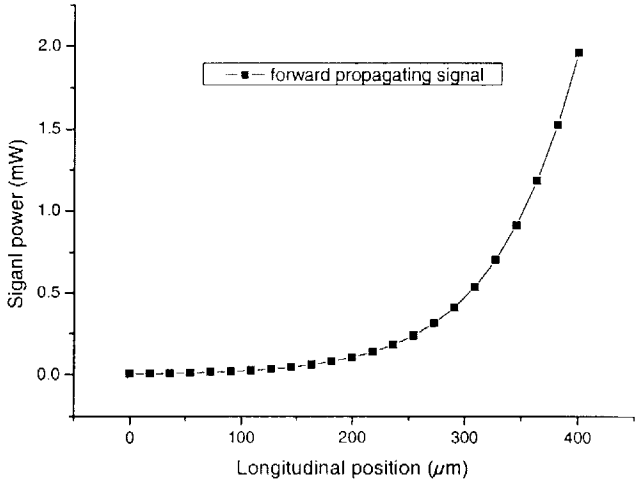

(b)

Figure 5.1.4 MQW SOA (a) carrier density, (b) forward propagating signal photon power spatial distributions with the input signal power is 10 μW (-20 dBm). Signal wavelength is 1550.12 nm.

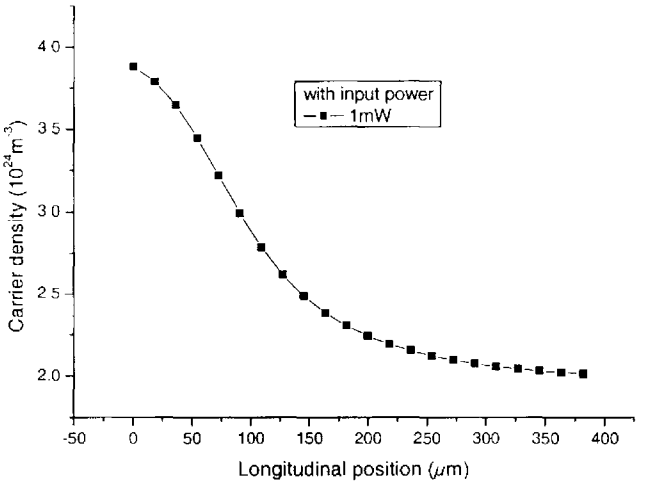

(a)

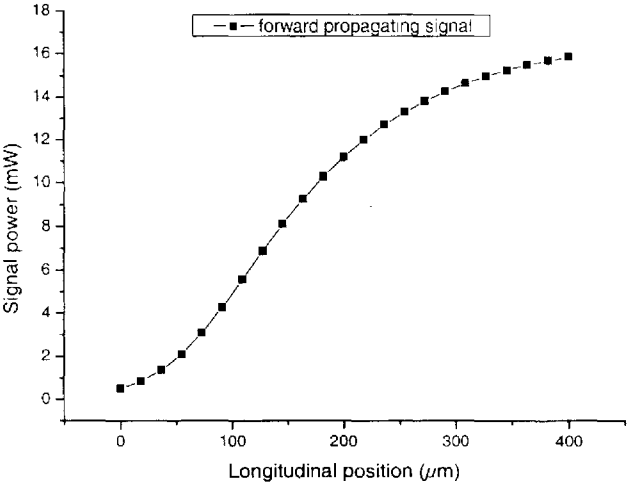

(b)

Figure 5.1.5 Bulk SOA (a) carrier density, (b) forward propagating signal photon power spatial distributions with the input signal power is 1 mW (0 dBm). Signal wavelength is 1550.12 nm.

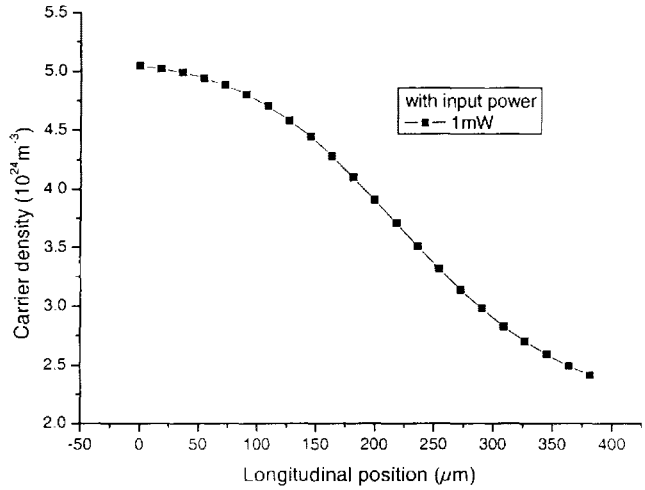

(a)

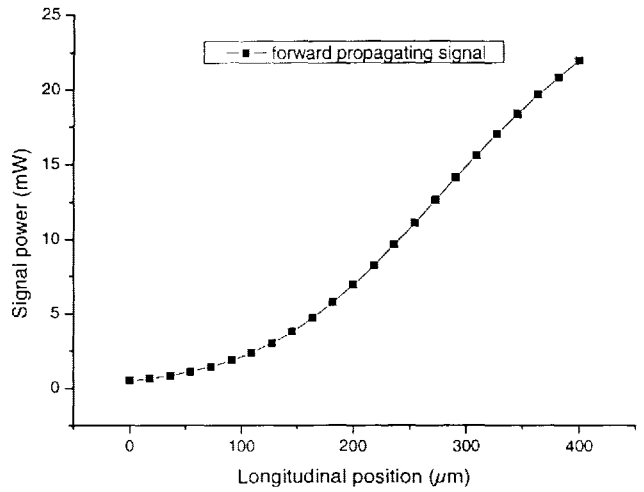

(b)

Figure 5.1.6 MQW SOA (a) carrier density, (b) forward propagating signal photon power spatial distributions with the input signal power is 1 mW (0 dBm). Signal wavelength is 1550.12 nm.

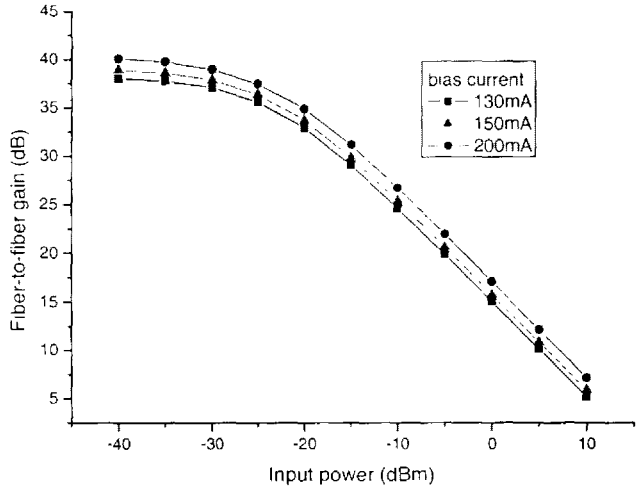

(a)

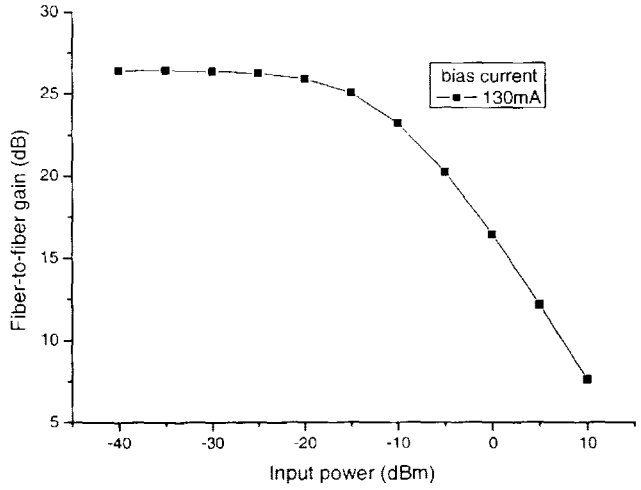

(b)

Figure 5.1.7 SOA fiber-to-fiber gain as a function of input signal power under a bias current of 130 mA. (a) Bulk SOA (b) MQW SOA.

In Fig.5.1.1 to 5.1.6, simulations are presented for the SOA under a variety of operating conditions. Three significant cases are performed to understand the properties of the amplifier, namely: (a) absence of input signal; b) regime of weak saturation ($P_{in,sig}$ =10 μW); (c) regime of strong saturation ($P_{in,sig}$ =1 mW). They show

the carrier density, ASE and signal photon power spatial distributions in the amplifier at these three input powers. At zero input powers, the carrier density profile has a symmetrical spatial distribution with the peak located at the center of device, and it is determined by the ASE photons that deplete the carriers at the input and output ends of the active waveguide. At low input power, the peak is tending to shift towards the input end, due to both signal and ASE photons can influence the carrier profile while they deplete the carriers increasingly in a way of proceeding to the amplifier end. At high input power, a strong saturation effect occurs. The carrier density spatial distribution becomes more asymmetrical, as shown in Fig.5.1.5a and Fig.5.1.6a, with the peak locating at the input facet. This is caused by the input signal power dominating over ASE power. Moreover, it can be observed that the Bulk SOA is more readily saturated than the MQW SOA, so it indicates that the later one has a higher saturation output power than the former. Fig. 5.1.7 compares the signal gain against input power at a signal wavelength 1550.12 nm for both bulk and MQW SOA at I =130 mA. When the input signal power exceeds a critical level, the output signal power becomes saturated and the fiber-to-fiber gain drops rapidly as the input power further increases.

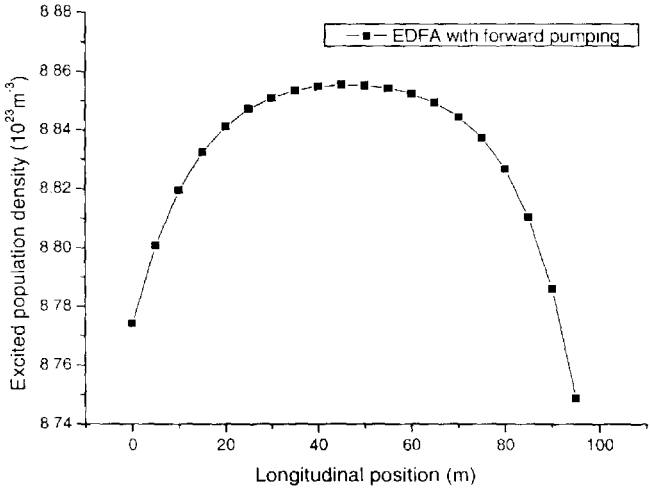

(a)

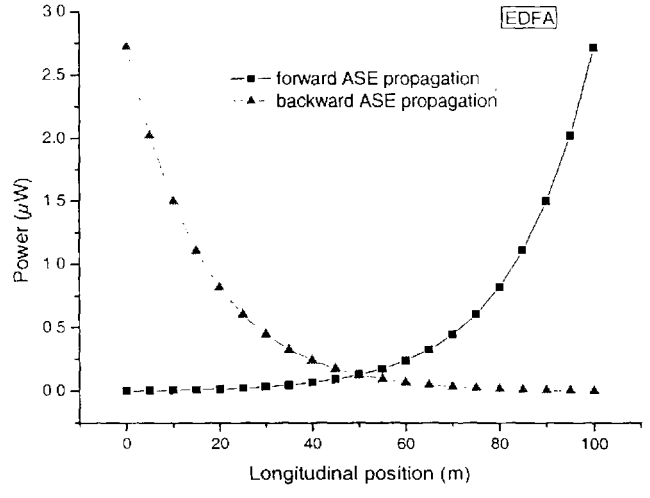

(b)

Figure 5.1.8 EDFA (a) poplulation density, (b) forward and backward propagating ASE photon power spatial distributions with zero input power.

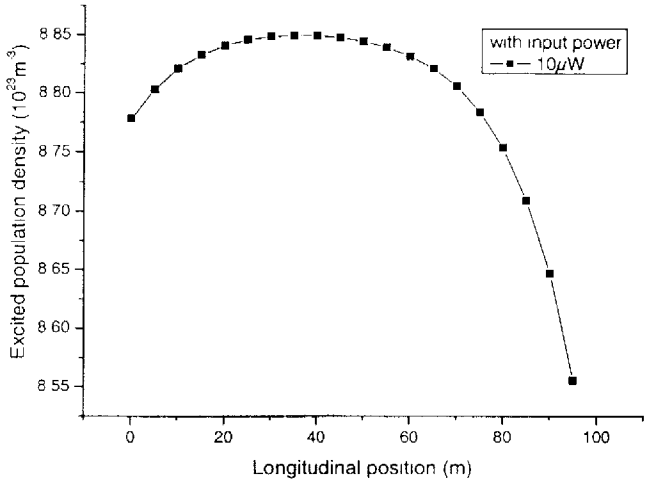

(a)

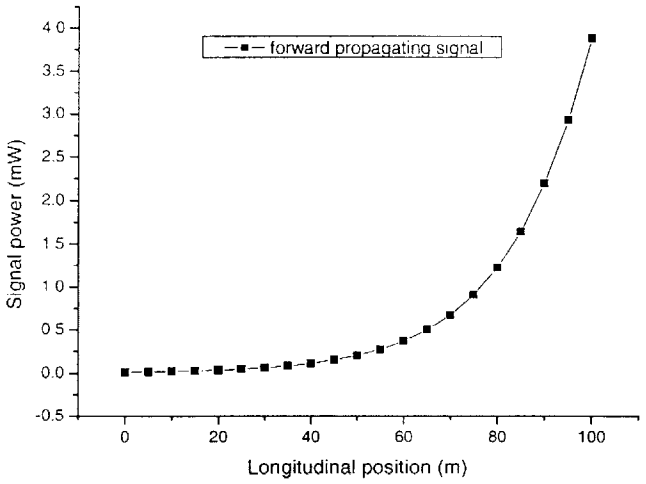

(b)

Figure 5.1.9 EDFA (a) population density, (b) forward propagating signal photon power spatial distributions with the input signal power is 10 μW (-20 dBm). Signal wavelength is 1550.12 nm.

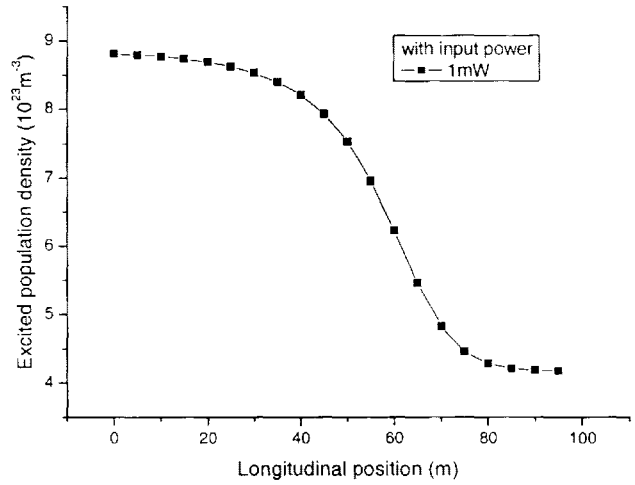

(a)

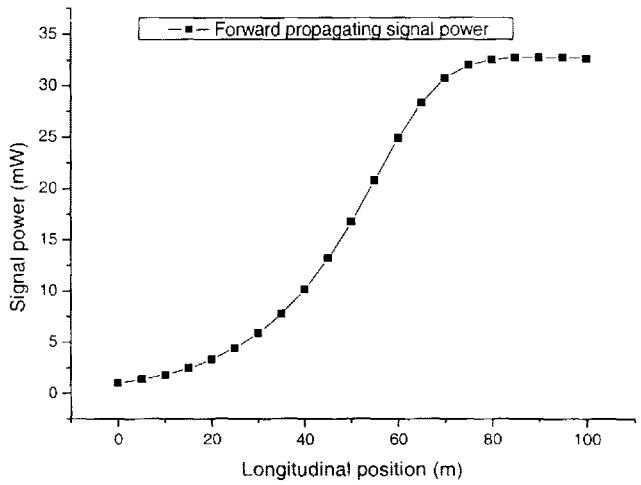

(b)

Figure 5.1.10 EDFA (a) population density, (b) forward propagating signal photon power spatial distributions with the input signal power is 1 mW (0 dBm). Signal wavelength is 1550.12 nm.

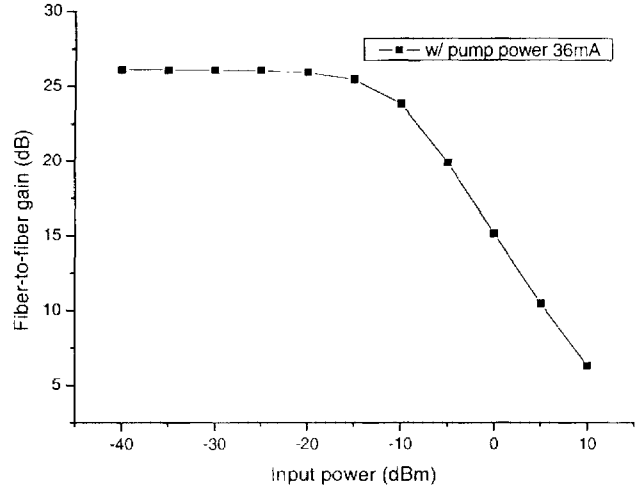

Figure 5.1.11 EDFA fiber-to-fiber gain versus input signal power under a forward pump power of 36 mW.

In Fig.5.1.8 to 5.1.11, the simulation results for the EDFA are shown as same as for the SOA in previous section. At zero input power, the population density profile has just a quite symmetrical spatial distribution due to the model utilizes a forward pumping scheme. An even symmetrical profile can be surely obtained by using dual pumping. Besides, the other results of EDFA with non-zero input power are also similar to that of SOA as well.

As far as this, a broadband SOA and EDFA steady state model and numerical solution has been described. The characteristics of optical amplifiers are investigated under a various operating conditions. In addition, steady-state simulations obtained the device material parameters used in the dynamic model.

5.2 Large signal dynamics results:

After having obtained the crucial parameters and results from the steady state model, we are able to simulate the dynamic model of optical amplifiers. In this section we consider a simple dynamic model for the optical amplifiers with digitally modulated inputs. A rectangular-wave input signal at wavelength 1550.12nm is adopted for a single channel simulation, to observe the transient characteristics of optical amplifiers.

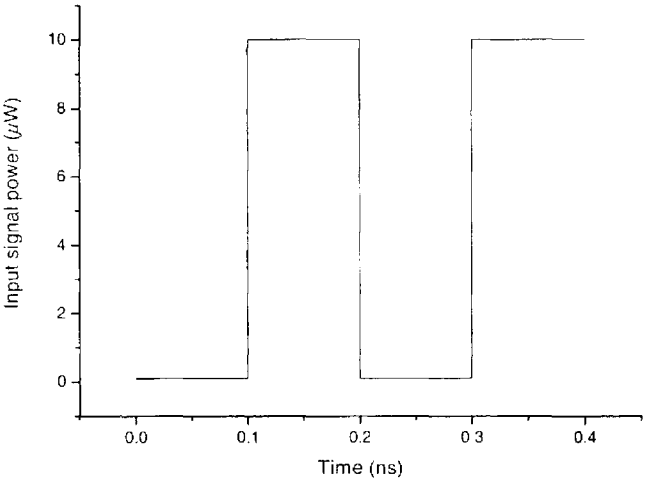

Figure 5.2.1 Four bits NRZ square-wave signal input at 10 Gbits/s with bit pattern 0101. Signal wavelength is 1550.12 nm. On and off states are 10μW and 0.1μW.

The effects of amplification by the SOA on an optical signal are shown in Fig. 5.2.2 and 5.2.3. It can be observed that signal distortion due to the gain saturation occurs in SOAs, although the multi quantum well SOA has less severely saturation than the bulk SOA. Generally speaking, gain saturation is induced by the reduction of carrier concentration from the depletion by signal and ASE noise photons. In mathematical point of view, equation (3.1.6) becomes negative, which implies that the carrier density is decreasing with respect to time all the way whenever the amplified signal and amplified spontaneous emission (ASE) term exists. In Fig. 5.2.2a, at the

leading edge of each pulse, carriers are beginning to emit photons correlated to input signal photons, so the population inversion is beginning to be reduced. As such leading part has already depleted large amount of carriers, the part followed by it could not acquire the same high gain. Therefore the pulse would be experienced a likely exponentially decay in bulk SOA and a slowly decay in MQW SOA as shown in Fig. 5.2.3. To see the signal outputs with ASE noise, there are random fluctuations on power caused by the ASE noise, which gives rise to further signal impairment. In cascaded amplifier system, the ASE accumulates over many amplifiers and makes the system performance severely degraded. In Fig.5.2.9, it can be observed that the random fluctuation becomes smaller as the input power increases. The reason is that a large amount of carriers are depleted by the high input power for amplification, it leaves only small portion of carriers for spontaneous emission. Therefore, in any situation the amount of ASE noise can be limited to the minimum when the optical amplifier operates under saturated condition. Thus the effect of ASE is negligible when the gain is small enough, or when the input powers are sufficiently high as it is commonly the case in WDM systems [18].

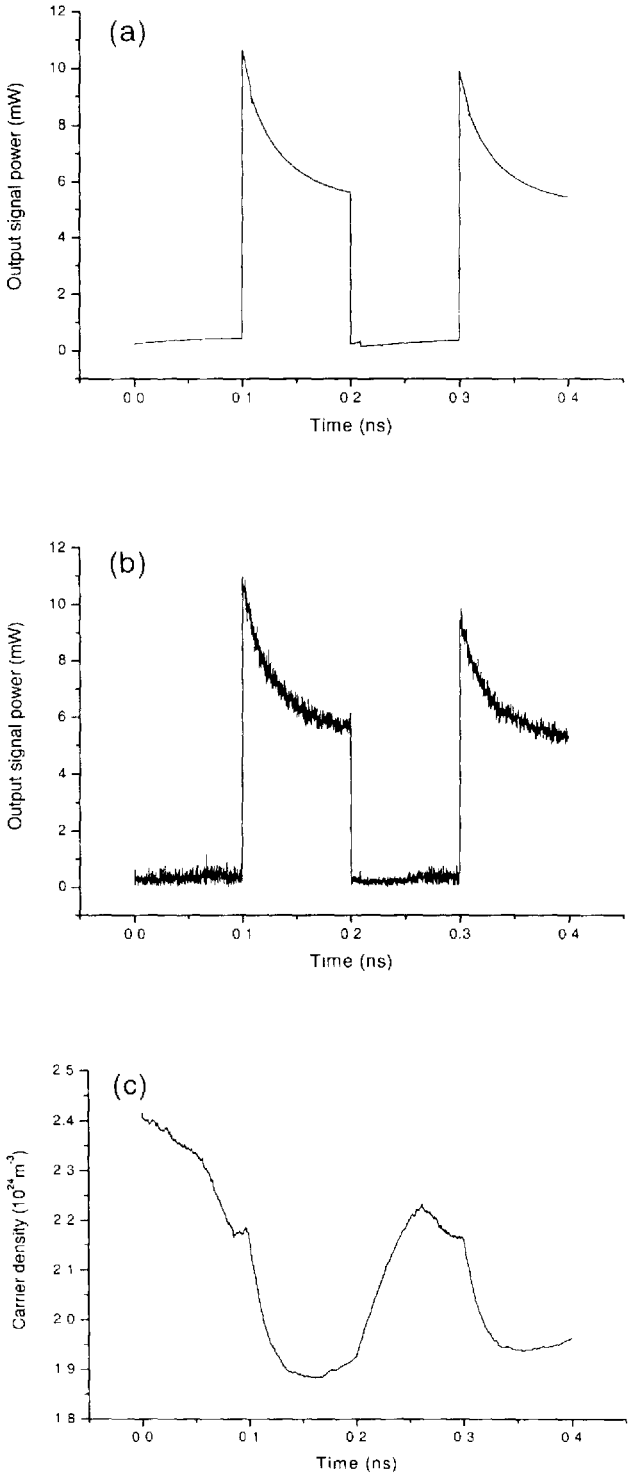

Figure 5.2.2 Dynamics output from Bulk SOA (a) signal without random ASE noise (b) signal with random ASE noise (c) dynamics of carriers under amplification according to (b).

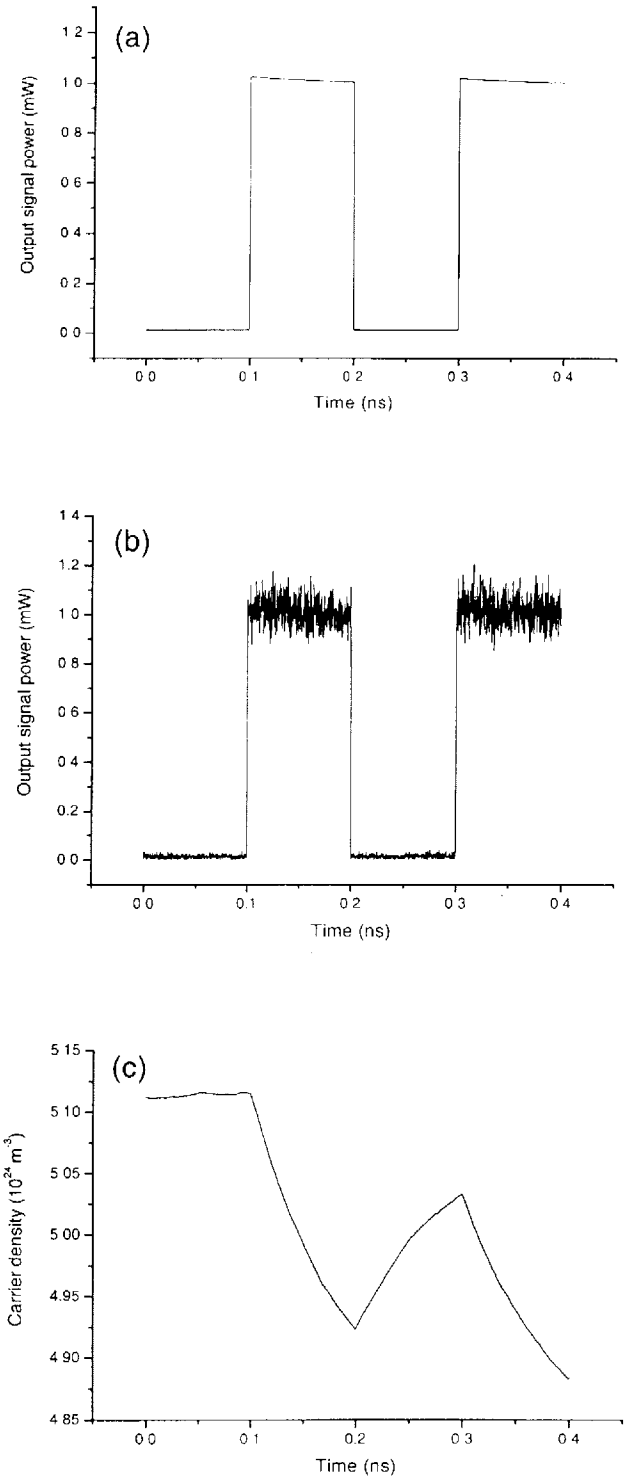

Figure 5.2.3 Dynamics output from MQW SOA (a) signal without random ASE noise (b) signal with random ASE noise (c) dynamics of carriers under amplification according to (b).

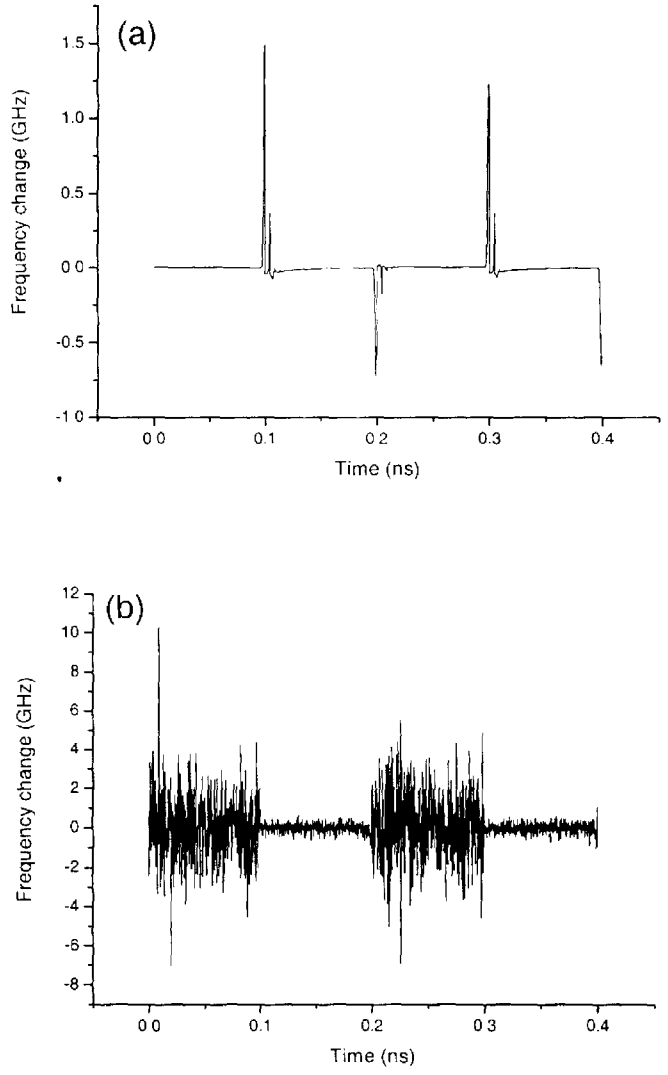

Figure 5.2.4 Frequency chirping from Bulk SOA (a) without random phase noise and (b) with random phase noise.

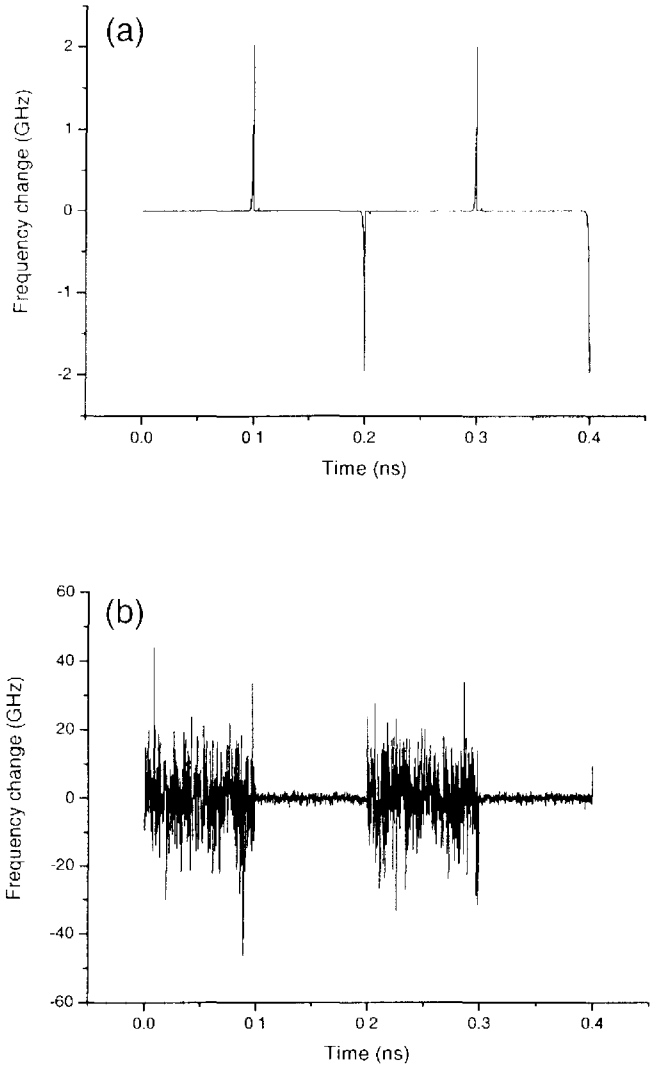

Figure 5.2.5 Frequency chirping from MQW SOA (a) without random phase noise and (b) with random phase noise.

Fig.5.2.4 and 5.2.5 show the frequency chirp imposed on the output signal pulse for Bulk SOA and MQW SOA. The chirp will become larger as the input power increases, while the signal is largely distorted due to gain saturation [27]. Without considering the phase fluctuation induced by ASE, the output pulse undergoes positive chirp during the rising edge and negative chirp during the falling edge. Then, the signals have positive chirping which cause pulse broadening when it is transmitted

through the fiber. But when the ASE noise induces the random fluctuation on the frequency, it is not obviously to see the chirps; we only can distinguish the portion contaminated with more noise as OFF state, likewise with less noise as ON state. It is because the phase fluctuation is inversely proportional to the photon power.

There is no doubt that gain saturation would be more severe as the signal power increasing. In addition, the modulation frequency is another factor to influence the gain saturation effect. At the signal bit rate 10 Gbs/s, the modulation period is at least 0.1ns, which is smaller than the carrier lifetime of SOAs [2]. In this case the carrier density has not enough time to be fully recovered by the continuous bias current between signal transitions (in Fig.5.2.2c), so giving rise to pattern effects by gain saturation. As shown in Fig.5.2.2b, the following pulse has a smaller initial gain than the previous one. This is in contrast to EDFA, since an erbium ions has a extremely long lifetime (of the order of ms), so the gain dynamics are a slow process which prohibit the excited population density keeping pace with changes in the signal as shown in Fig.5.2.6. Thus there is negligible gain saturation or pattern effects in EDFAs for modulation frequency well above the population density response. Most importantly, this slow response reduces the effects of saturation-induced crosstalk and intermodulation distortion associated with multichannel signal amplification in high-speed WDM systems.

Moreover, in Fig. 5.2.8, the eye diagrams of the output after single amplifier are shown. Though all of the three cases are showing clear open eyes in a single amplifier stage, we can still observe that EDFA can provide a better noise performance than SOAs as its eye is a little bit wider.

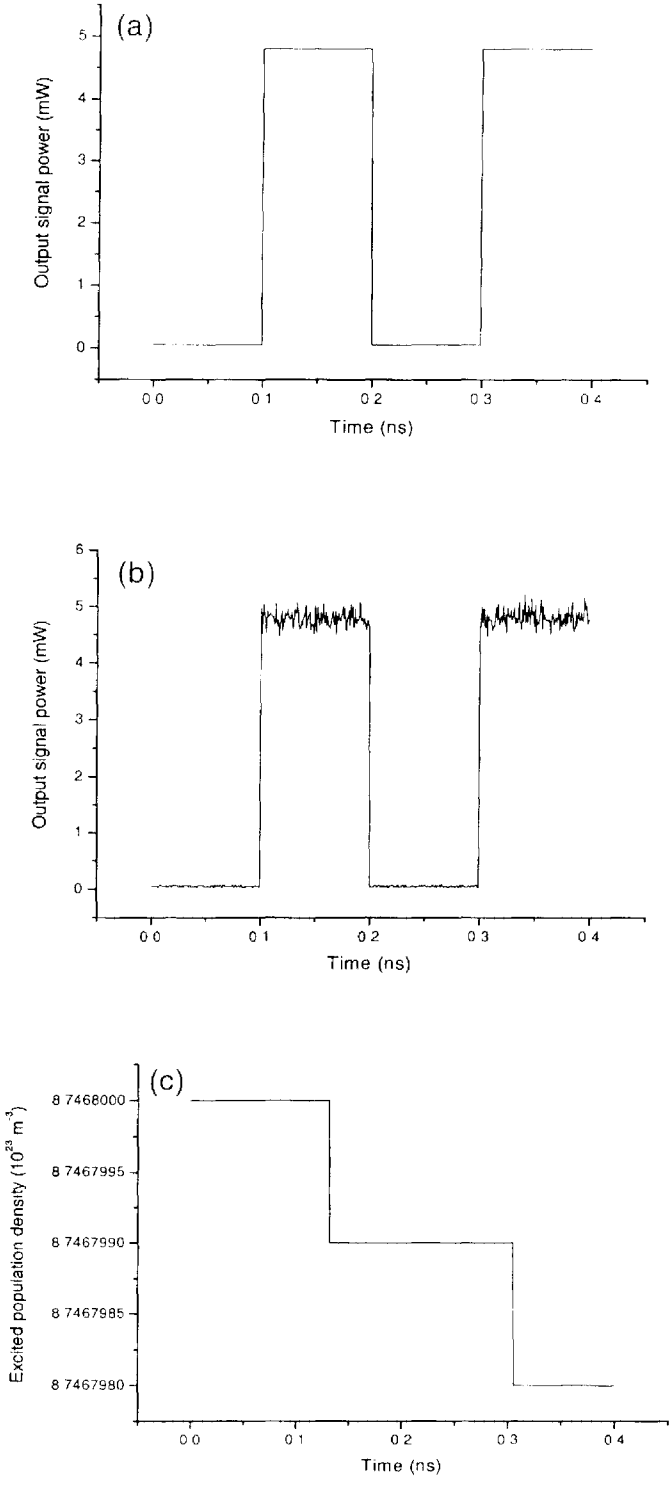

Figure 5.2.6 Dynamics output from EDFA (a) signal without random ASE noise (b) signal with random ASE noise (c) dynamics of population under amplification according to (b).

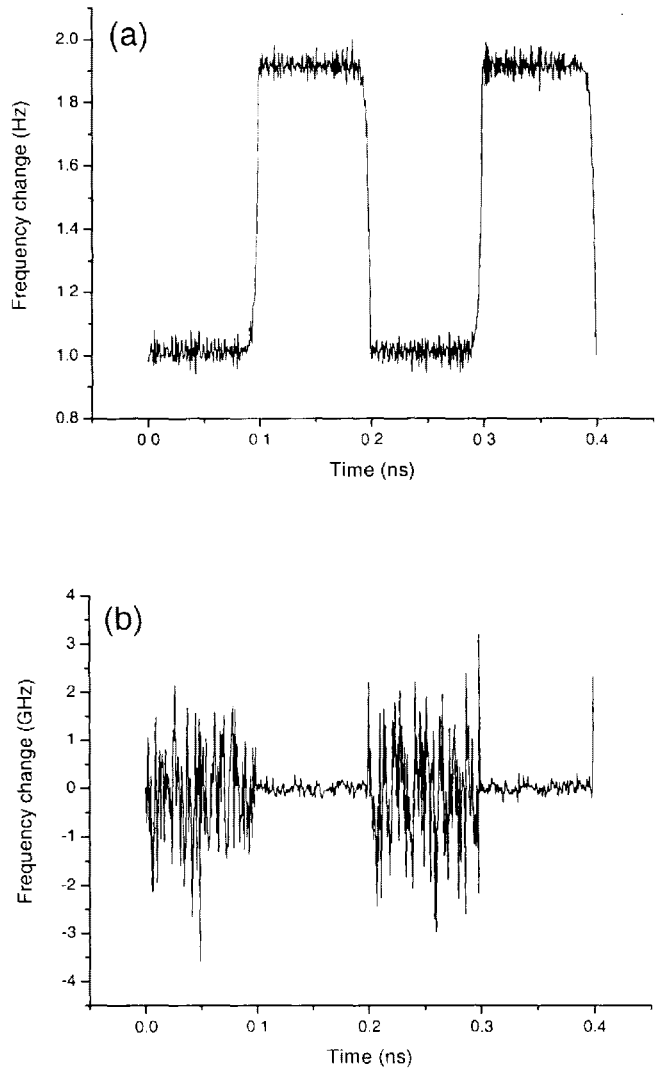

Figure 5.2.7 Frequency chirping from EDFA (a) without random phase noise and (b) with random phase noise.

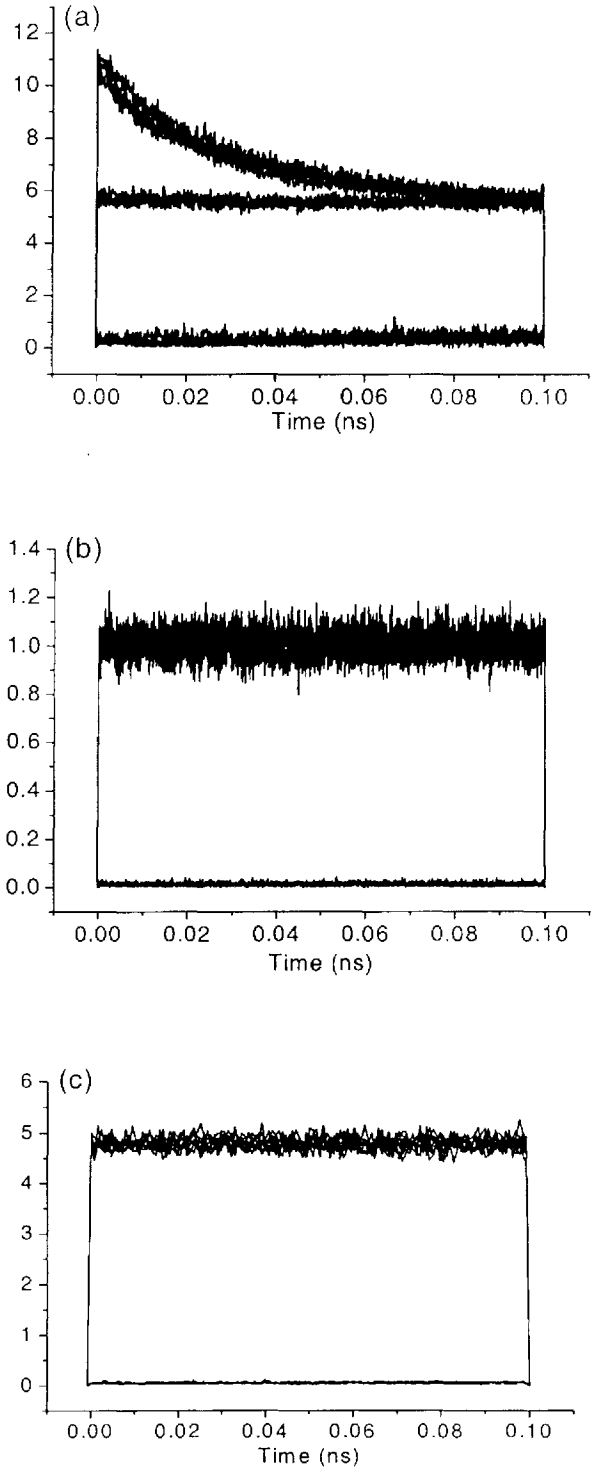

Figure 5.2.8 The one-bit eye diagrams at the output of the single optical amplifier a) Bulk SOA b) MQW SOA c) EDFA.

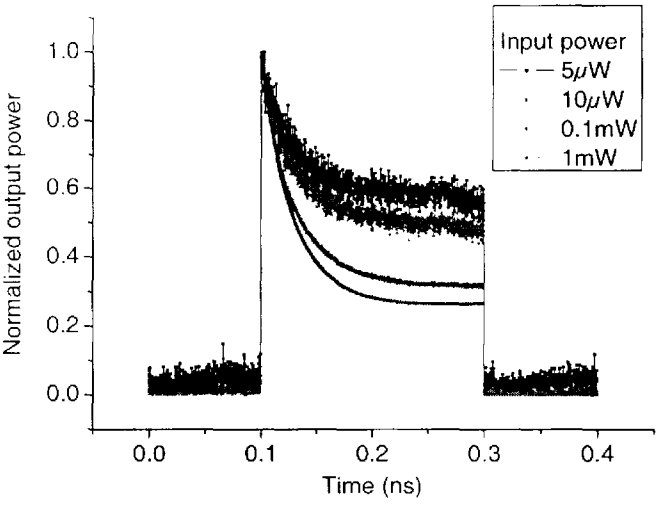

Figure 5.2.9 Gain saturation and ASE noise effects depend on various input signal powers in Bulk SOA . The random fluctuation of amplitude becomes smaller as the input power increases.

5.3 WDM channels dynamics results:

An advantage of optical amplifiers is that they can be used to amplify several communication channels simultaneously as long as the bandwidth of the multichannel signal is smaller than the amplifier bandwidth [5]. The bandwidths of both SOAs and EDFAs are broad enough to be used for multichannel amplification. Multiple channels sharing the limited pool of photons for amplification in an optical amplifier leads to gain saturation. As the input power increases, the carriers or ions are depleted from the active region, resulting in a reduction of the gain. Therefore, the actual gain seen by a particular channel depends on the power level as well as total number of other coexisting channels at the amplifier. In this section, the cross gain saturation effect can be studied through the transient power variation results in a case of two-channel amplification.

In Fig. 5.3.1, one laser, operating continuous wave at λ_1= 1555.12 nm, is used as a surviving channel, and the other laser, emitting at λ_2= 1550.12 nm, is used as an added input channel. As can be seen for Bulk and MQW SOAs from Fig. 5.3.2-5.3.3, the surviving channel experiences an output power excursion once the added channel is switched on. The gain of the surviving channel decreases with the characteristic time equal to that of the saturating signal overshoot in the added channel. It is because the gain of the surviving channel is saturated not only by its power but also by the total input power from all channels to the amplifier. As well as, the output power of surviving channel also need some more time to reach back its initial value after the added channel is switched off. However, the same phenomenon cannot be seen from the results of EDFA, it is due to its very slow gain response time. The dynamics of EDFA is generally considered to be slow as a result of the long spontaneous lifetime of around 10ms, which is much longer compared to that of SOA. For transmission of

high-speed data, the gain of EDFA is undisturbed by the signal modulation, and EDFA does not introduce saturation induced crosstalk among channels in WDM systems.

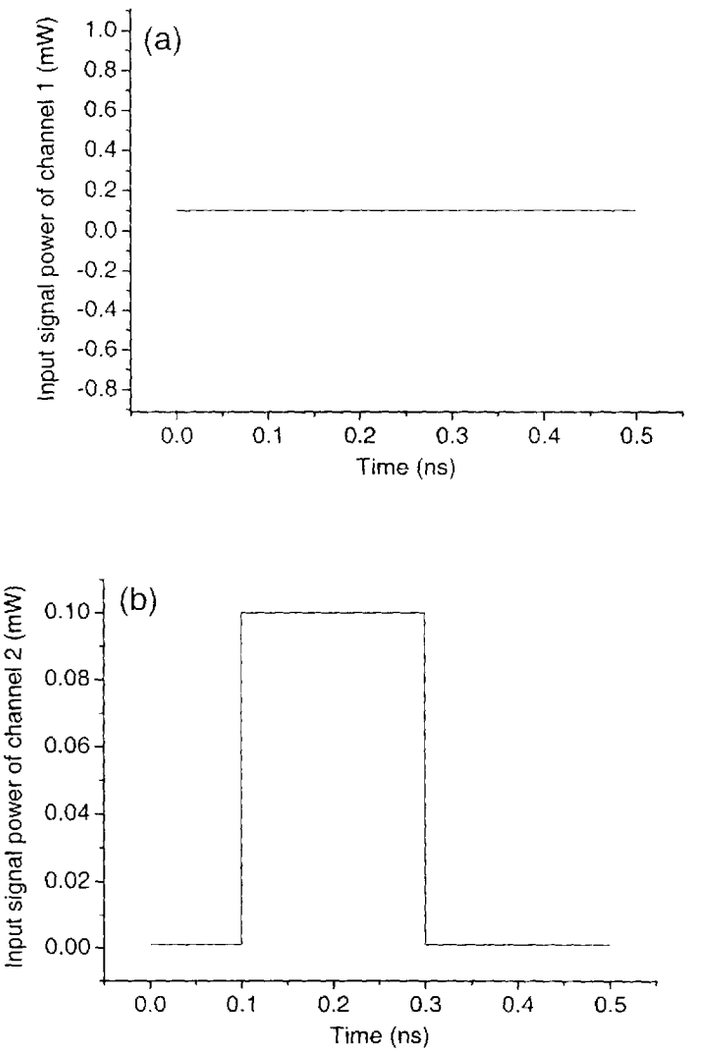

Figure 5.3.1 The input signals of two channels a) a constant input power (0.1mW) of channel 1, b) suddenly switched on power of channel 2.

Therefore, this property makes EDFAs suitable for WDM lightwave systems [5]. In contrary, the noise behavior, cross gain modulation and cross gain saturation restrain the use of SOAs in WDM systems.

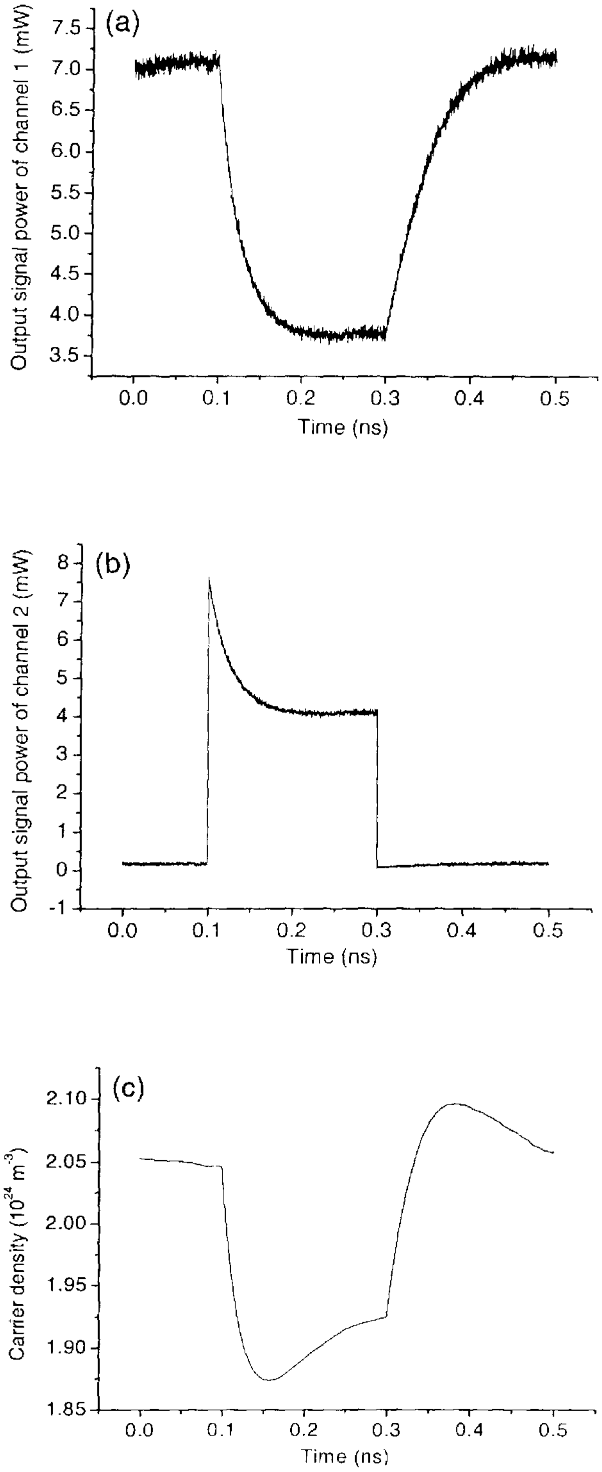

Figure 5.3.2 Transient output power variations in a two-channel Bulk SOA a) & b) output signal powers of channel 1 and 2. c) carrier dynamics changes with input signals.

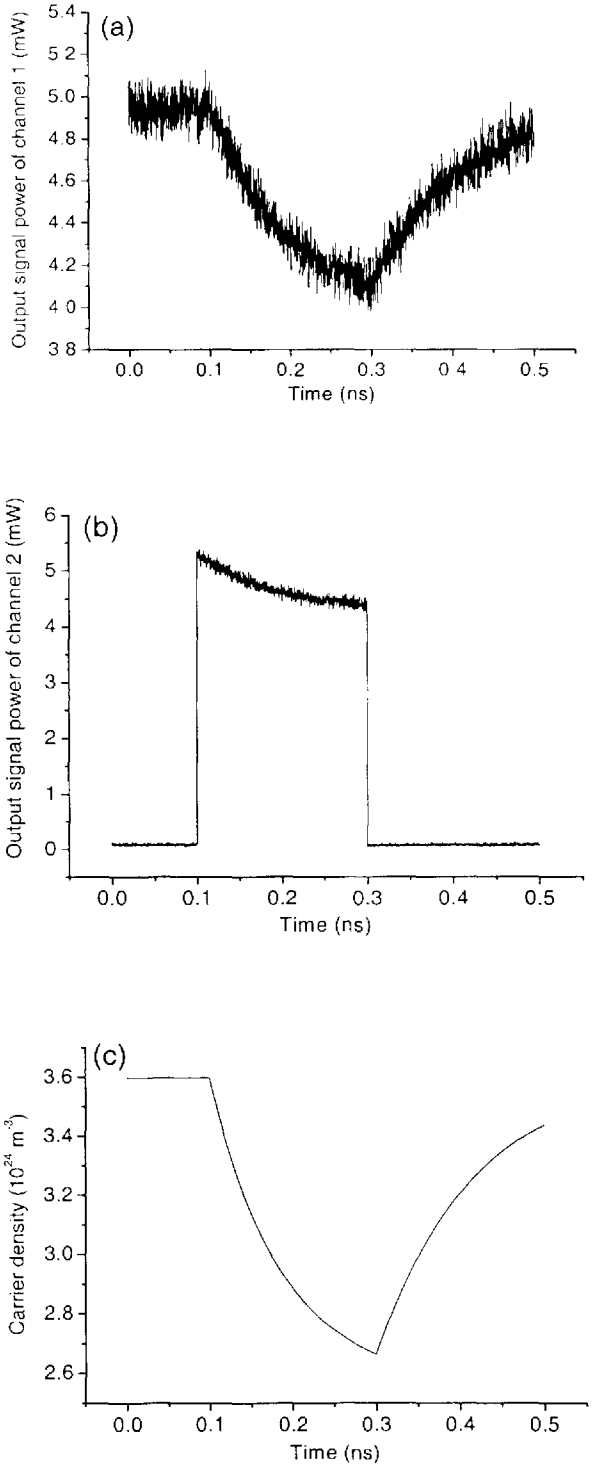

Figure 5.3.3 Transient output power variations in a two-channel MQW SOA a) & b) output signal powers of channel 1 and 2. c) carrier dynamics changes with input signals.

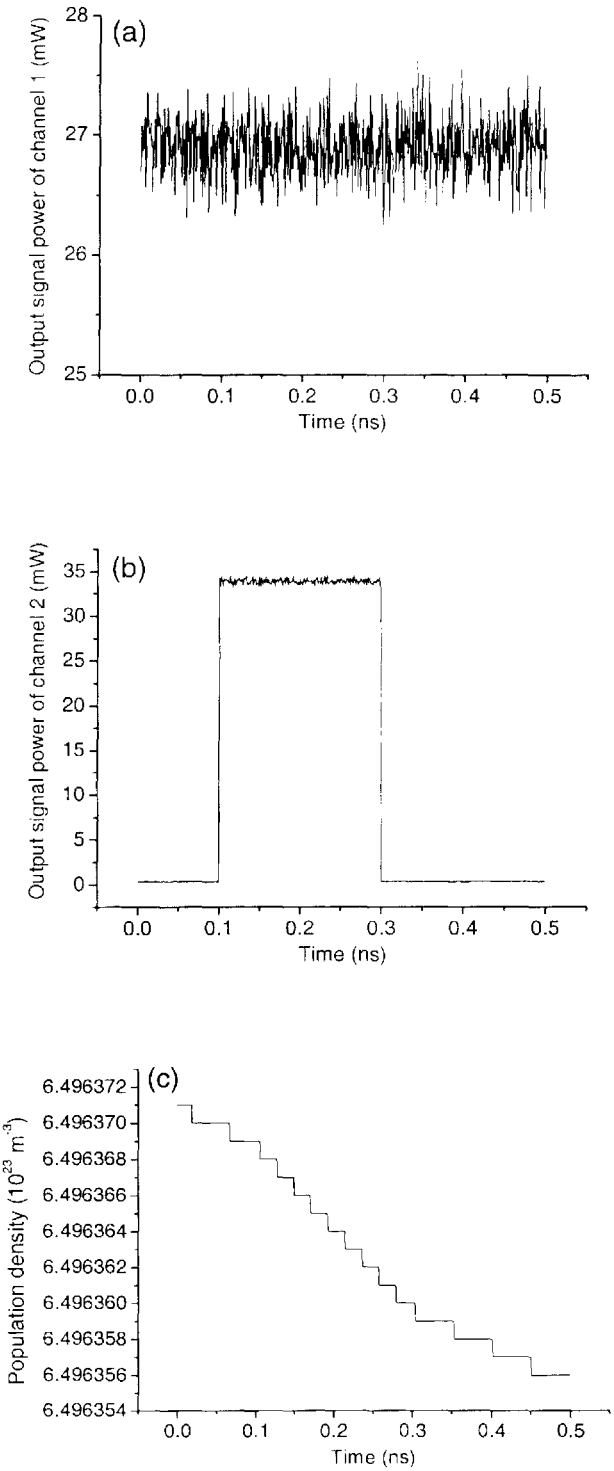

Figure 5.3.4 Transient output power variations in a two-channel EDFA
a) & b) output signal powers of channel 1 and 2. c) excited population dynamics changes with input signals.

5.4 Noise Power Spectrum

The expression of the slowly varying output complex field is $E_{out}(t) = \sqrt{P_{out}(t)}e^{j\Delta\phi_{out}(t)}$. After performing the Fourier transform on the time domain output signal by using fast Fourier transform (FFT) function, the noise characteristics in frequency domain can be obtained. The results for both of SOAs and EDFA are shown below.

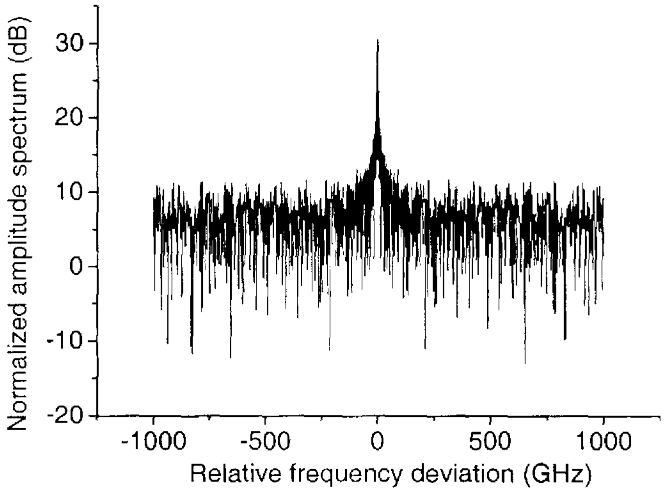

Figure 5.4.1: The normalized amplitude spectrum of the ASE noise in Bulk SOA.

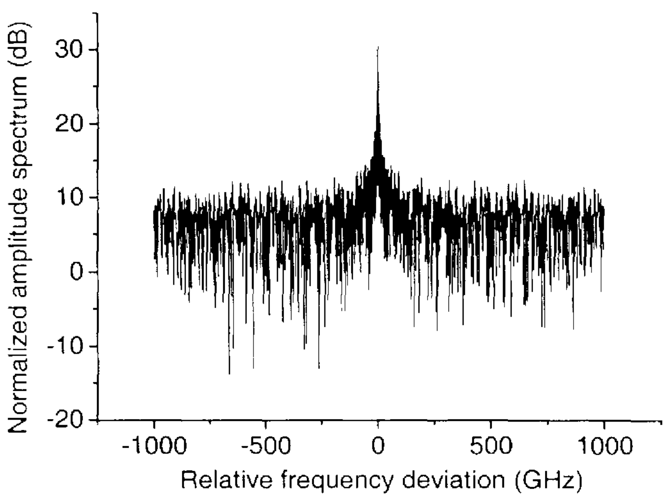

Figure 5.4.2: The normalized amplitude spectrum of the ASE noise in MQW SOA.

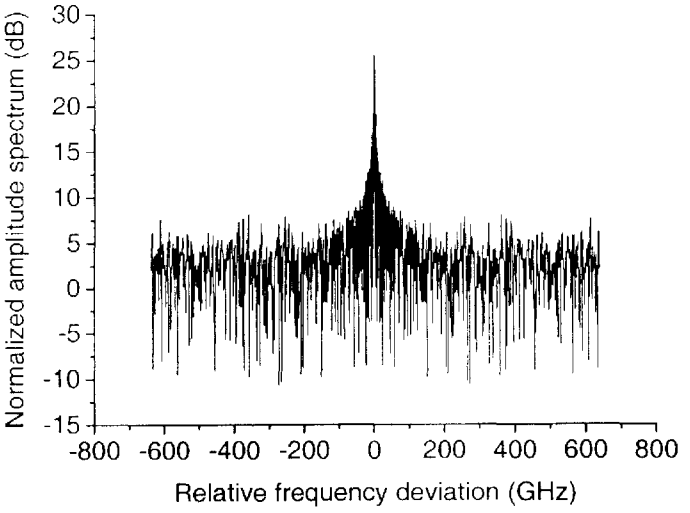

Figure 5.4.3: The normalized amplitude spectrum of the ASE noise in EDFA.

Chapter 6
Transmission Link Simulations

Our major task is to set up a simulation platform for investigating the performance of a typical single and multichannel fiber-optic transmission system. As all of the other individual optical component solvers are connected together, we are able to demonstrate the performance simulation of the entire fiber-optic transmission link. By making use of this, we are also able to examine the characteristics of different applications of optical amplifiers and the ASE noise effects in a cascaded amplifier system. As a representative simulation model for long-haul transmission links, we used the flow diagram depicted in Fig. 6.1 to illustrate the system simulation scheme. The system configuration can be adjusted freely as desired for flexibility.

The RCG was modeled as M independent signal generators that were multiplexed before launching into the link. We adopted a 32 pseudorandom bit sequence modulation format to limit the simulation time and memory requirements. An external or internal modulation scheme can be chosen to use at the transmitter. For external modulation, the continuous lightwave with constant intensity from a laser is modulated by an Electroabsorption (EA) or Mach-Zehnder (MZ) modulator. After that, we can select from which configuration composing of fiber, EDFA, or SOA, in order to examine the performance of different system schemes. After the lightwave signal is amplified by a power booster to boost the transmitted optical power, the optical pulses are transmitted through standard single mode fiber. The attenuation of

optical signal level due to the fiber loss could be restored by a number of in-line amplifiers. At the receiver, a preamplifier amplifies the received optical signal and a pin photodiode is used for optical signal detection and convert the signal back to an electrical pulse. The electrical signal resulting from the photodetector is amplified, and then sampled and compared with a threshold using a decision circuit to recover the transmitted digital signal. Finally, an eye-diagram can be used to evaluate the performance of the communication channel.

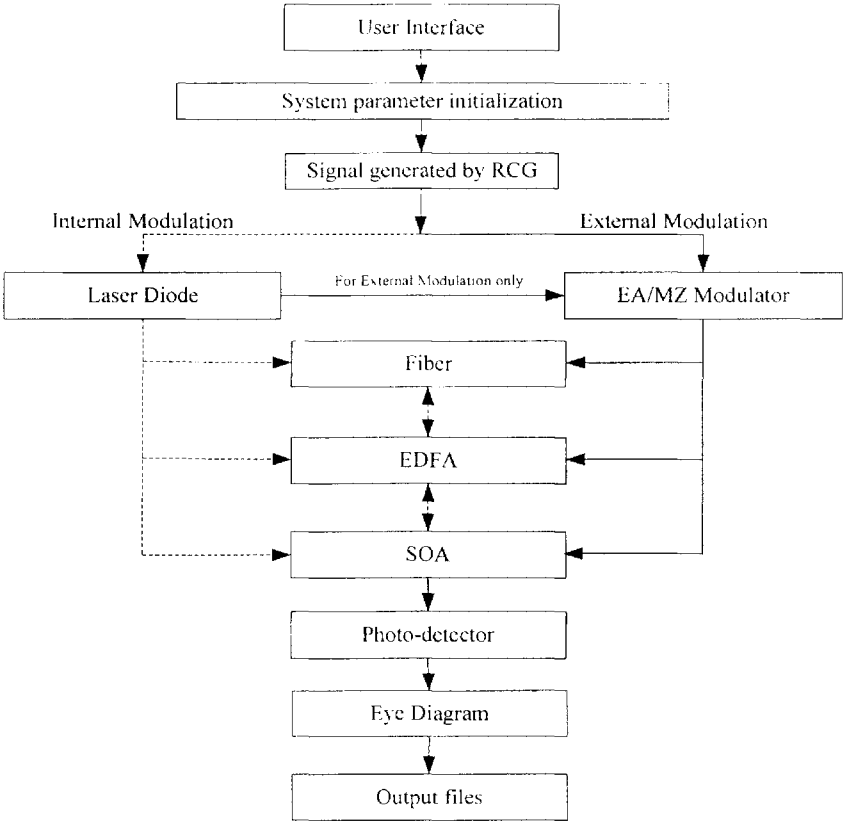

Figure 6.1 Flow diagram of the system simulation scheme

6.1 Single-channel system simulation

In this section, all types of the previous mentioned amplifier applications were discussed based on single channel transmission systems.

6.1.1 Case 1: Power Boost amplifier

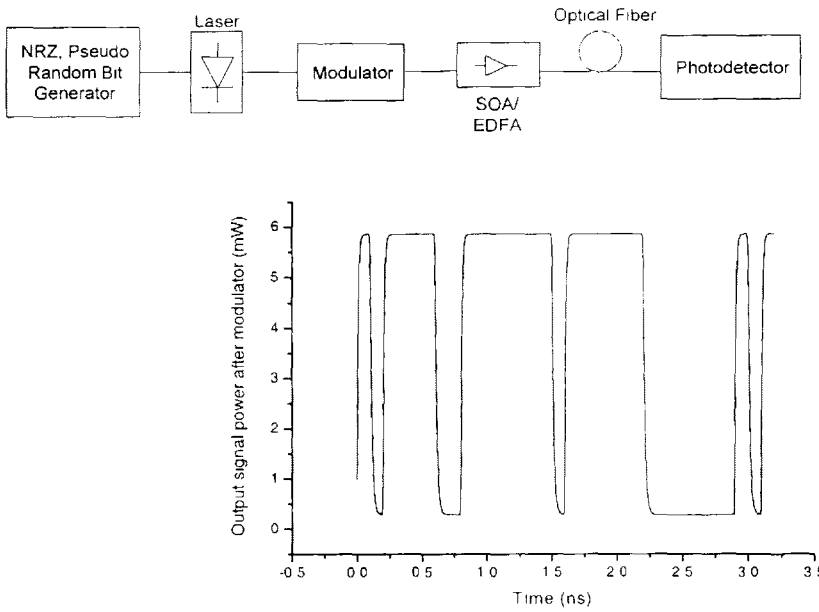

Figure 6.1.1 Input signal power of the power booster from modulator.

A power boost amplifier is used to launch high power signals, to extend the transmission distance, or to increase the link power budget. Because there is little or no loss between the transmitter and the power amplifier, the amplifier usually operates in deep saturation as shown in Fig. 6.1.2a and 6.1.3a. As can be seen from Fig. 6.1.2a, it is important to note that the signal transmitted after the bulk SOA is severely distorted and it even misread the original bit "0" as bit "1". Therefore in our case, the bulk SOA is not suitable to be used as power booster in our transmission system. Typical gain compression for power amplifiers is between 20 and 40dB [29]. At these levels of saturation, the ASE noise output is reduced and the optical SNR at the output

of the amplifier is extremely high. Thus, the noise figure is not an important design parameter for power amplifiers. On the other hand, the most important parameter for power amplifiers is maximum saturated output power. If this is high enough, the pattern effects due to gain saturation can be reduced. Fig.6.1.3 and 6.1.5 show the vertical closure of the eye is mainly due to the signal distortion by gain saturation when using SOA. In contrast to the case of using SOA, the eye pattern for using EDFA in Fig. 6.1.7 shows a clear open eye, as the gain does not respond to the signal modulation in EDFA due to its slow gain response time.

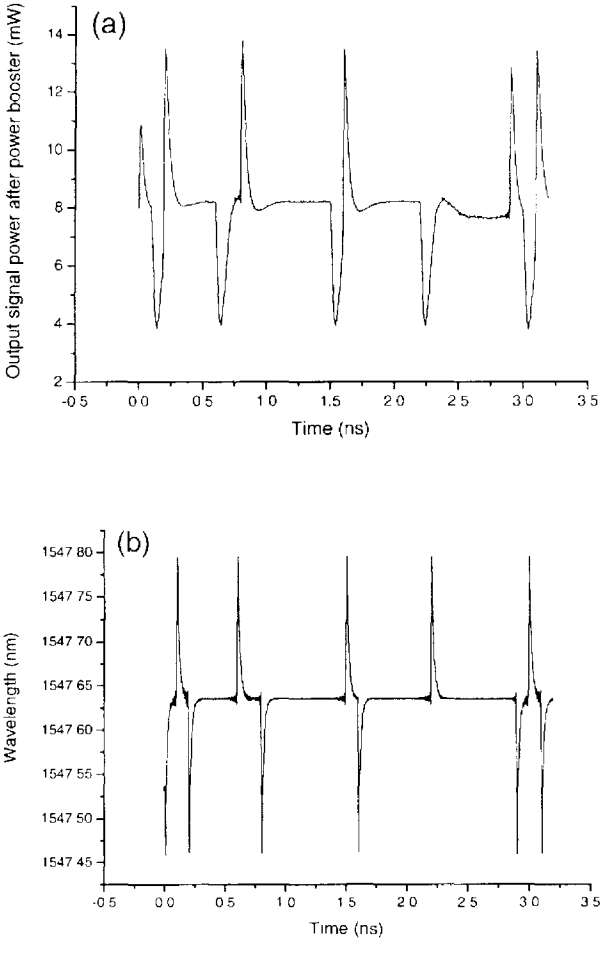

*Figure 6.1.2 Output results after the **Bulk SOA** power booster a) output signal power , b) dynamic wavelength changes due to chirp.*

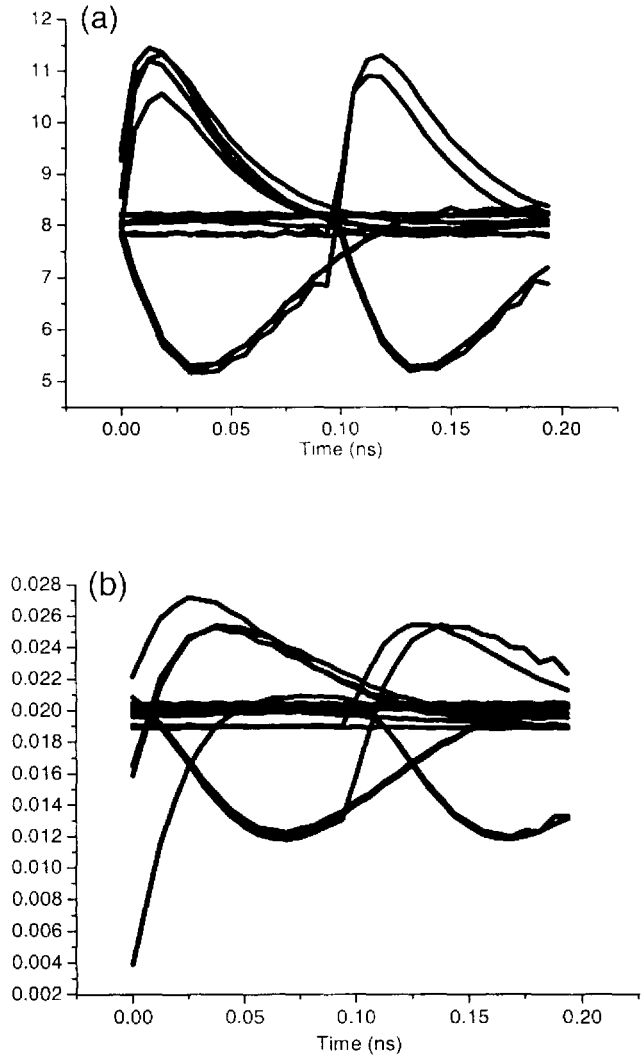

Figure 6.1.3 Eye diagrams of the output a) right after the ***Bulk SOA*** *power booster amplifier , b) at the receiver after low pass filter.*

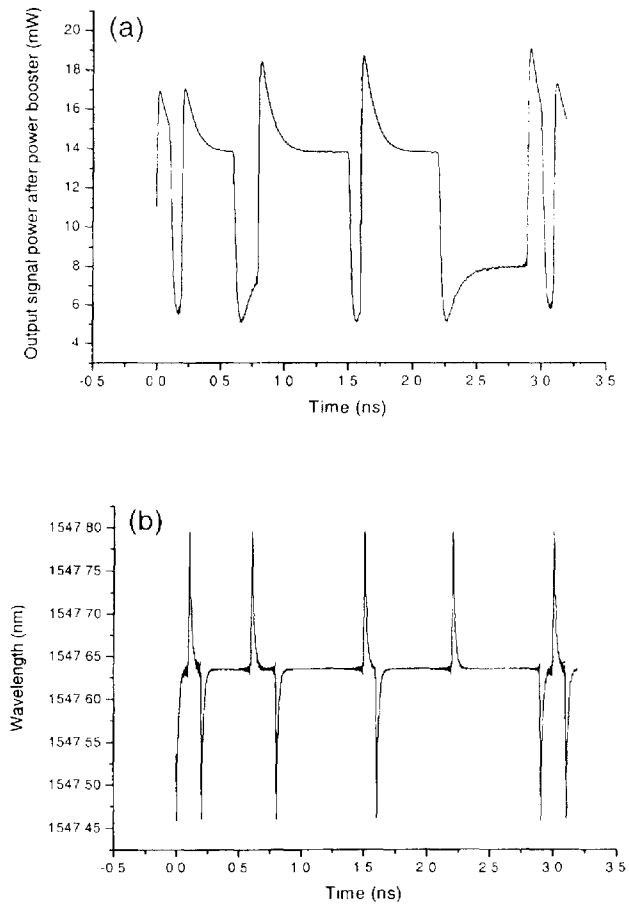

*Figure 6.1.4 Output results after the **MQW SOA** power booster a) output signal power , b) dynamic wavelength changes due to chirp.*

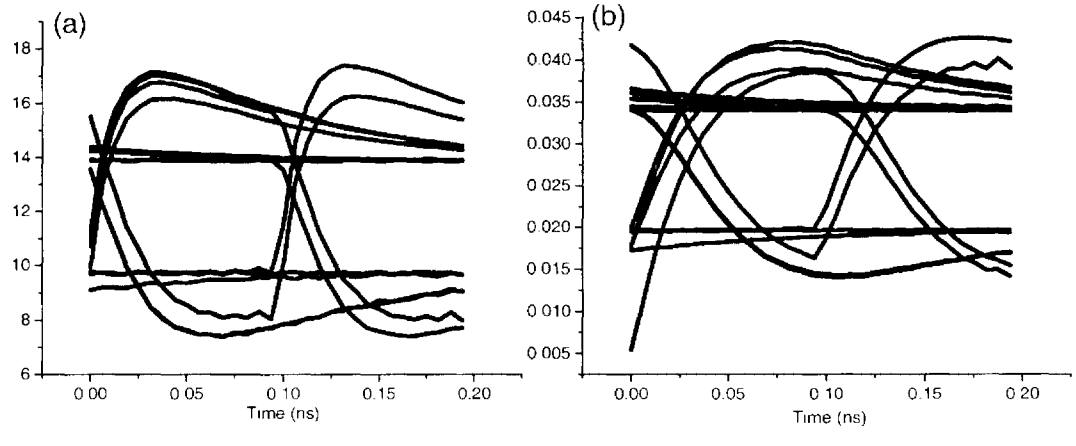

*Figure 6.1.5 Eye diagrams of the output a) right after the **MQW SOA** power booster amplifier, b) at the receiver after low pass filter.*

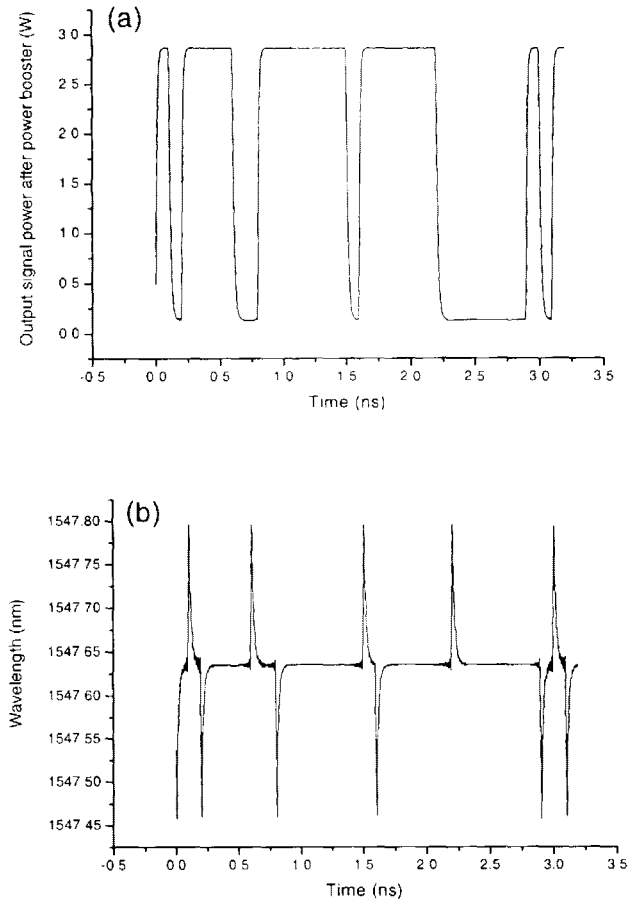

Figure 6.1.6 Output results after the ***EDFA*** *power booster a) output signal power , b) dynamic wavelength changes due to chirp.*

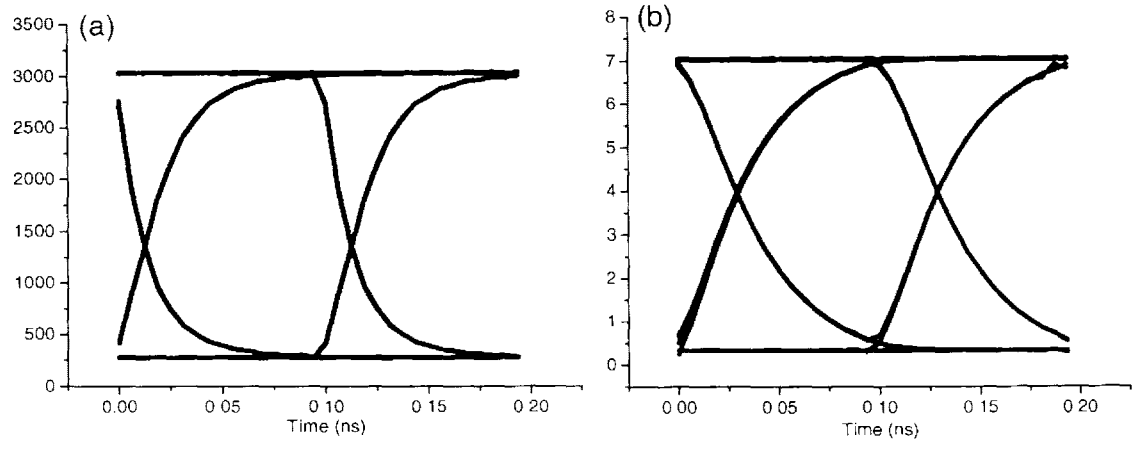

Figure 6.1.7 Eye diagrams of the output a) right after the ***EDFA*** *power booster amplifier, b) at the receiver after low pass filter.*

6.1.2 Case 2: In-line Amplifiers

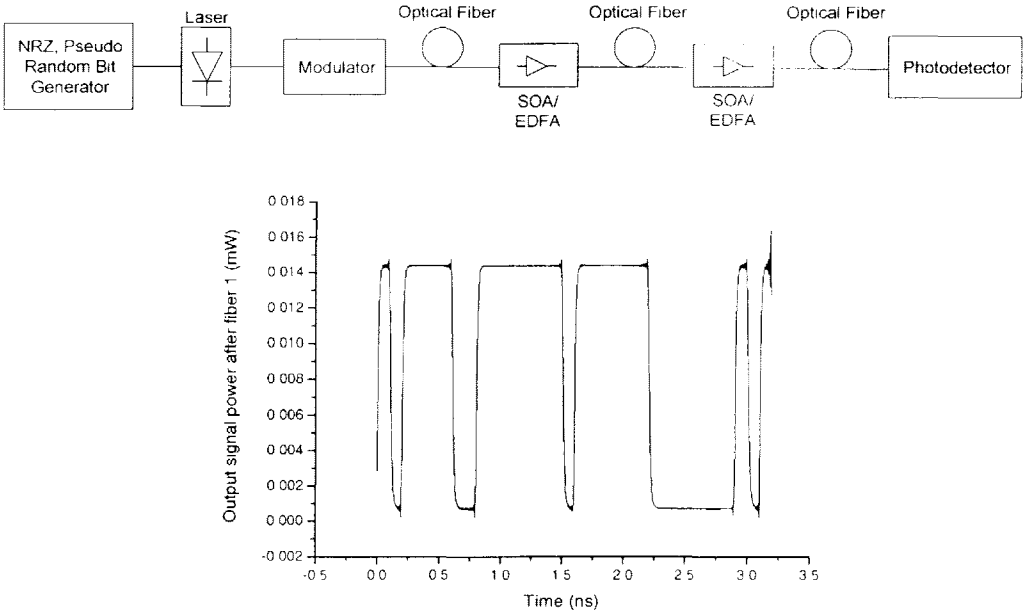

Figure 6.1.8 Input signal power of the inline amplifier from the first optical fiber.

Secondly, we consider two cascaded in-line amplifiers used as repeaters to boost the signal power. Because in-line amplifiers are used to extend the transmission distance, high output power is required. However, the signals entering in-line amplifiers are weak, so that noise added by each in-line amplifier is important. Fig. 6.1.9, 6.1.11 and 6.1.13 show clearly that the transmitted signal is contaminated by the accumulated ASE noise in a cascaded in-line amplifiers system for both SOAs and EDFAs. Therefore, a low noise figure and high gain both are also required. At this time, the degraded eye diagrams in Fig. 6.1.10, 6.1.12 and 6.1.14 show that the partial closing of eye is caused by both of the accumulated ASE noise and gain saturation effect. However, the EDFA not only have a higher gain and is immune to gain saturation, but also it does give a better noise performance compared to the SOA. Since in-line amplifiers must be designed with high gain, high output power, and a low noise figure, all realized for a wide dynamic range of input signals. However, it is

difficult to optimize all these three parameters simultaneously. For example, high gain is reached by using a long device length. In contrast, the best noise figure is obtained by maintaining a high inversion at the input and is usually achieved with short device length [29]. One of the solutions is to use multistage designs in which the first stage is designed to function as an efficient preamplifier and the succeeding stages as a power booster.

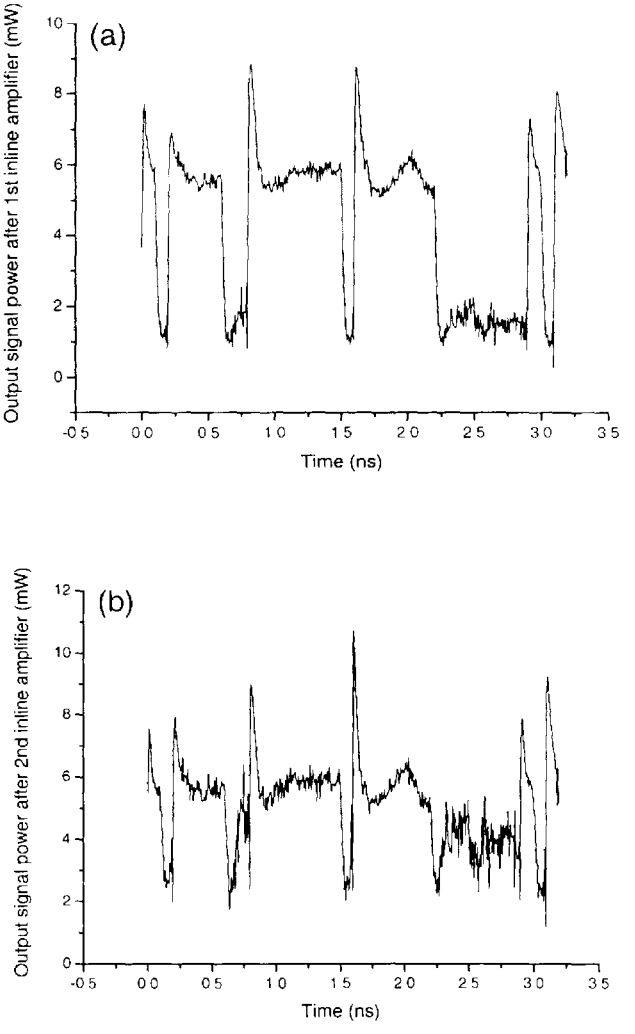

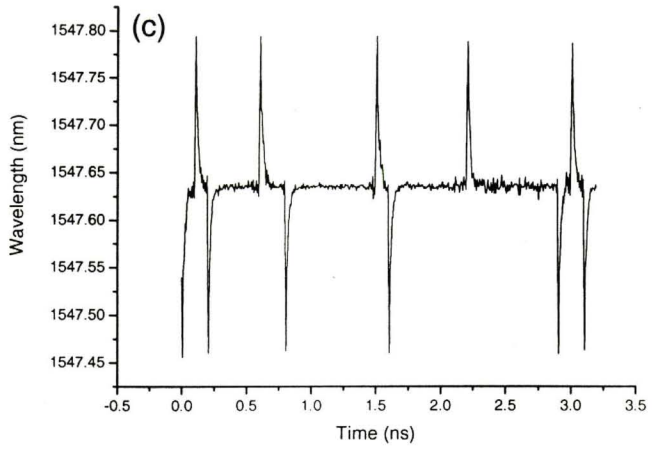

Figure 6.1.9 Output results for the in-line ***Bulk SOAs*** *a) output signal power after the 1st in-line , b) output signal power after the 2nd in-line , c) dynamic wavelength changes due to chirp.*

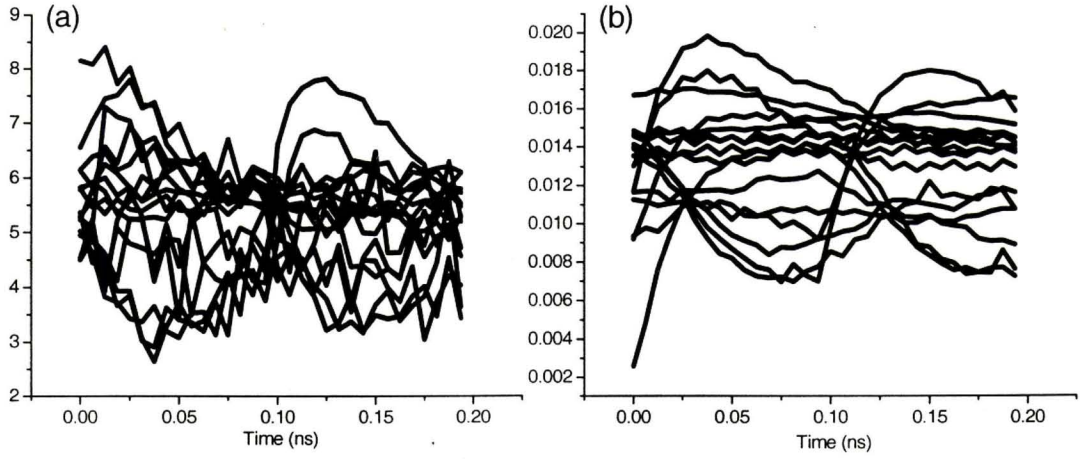

Figure 6.1.10 Eye diagrams of the output a) right after the ***Bulk SOA*** *2nd in-line amplifier, b) at the receiver after low pass filter.*

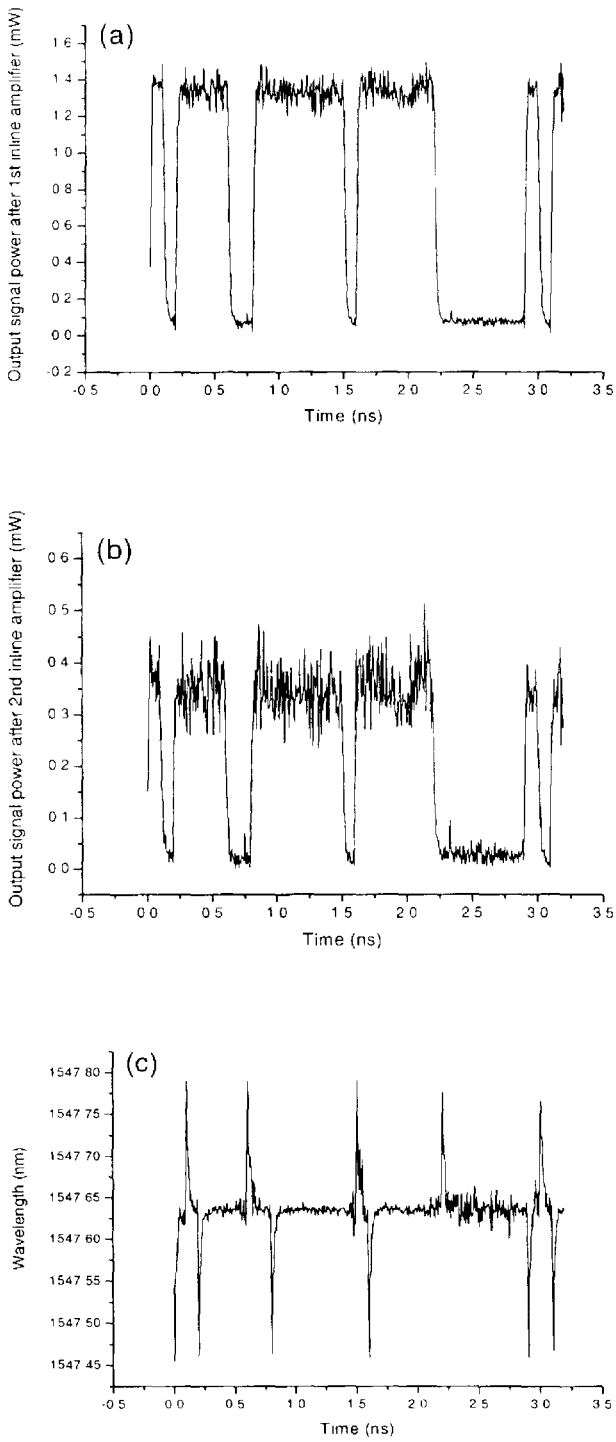

Figure 6.1.11 Output results for the ***in-line MQW SOAs*** *a) output signal power after the 1st in-line , b) output signal power after the 2nd in-line , c) dynamic wavelength changes due to chirp.*

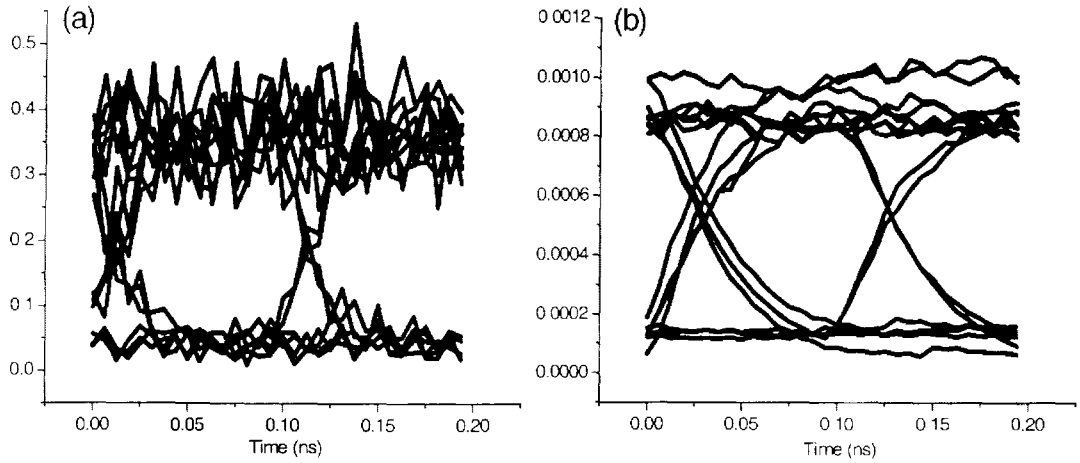

Figure 6.1.12 Eye diagrams of the output a) right after the ***MQW SOA 2nd in-line amplifier,*** *b) at the receiver after low pass filter.*

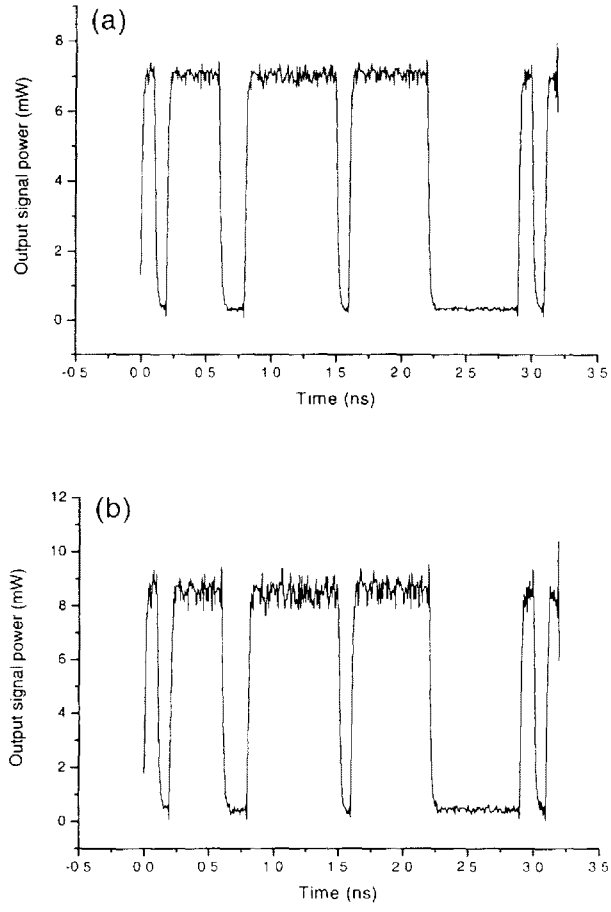

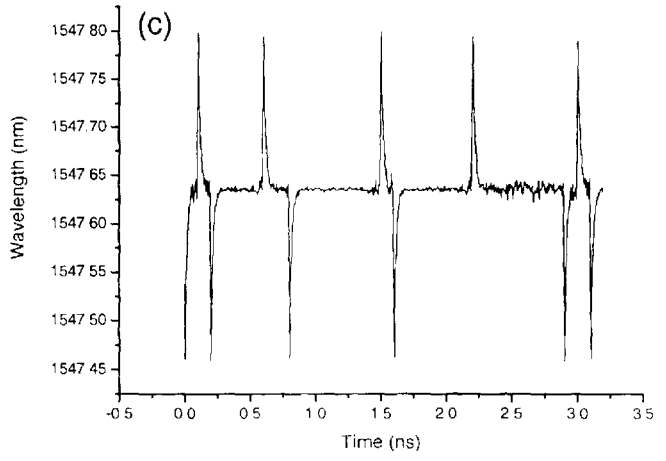

Figure 6.1.13 Output results for the ***in-line EDFAs*** *a) output signal power after the 1st in-line , b) output signal power after the 2nd in-line , c) dynamic wavelength changes due to chirp.*

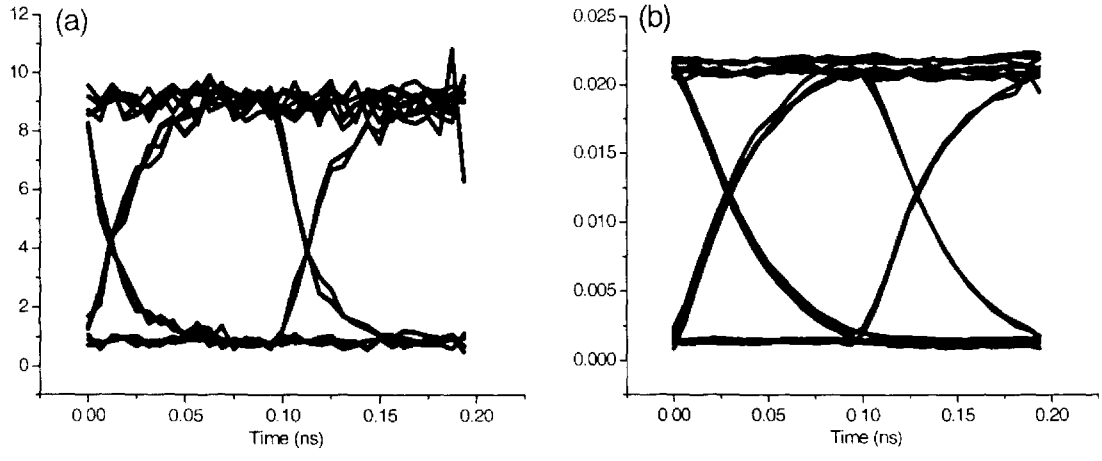

Figure 6.1.14 Eye diagrams of the output a) right after the ***EDFA 2nd in-line amplifier****, b) at the receiver after low pass filter.*

6.1.3 Case 3) Preamplifier

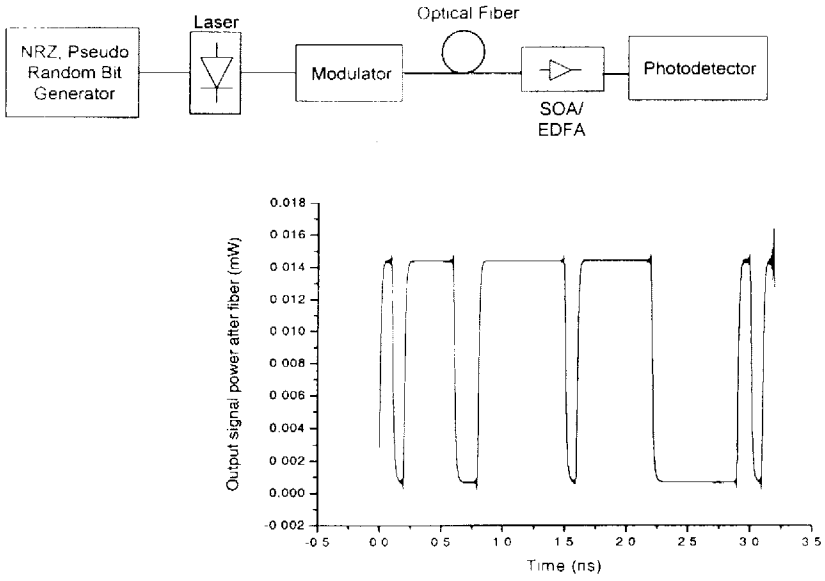

Figure 6.1.15 Input signal power of the preamplifier from the fiber.

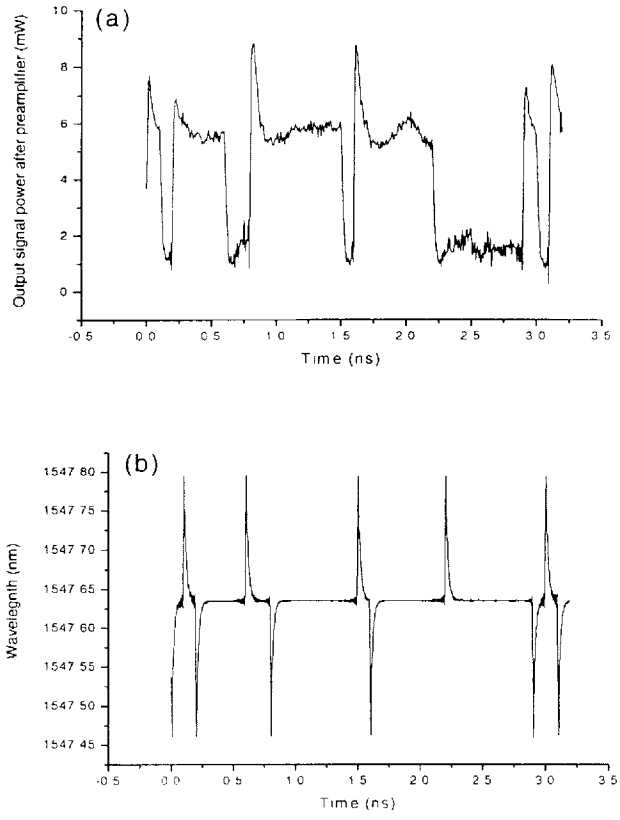

*Figure 6.1.16 Output results after the **Bulk SOA preamplifier** a) output signal power , b) dynamic wavelength changes due to chirp.*

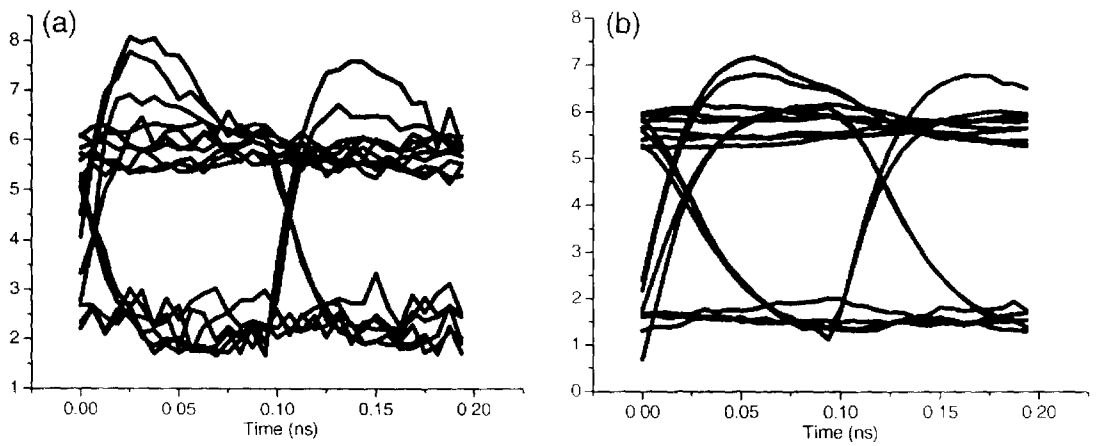

Figure 6.1.17 Eye diagrams of the output a) right after the ***Bulk SOA preamplifier****, b) at the receiver after low pass filter.*

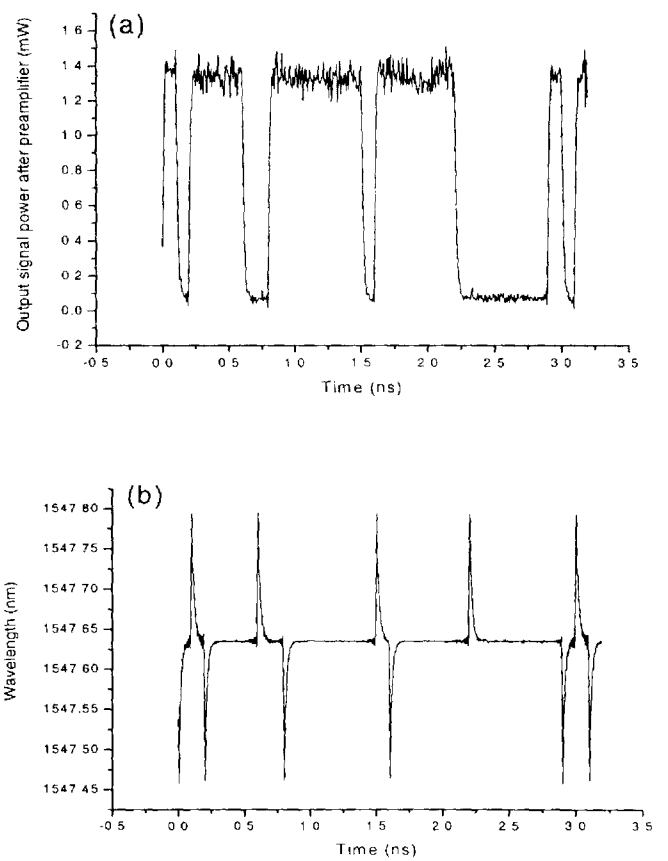

Figure 6.1.18 Output results after the ***MQW SOA preamplifier*** *a) output signal power , b) dynamic wavelength changes due to chirp.*

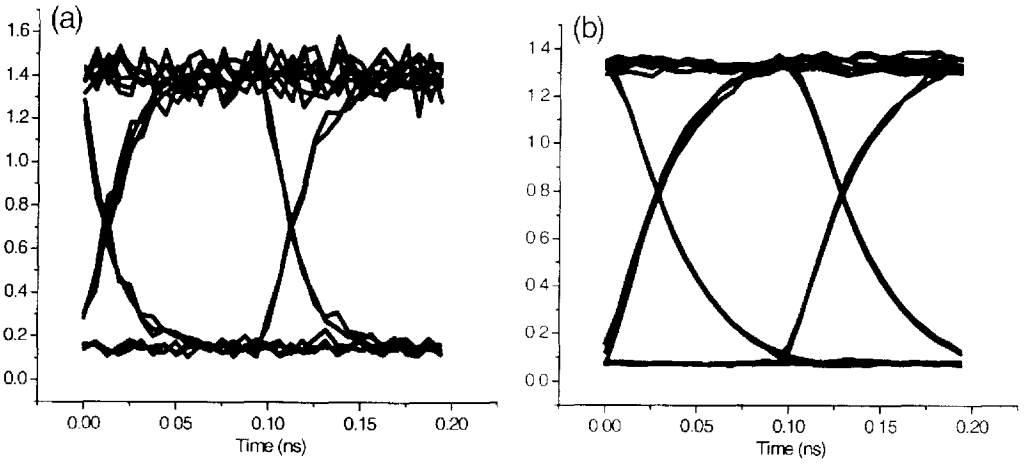

Figure 6.1.19 Eye diagrams of the output a) right after the ***MQW SOA preamplifier****, b) at the receiver after low pass filter.*

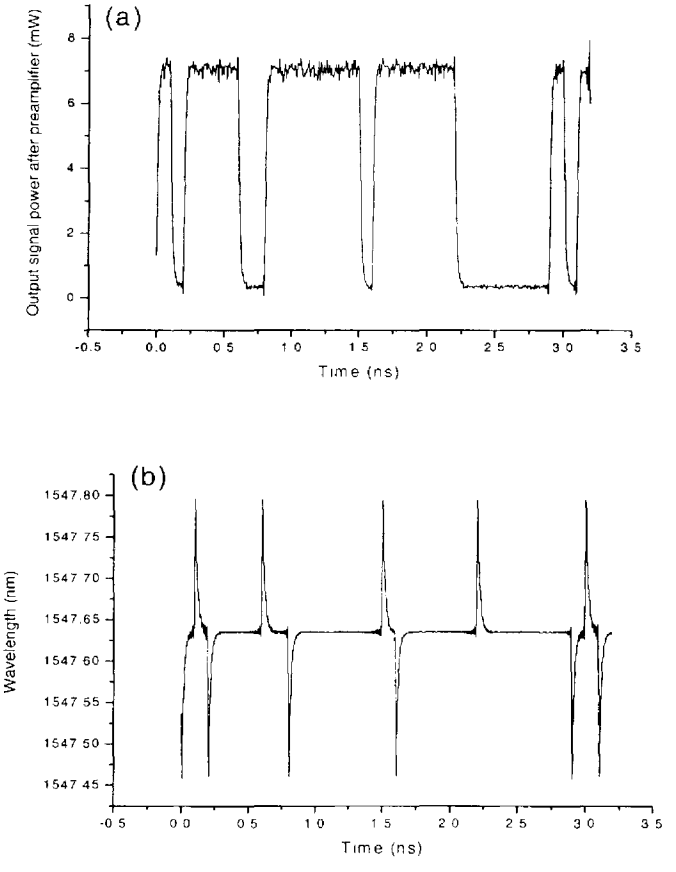

Figure 6.1.20 Output results after the ***EDFA preamplifier*** *a) output signal power , b) dynamic wavelength changes due to chirp.*

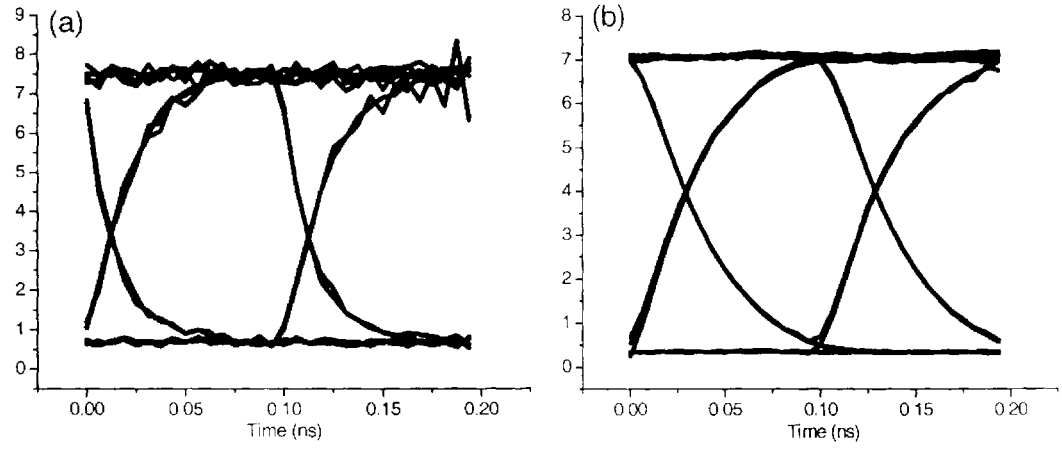

Figure 6.1.21 Eye diagrams of the output a) right after the ***EDFA preamplifier****, b) at the receiver after low pass filter.*

6.1.4 Case 4) Combination of Power Booster, In-line amplifier and Preamplifier:

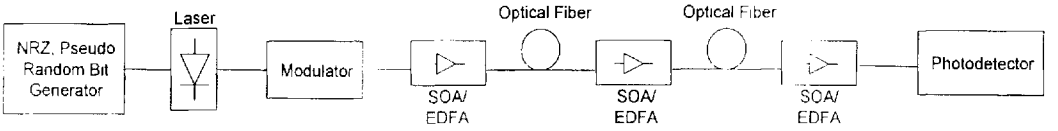

Finally, we consider the case of the combination of power booster, in-line amplifier, and preamplifier, which is used to improve the system performance in long-haul transmission links. An optical preamplifier is used at the end of a transmission link, just before the photodetecting receiver. The sensitivity of a direct detection receiver can be improved significantly by using low noise figure (3- to 5-dB) optical preamplifiers [29]. Fig. 6.1.22 and 6.1.24 give us the output results of both MQW SOA and EDFA. As usual, the input signal power level of the preamplifier is extremely low because the signal has lost power in the transmission link. Hence, the output power of the preamplifier needs to be sufficiently high so that at the photodetector the noise is dominated not by its receiver noise but by the signal to spontaneous beat noise of the optical preamplifier [31]. In Fig. 6.1.23a shows us a completely close eye and indicates that the signal transmitted through the cascaded MQW SOAs is severely impaired by the largely accumulated ASE noise in successive amplifiers. Thus we can conclude that ASE is trivial and does not constitute a serious problem in a single amplifier stage, but with many stages of amplification ASE can makes system degradation even worse.

Moreover, we can observe a widely open eye from Fig. 6.1.25 and conclude that EDFAs are capable of providing high signal gain, high saturation output power and low noise over a broad optical bandwidth. These nearly ideal characteristics of EDFAs enable them to be widely used in presently optical transmission system, though commercial considerations like costs and compactness of these devices can change the balance in favor of the SOAs.

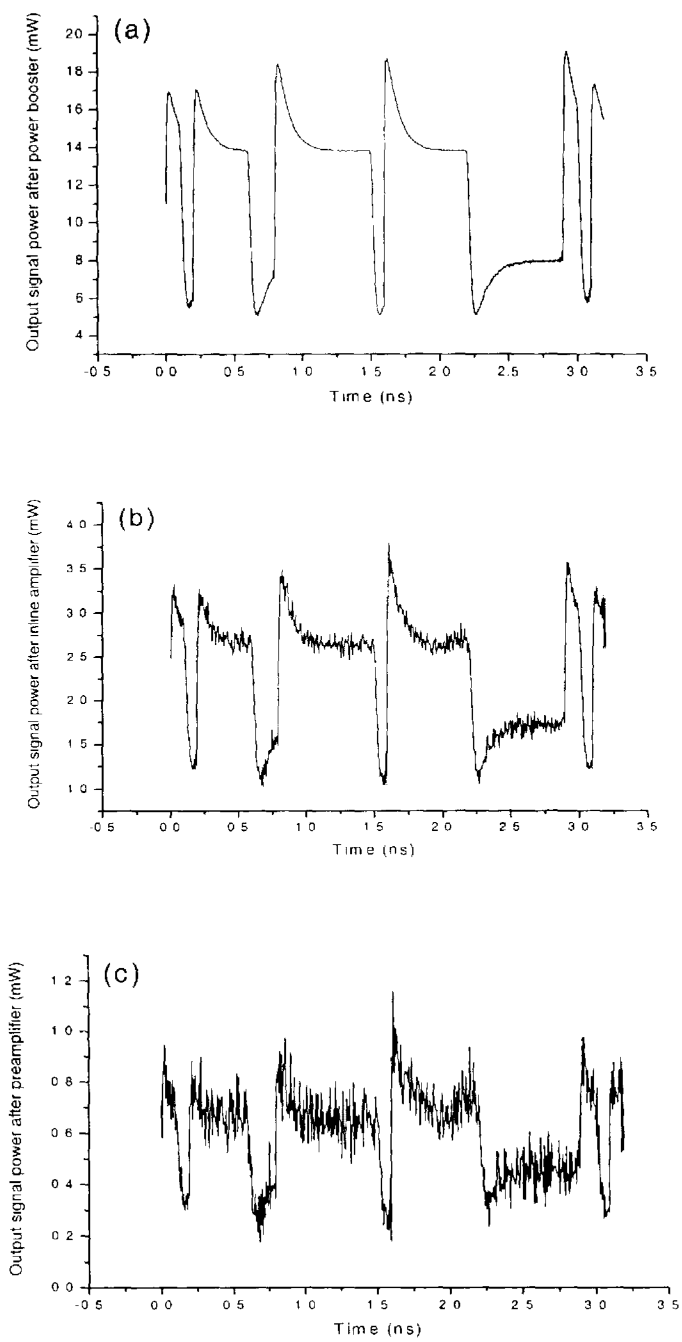

Figure 6.1.22 Output results for the ***combination of MQW SOAs*** *a) output signal after the booster, b) output signal after the in-line, c) output signal after the preamp.*

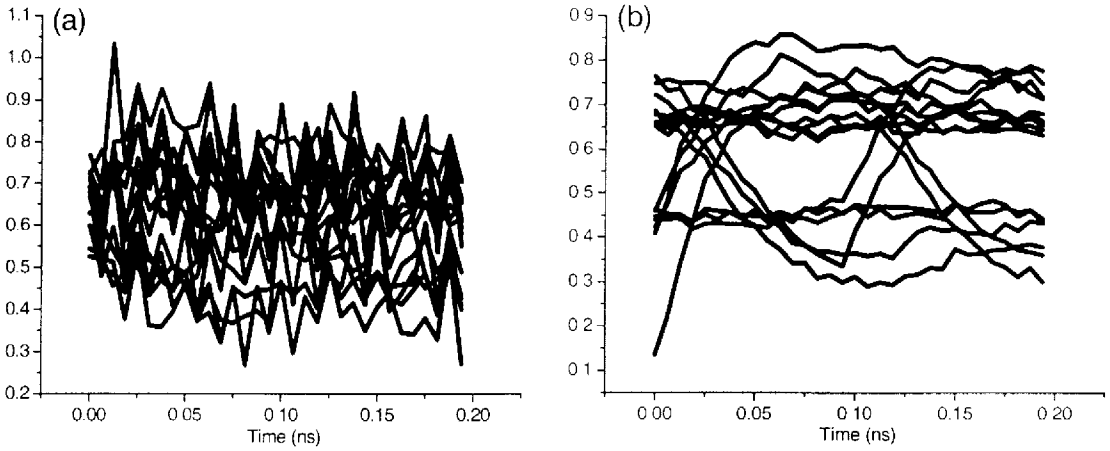

Figure 6.1.23 Eye diagrams of the output a) right after the ***MQW SOA preamplifier of the combination****, b) at the receiver after low pass filter.*

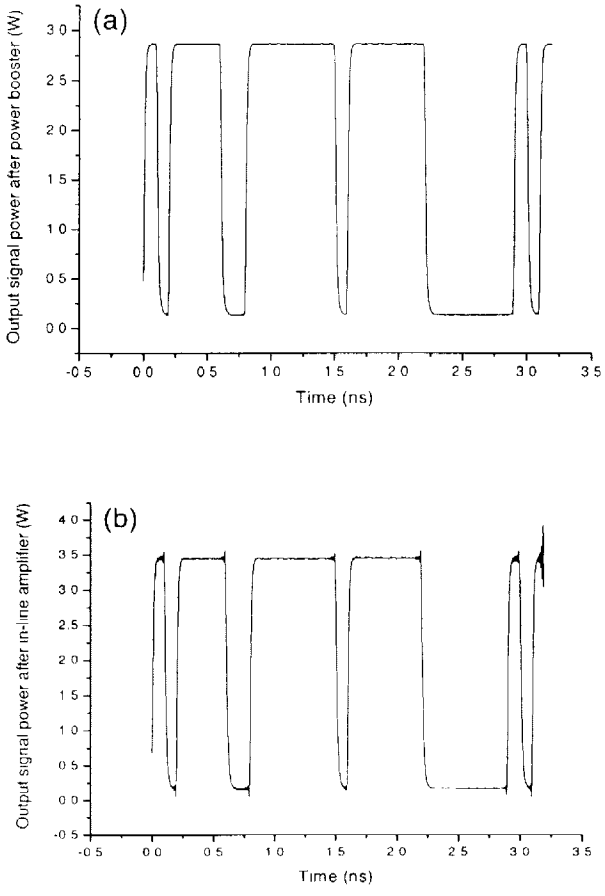

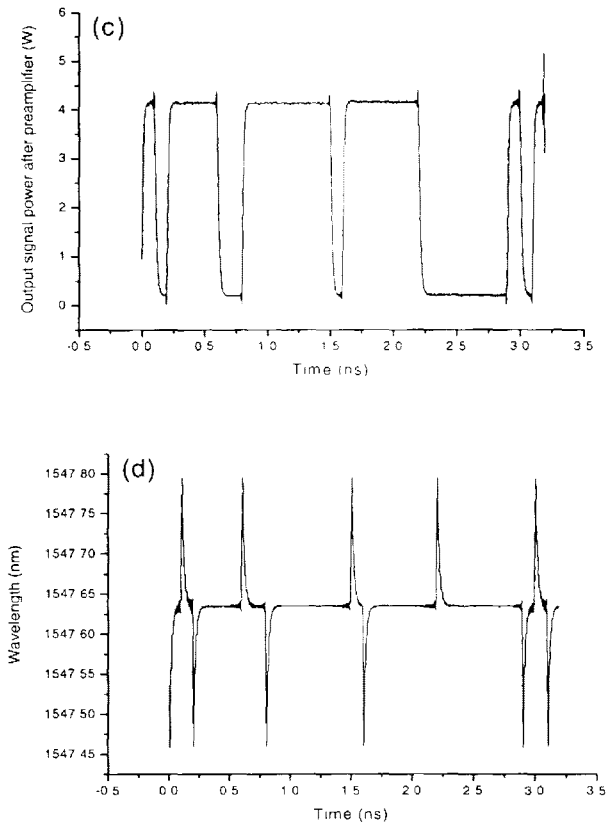

Figure 6.1.24 Output results for the ***combination of EDFAs*** *a) output signal after the booster , b) output signal after the in-line , c) output signal after the preamp , d) dynamic wavelength changes due to chirp.*

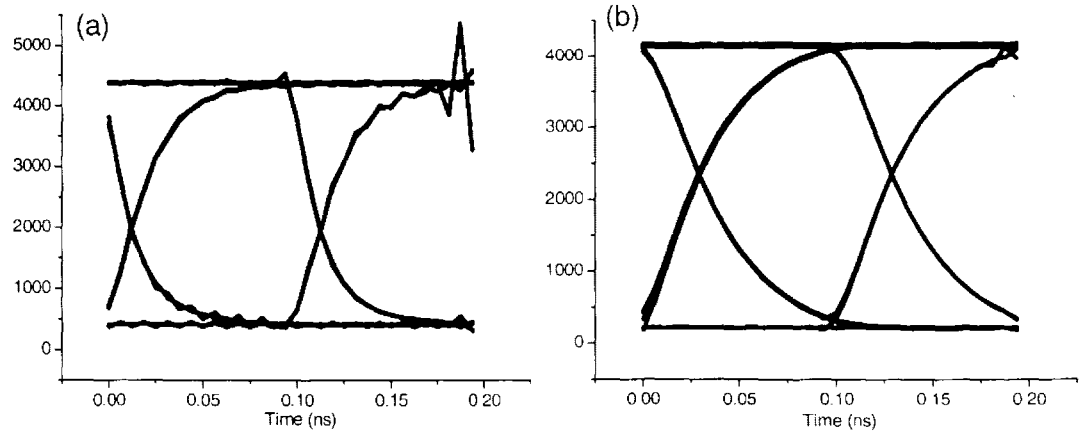

Figure 6.1.25 Eye diagrams of the output a) right after the ***EDFA preamplifier of the combination,*** *b) at the receiver after low pass filter.*

6.2 WDM system simulations

WDM transmission can be used to greatly enhance the capacity of optical fiber. In this section, we focus on WDM in transmission systems that contain all of the optical amplifiers mentioned before. To determine the influence of ASE noise on WDM system behaviour, we performed on $4\times10Gbit/s$ transmission systems employing different amplifier types [33], [34].

6.2.1 Case 1: DWDM 4 channels with MQW SOAs in the 1550nm window

System Parameters for both case 1 and 2:	
System description:	External modulation (With power booster, inline amplifier, and preamplifier)
Number of channel:	4
Bit-rate:	10 Gb/s
Bit per frame:	16
Number of frame:	2
Total fiber length:	2 x 60 km
Optical bandwidth:	C-band (1530nm-1563nm)
Type of signal:	Gaussian pulse
Channel wavelengths:	1550.12, 1549.32, 1548.52, 1551.72 (nm)

Fig. 6.2.2-6.2.8 show the output signal powers and wavelengths of four channels after modulator, power booster, inline amplifier, and preamplifier. It can be clearly observed that more noises are accumulated through the cascaded amplifiers. After passing through the photodetecting receiver, four electrical signals could be recovered as shown in Fig. 6.2.11. Obviously, there is intersymbol interference effect between

the channels caused by the signal dispersion in the transmission system. Moreover, Fig. 6.2.9 shows all the output eye diagrams after the preamplifier, these severely degraded eye diagrams are mainly caused by the largely accumulated ASE noise along the transmission line. Although most of the high frequency noises would be filtered out by low pass filter at the receiver, there is still a considerable amount of noise accompanying with the information signal so as to degrade the system performance. The results for EDFA are shown as same manner as in SOA. The widely open eyes in Fig. 6.2.20 show us that EDFA not only can be immune to cross-gain saturation effect in WDM systems, but also it does give a much better noise performance compared to SOA in any cases.

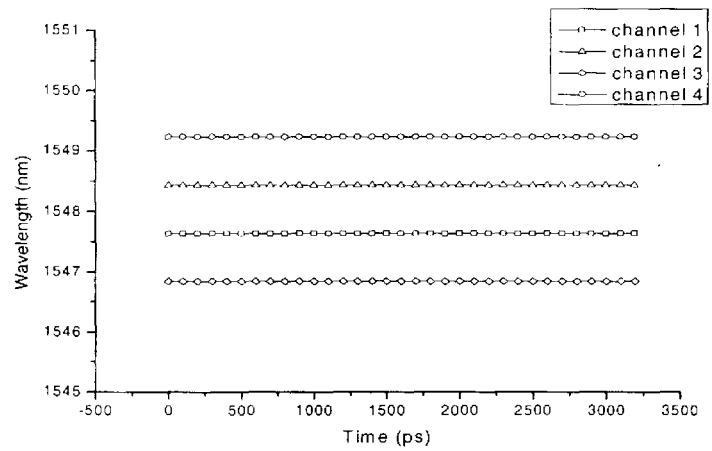

Figure 6.2.1: Four different wavelength channels generated from the Laser diode.

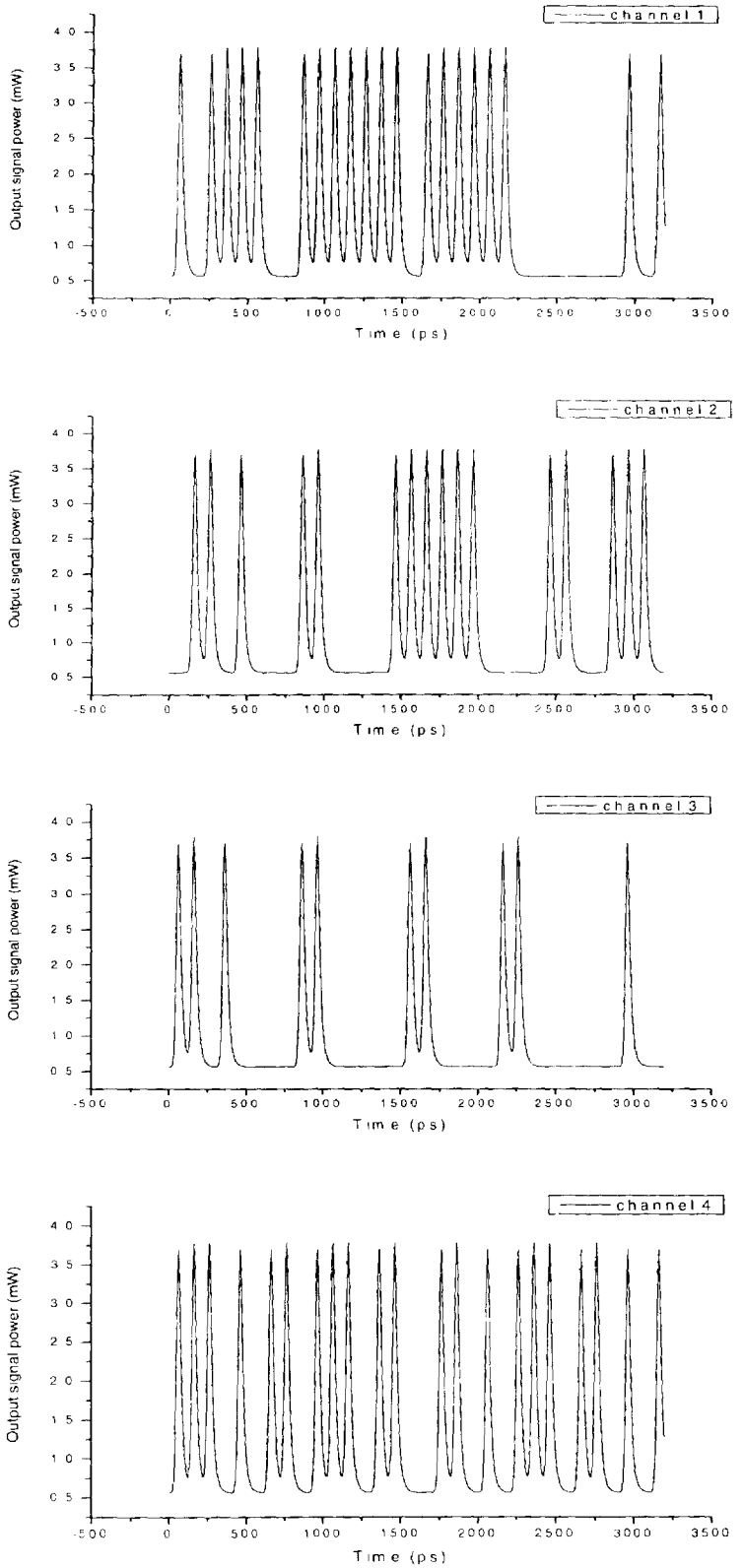

Figure 6.2.2 : Output signal by external modulation for 4 different channels.

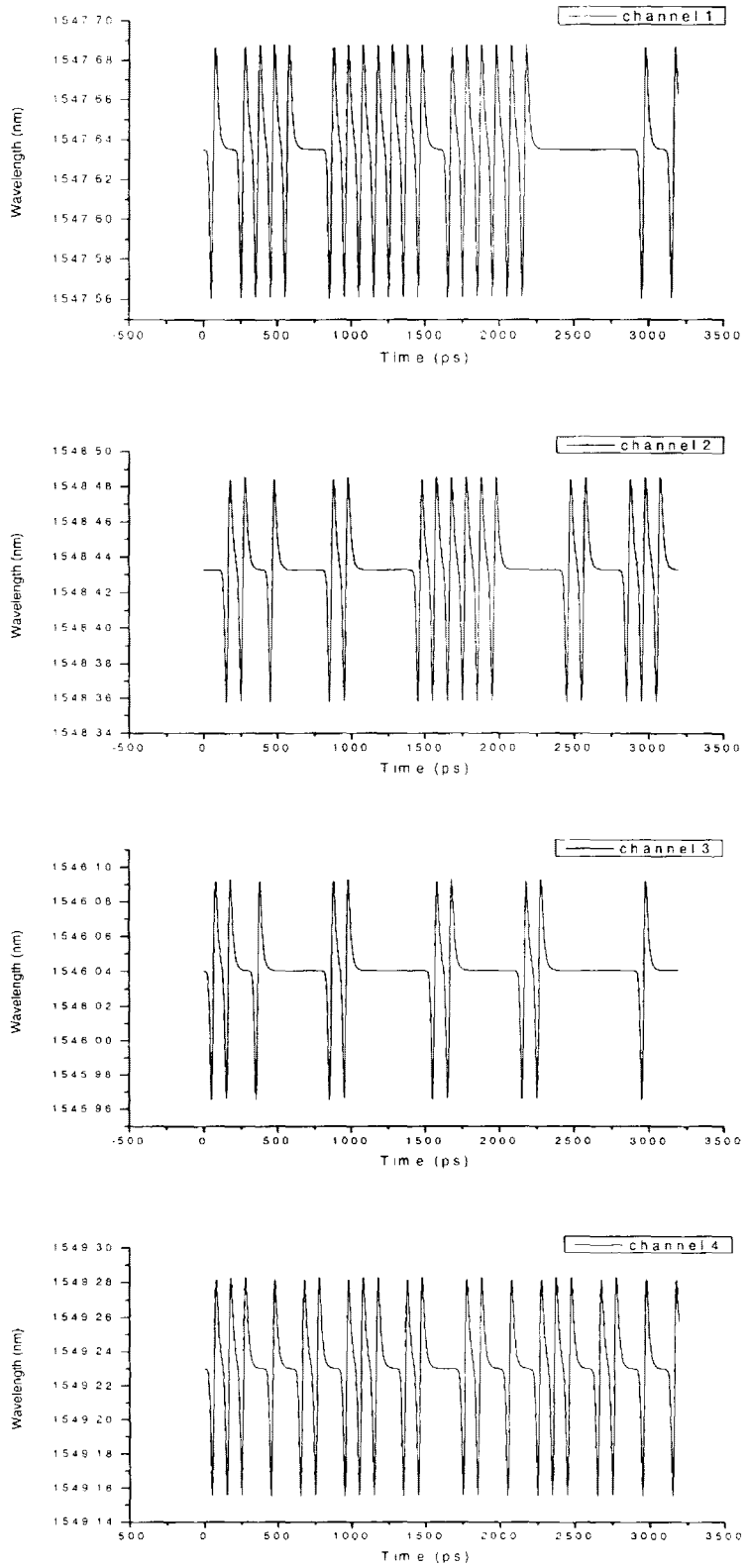

Figure 6.2.3 : Output wavelength after the modulator for 4 different channels.

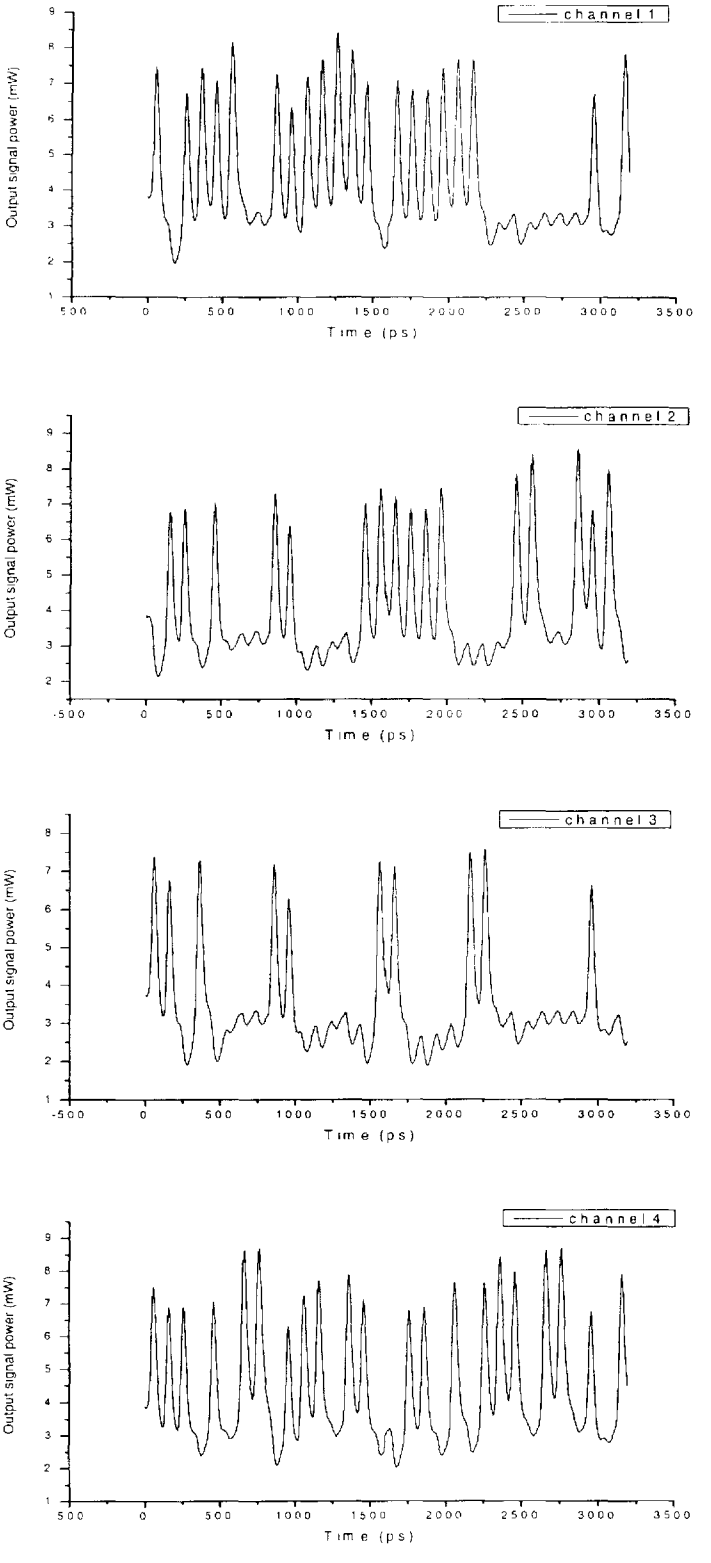

Figure 6.2.4: Output signal after the ***MQW SOA power booster*** *for 4 different channels.*

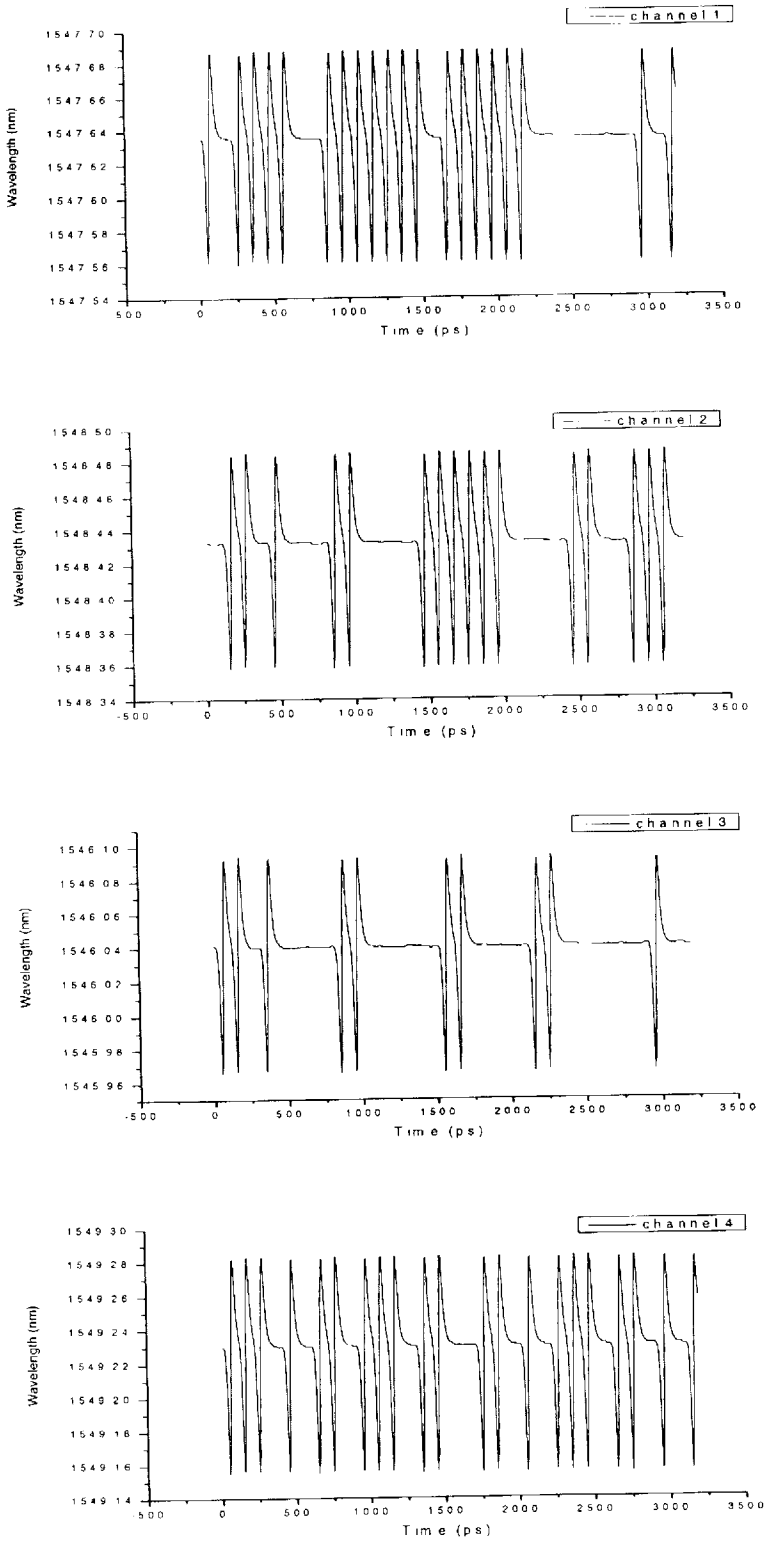

*Figure 6.2.5: Output wavelength after the **MQW SOA power booster** for 4 different channels.*

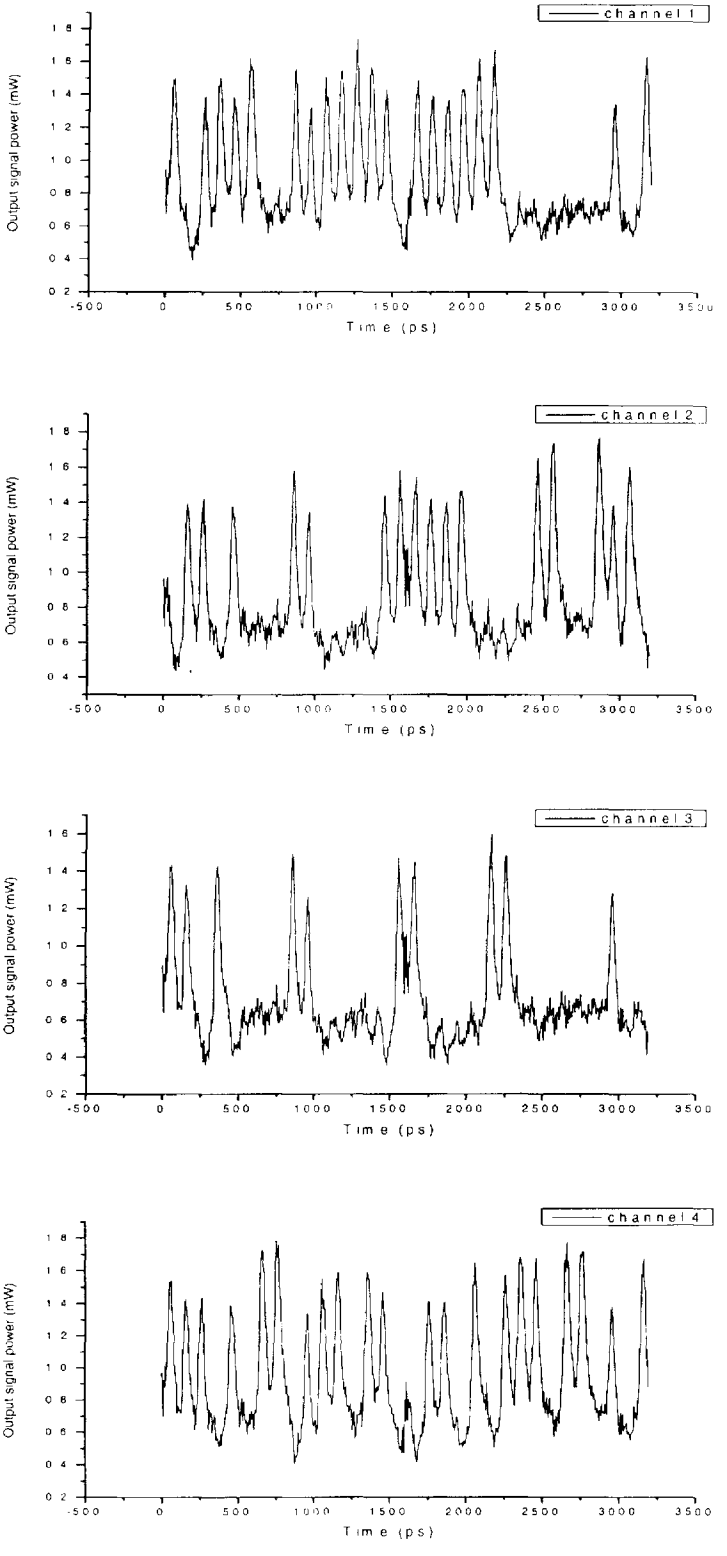

Figure 6.2.6 : Output signal after the ***MQW SOA inline amplifier*** *for 4 different channels.*

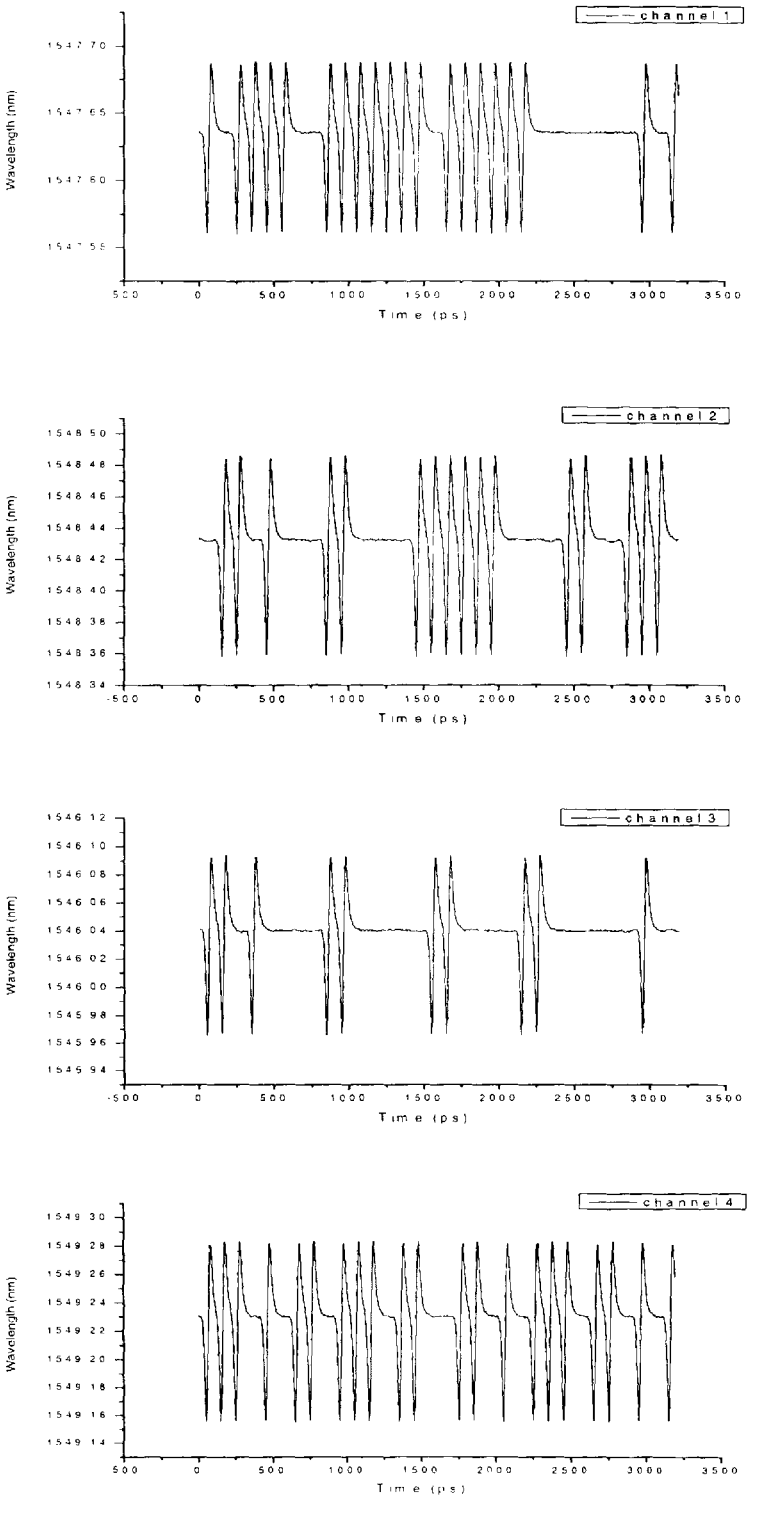

Figure 6.2.7: Output wavelength after the ***MQW SOA inline amplifier*** *for 4 different channels.*

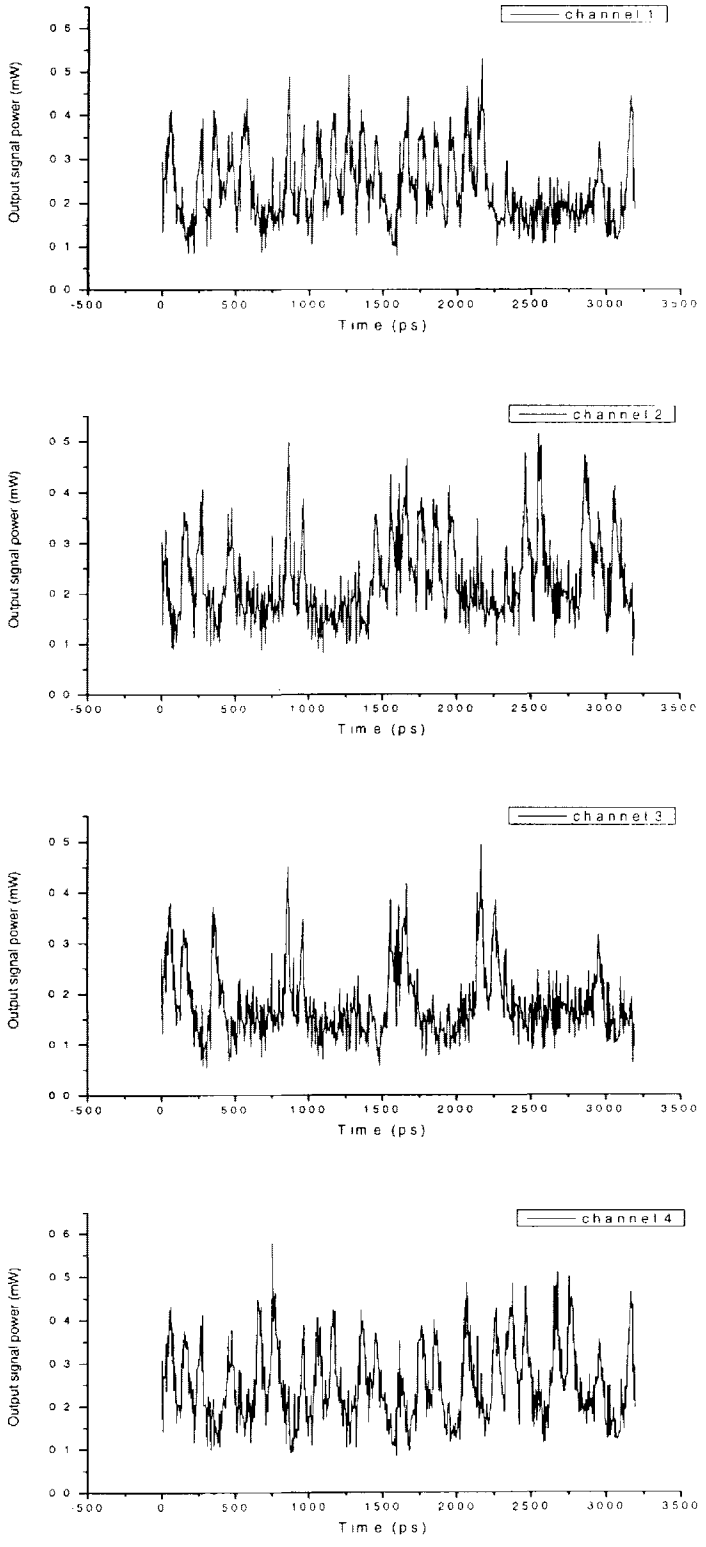

Figure 6.2.8: Output signal after the ***MQW SOA preamplifier*** *for 4 different channels.*

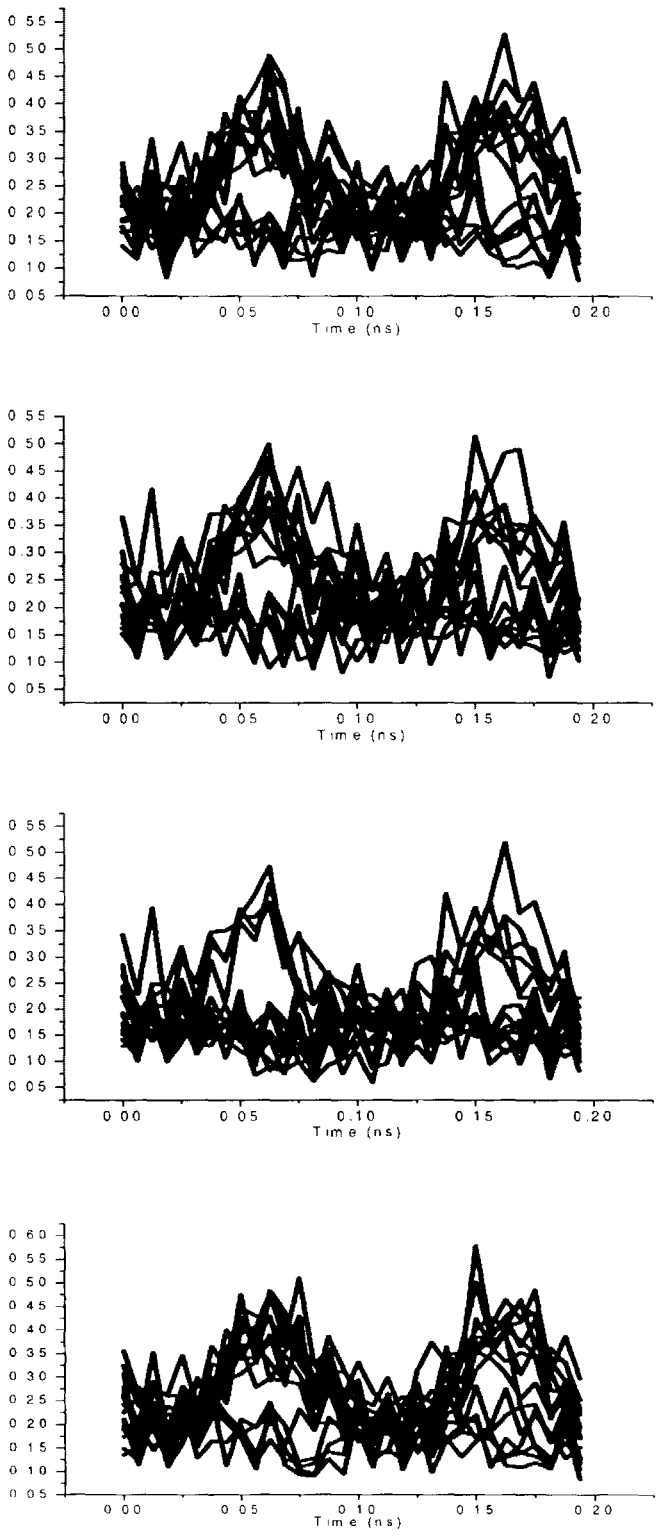

Figure 6.2.9: Eye diagram output just after the ***MQW SOA preamplifier*** *for 4 different channels.*

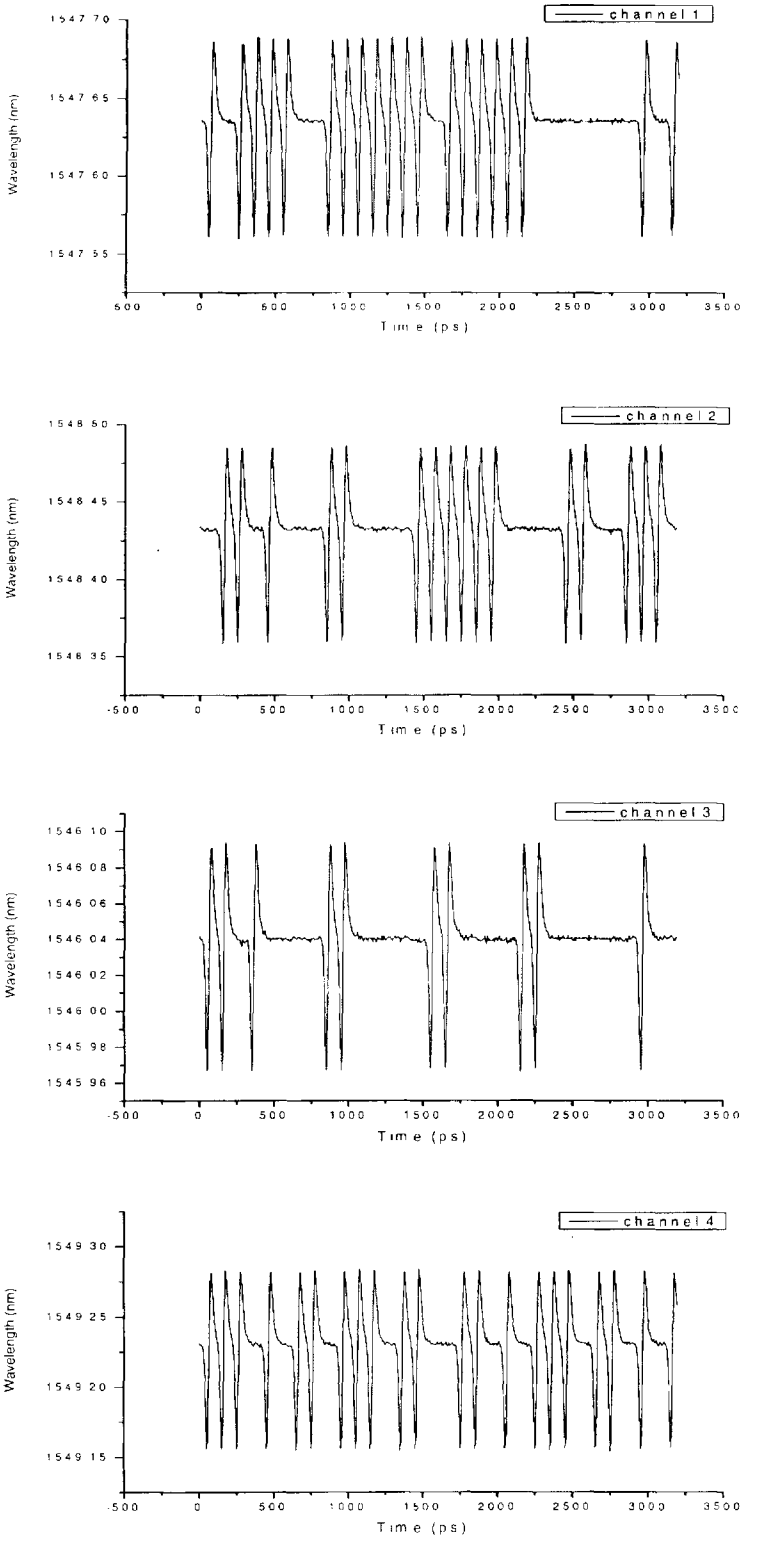

Figure 6.2.10: Output wavelength after the transmission link for 4 different channels.

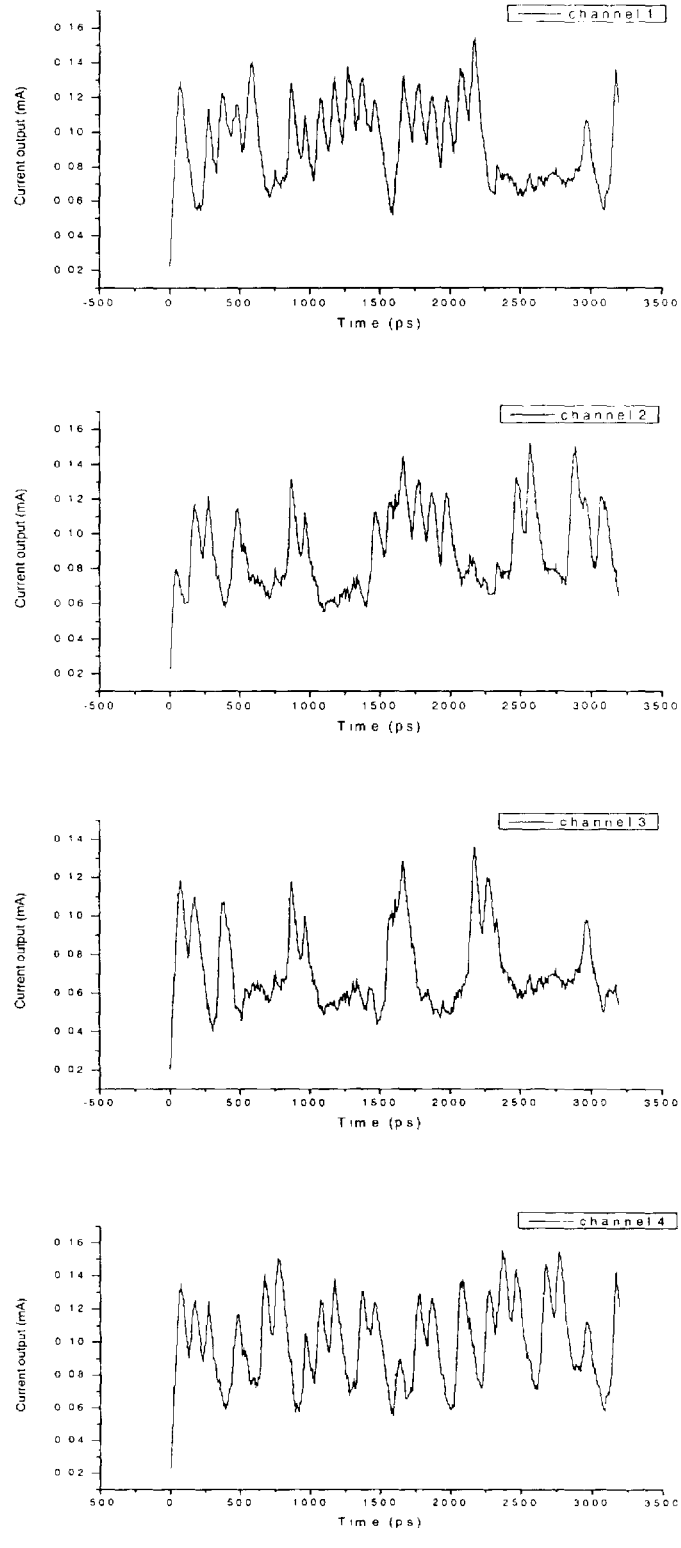

Figure 6.2.11: Output signal after the photo-detector at the end for 4 different channels.

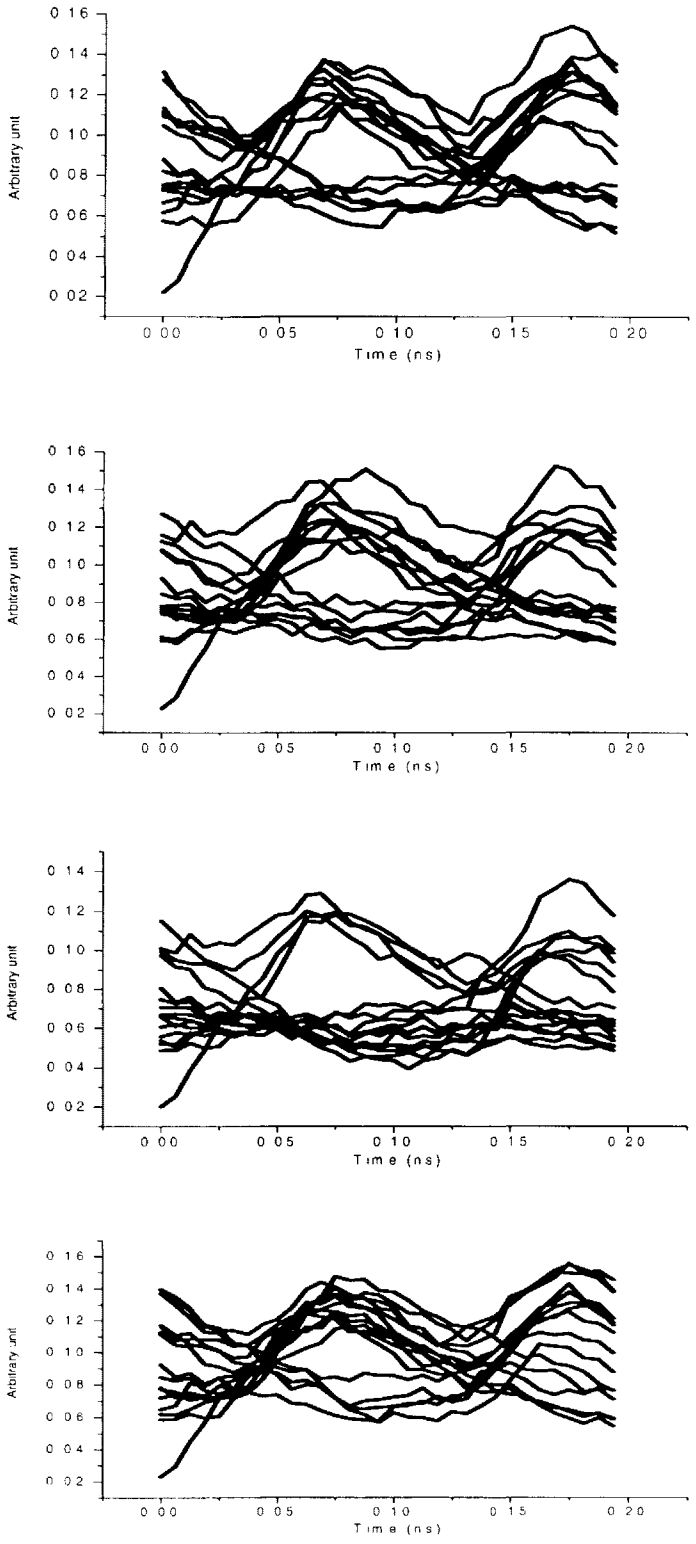

Figure 6.2.12: Eye diagram output at the end of the ***SOA-based transmission link*** *for 4 different channels.*

6.2.2 Case 2: DWDM 4 channels with EDFAs in the 1550nm window

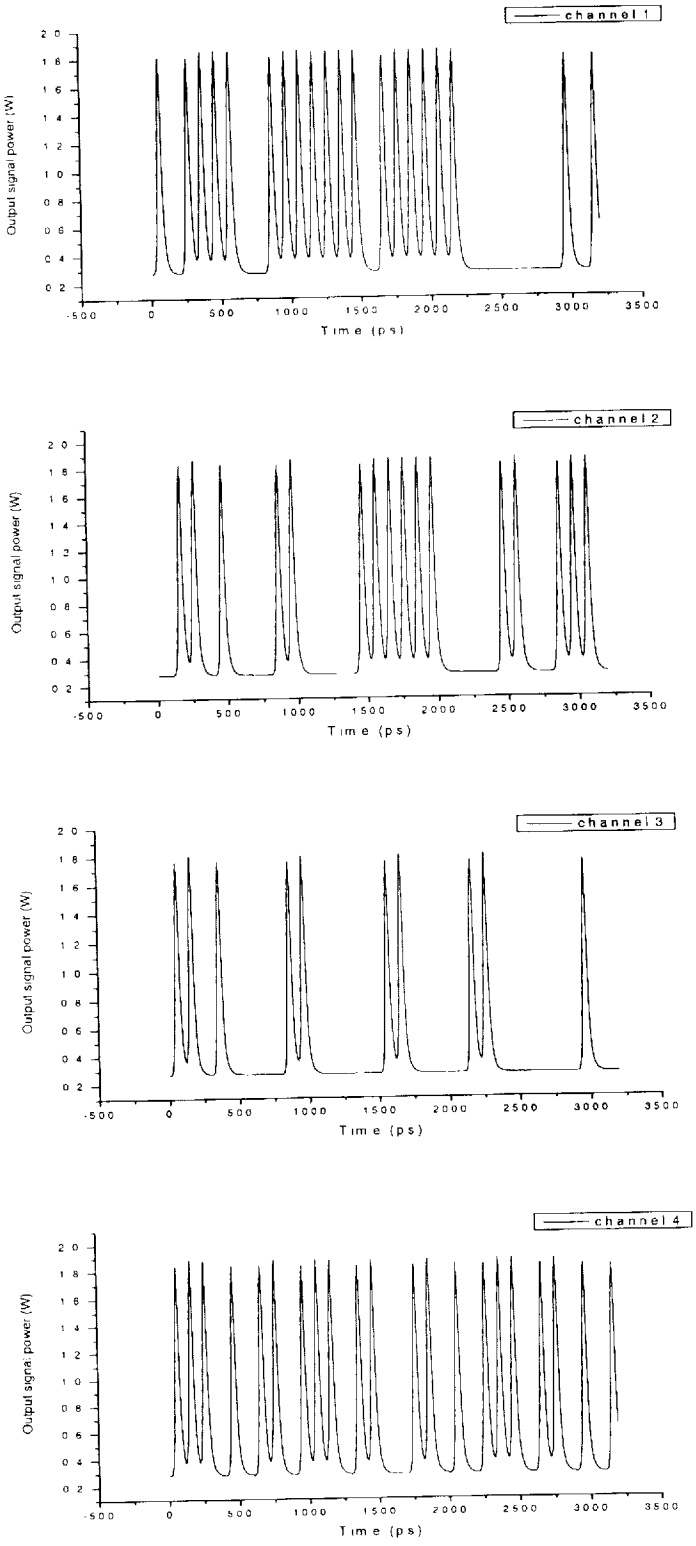

*Figure 6.2.13: Output signal after the **EDFA power booster** for 4 different channels.*

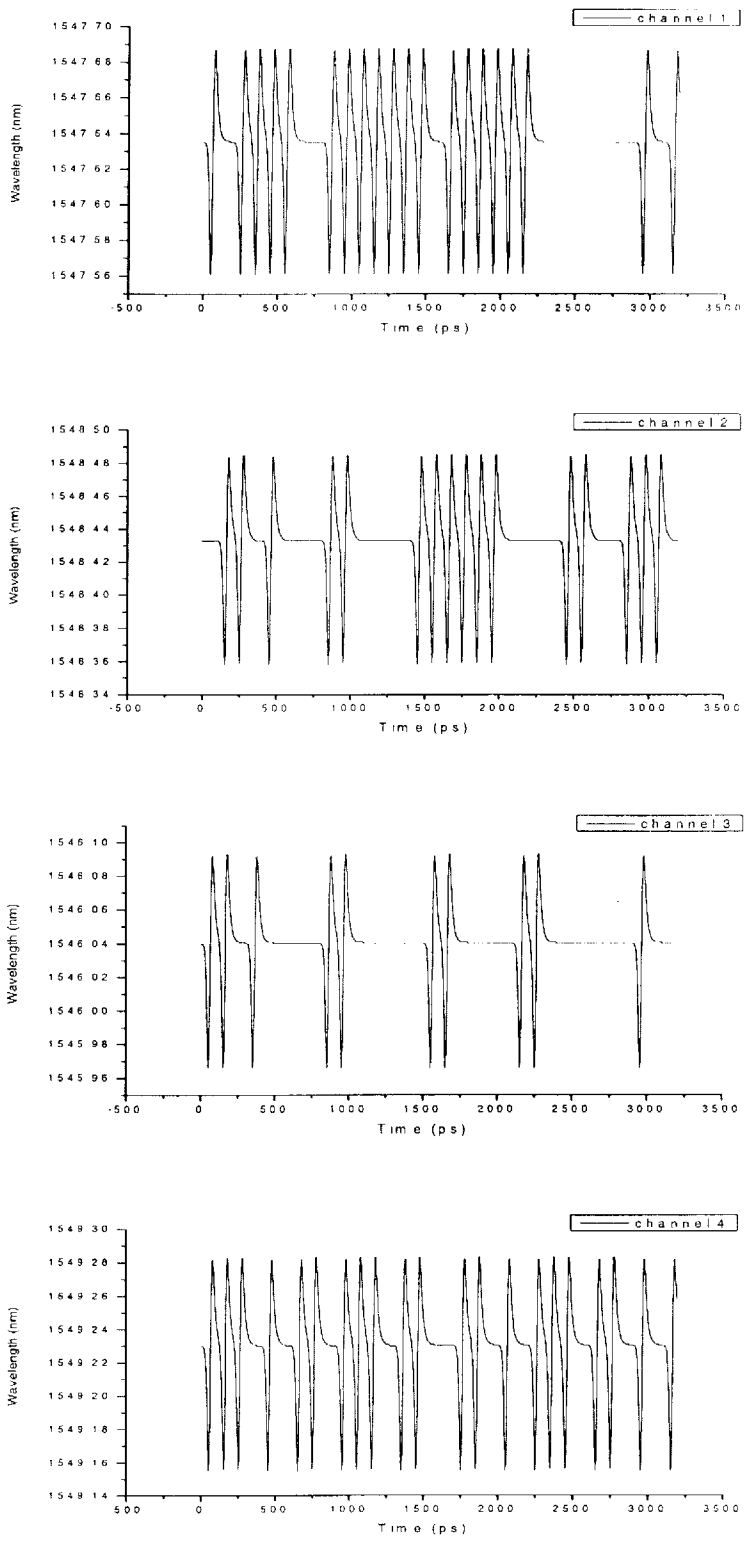

*Figure 6.2.14: Output wavelength after the **EDFA power booster** for 4 different channels.*

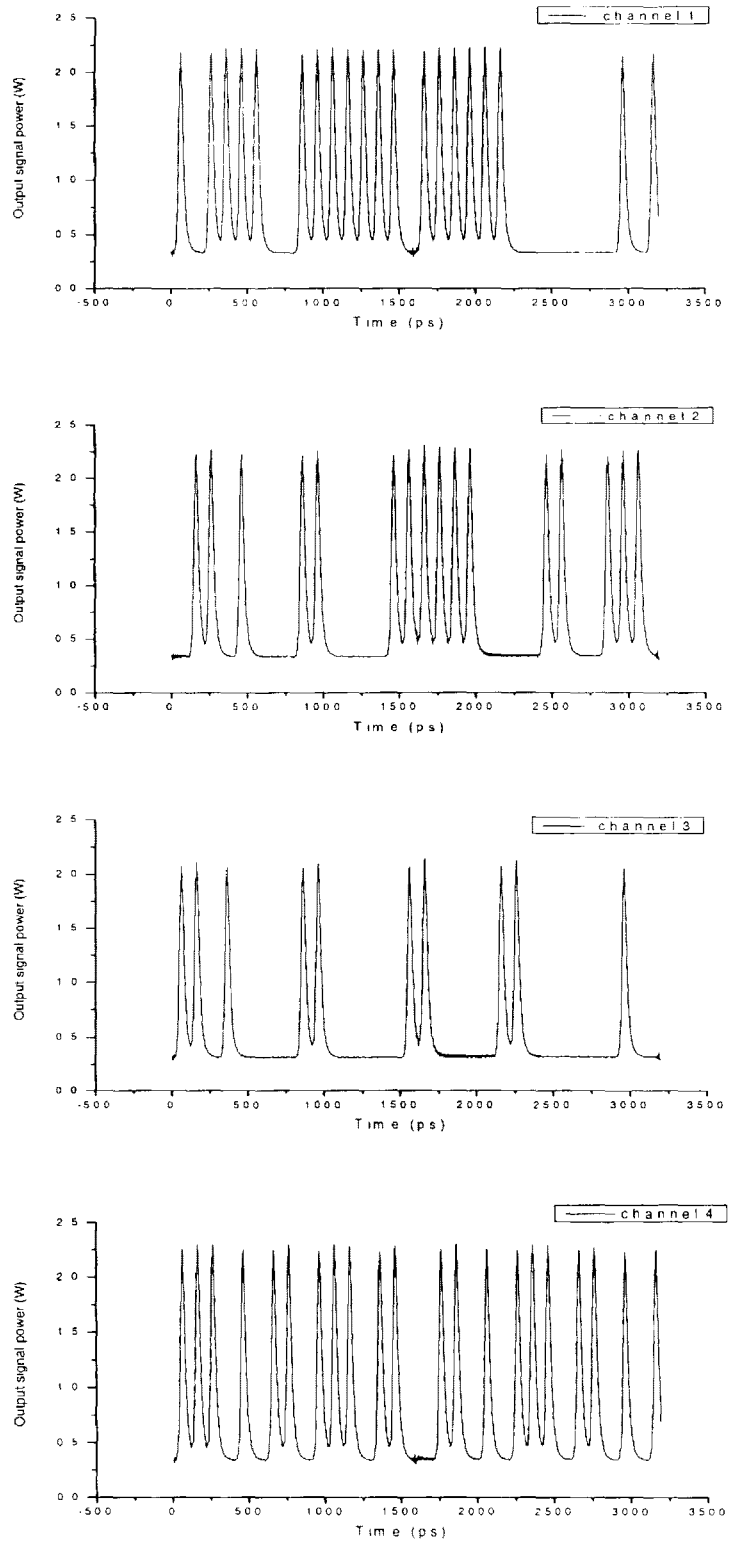

Figure 6.2.15: Output signal after the ***EDFA inline amplifier*** *for 4 different channels.*

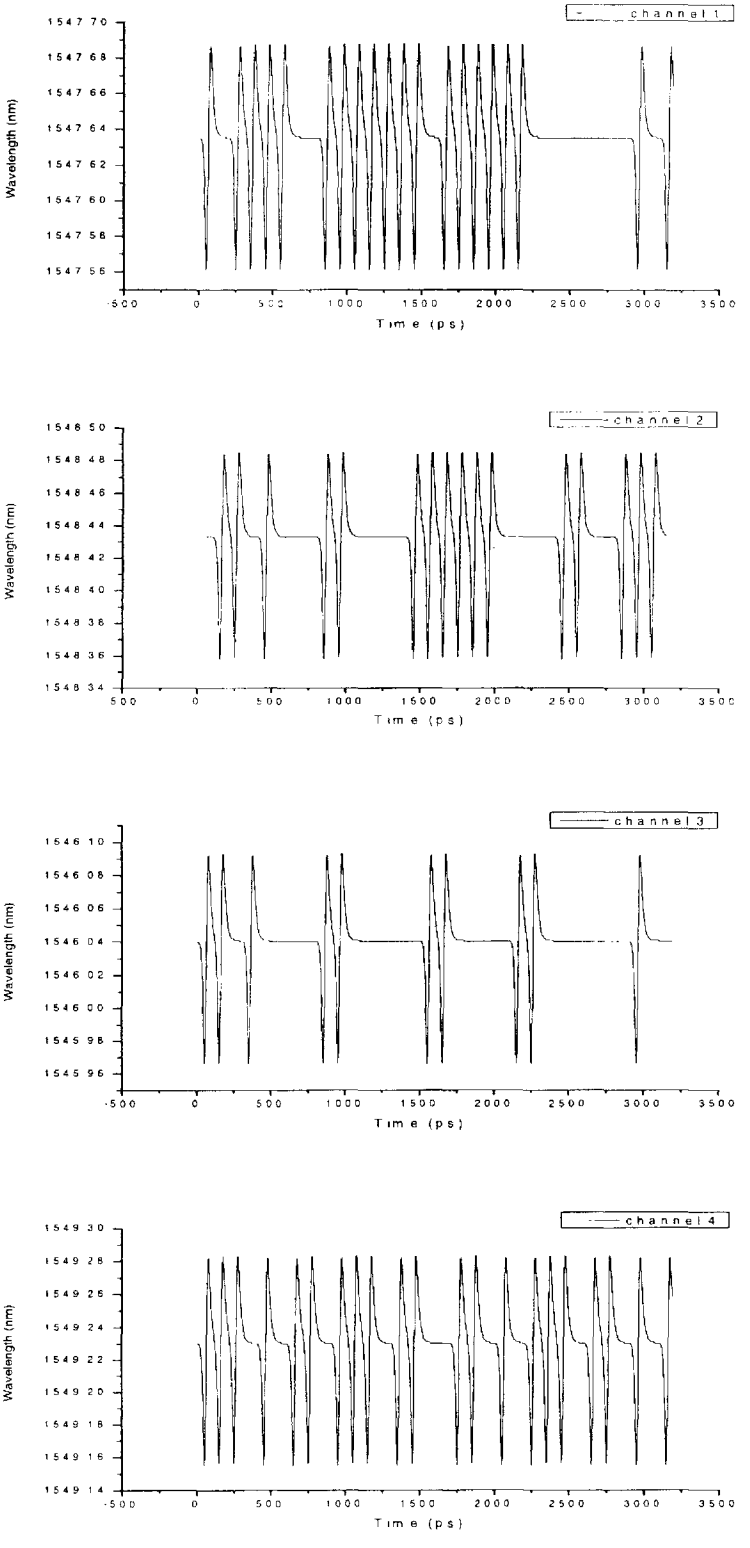

Figure 6.2.16: Output wavelength after the ***EDFA inline amplifier*** *for 4 different channels.*

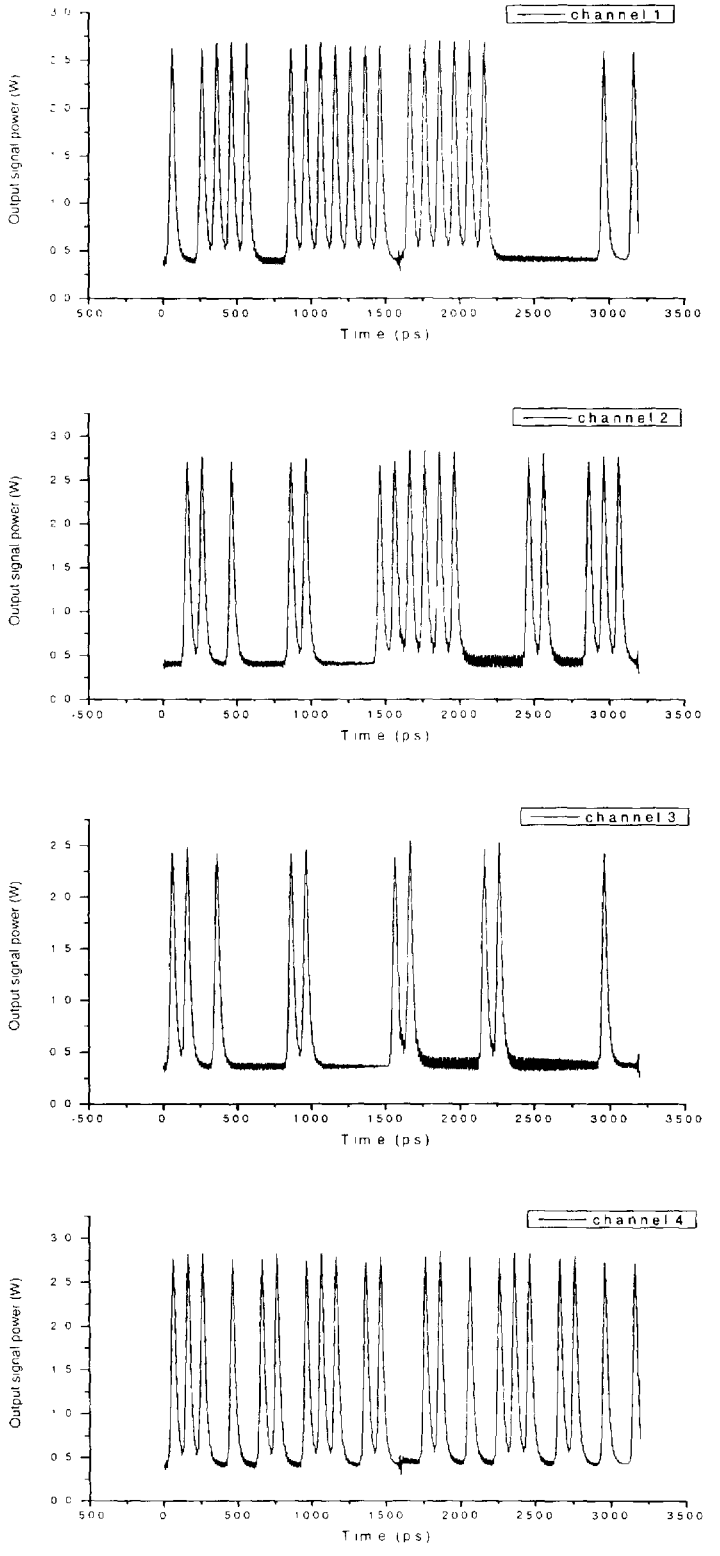

*Figure 6.2.17: Output signal after the **EDFA preamplifier** for 4 different channels.*

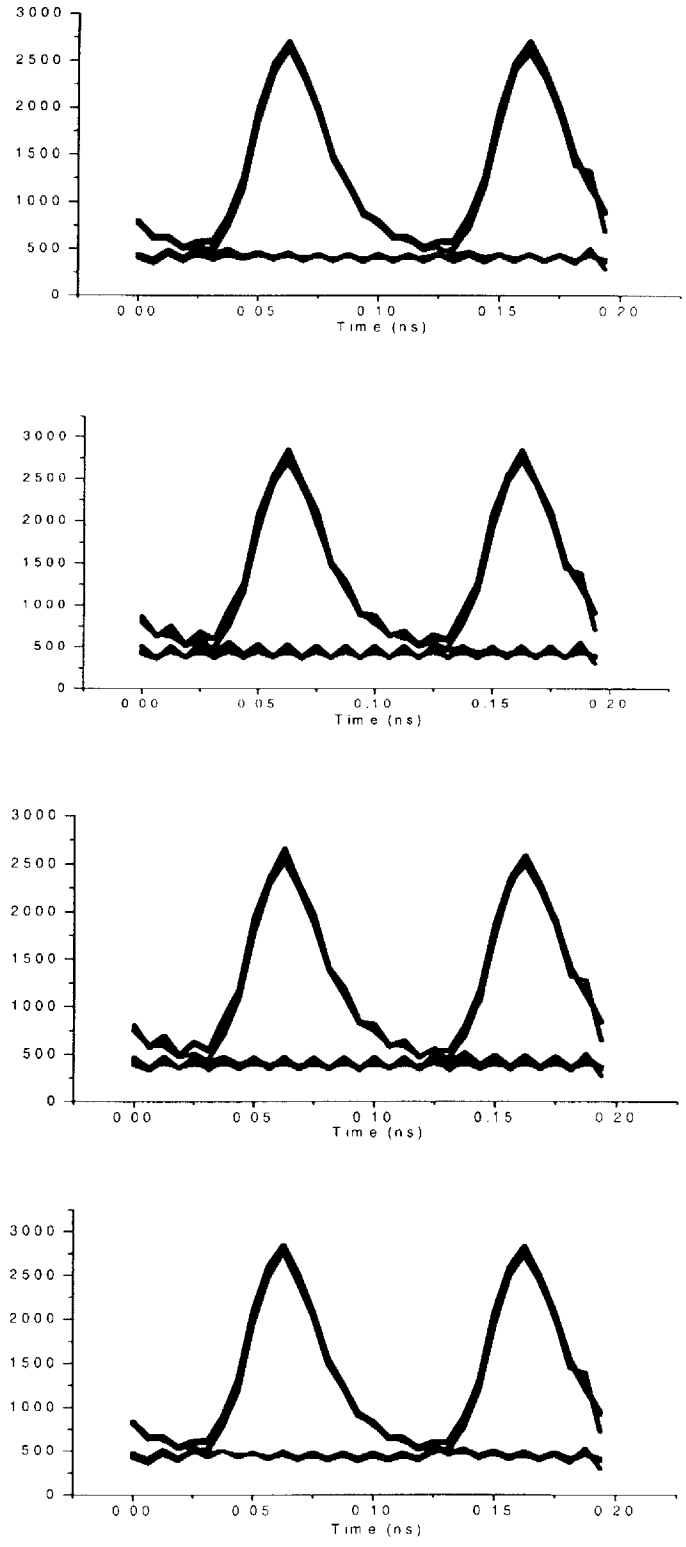

*Figure 6.2.21: Eye diagram output after the **EDFA preamplifier** for 4 different channels.*

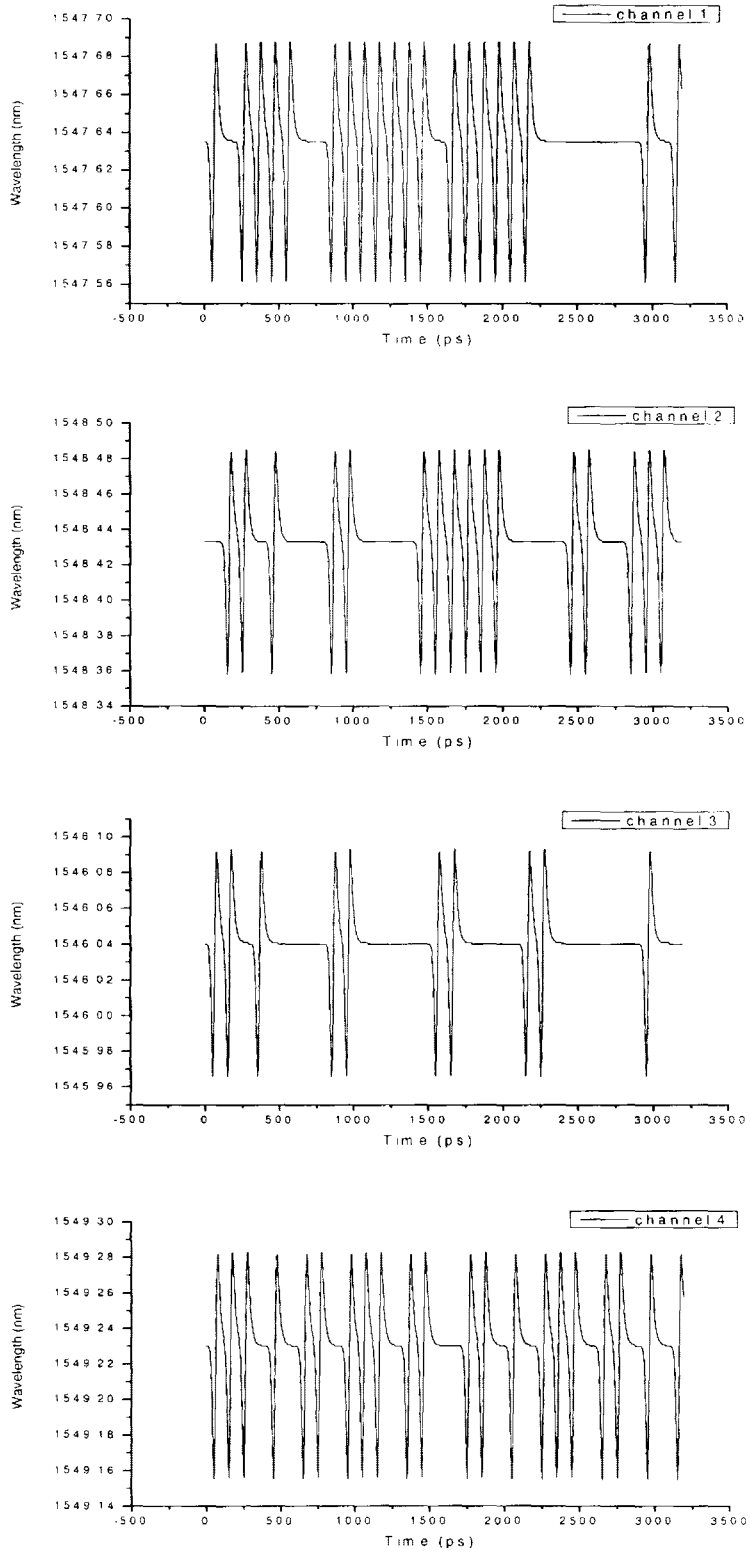

Figure 6.2.19: Output wavelength after the ***EDFA preamplifier*** *for 4 different channels.*

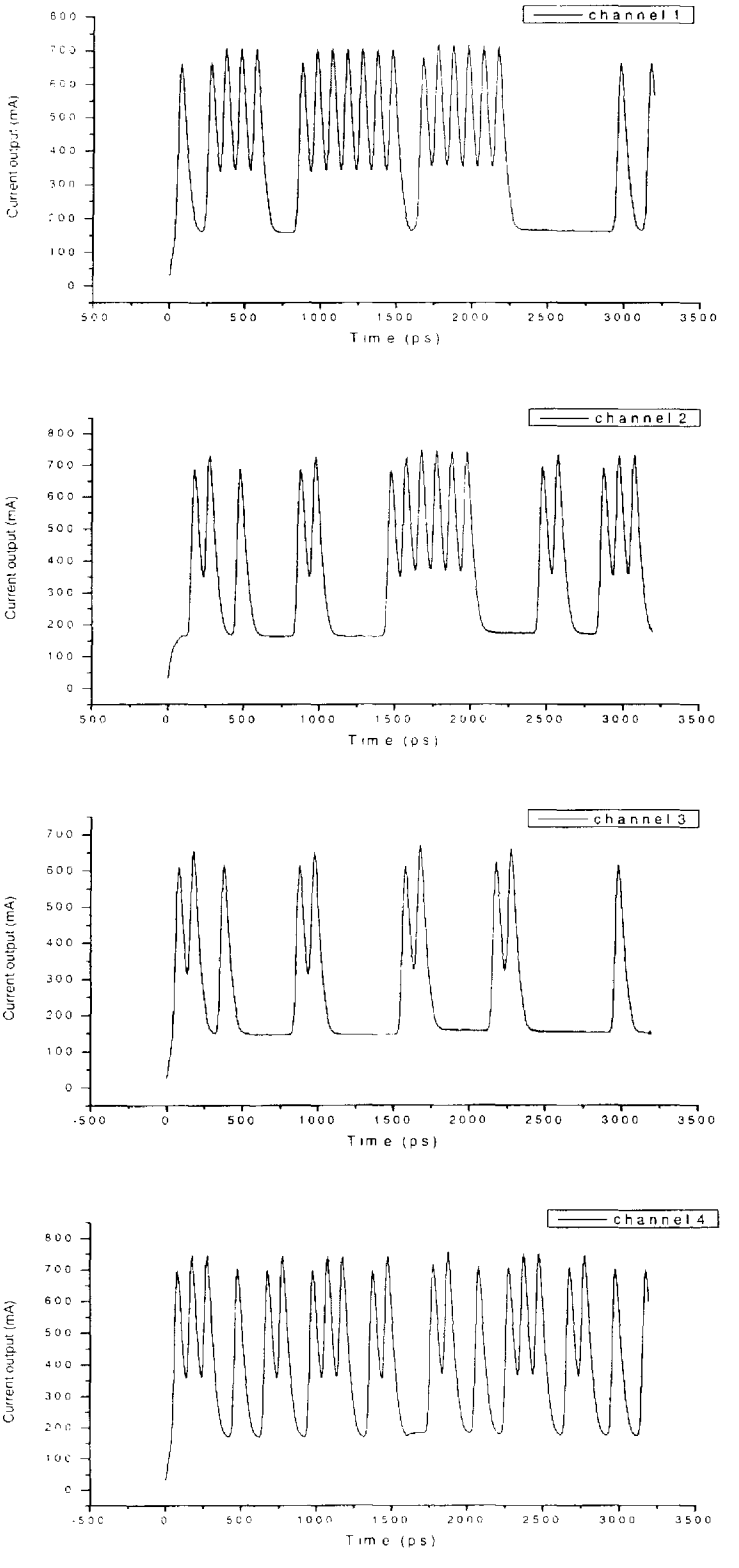

Figure 6.2.20: Output signal after the photo-detector at the end for 4 different channels.

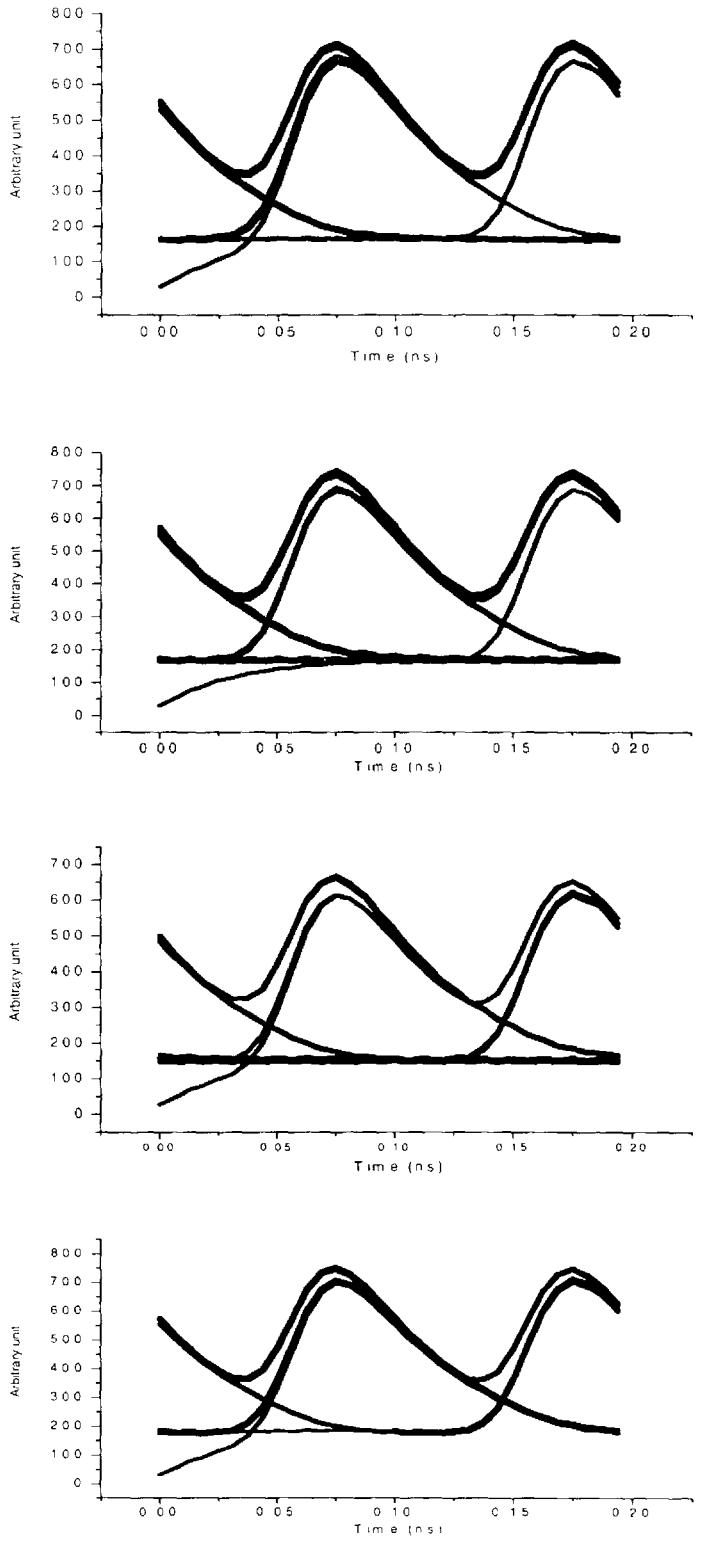

Figure 6.2.21: Eye diagram output at the end of the ***EDFA-based transmission link*** *for 4 different channels.*

Chapter 7
Conclusion

The amplified spontaneous emission (ASE) noise constitutes a serious factor in optical system performance, and thus it plays an important role in designing fiber-optic transmission links employing optical amplifiers. In this work, a time domain model including the ASE noise effect for both semiconductor optical amplifier (SOA) and erbium-doped fiber amplifier (EDFA) has been successfully developed within a reasonable computational complexity. It shows accurate results for both single channel and WDM transmission. Moreover, this newly optical amplifier simulator has been integrated with the existing time-domain simulation platform that has many other optical components assembled, in order to obtain a more realistic picture to examine the system performance of various transmission links. The system platform is capable of dealing with point-to-point multichannel optical transmission links with arbitrary configurations, transmission formats and device parameters. Thus, we can further study the ASE noise effect during single and multichannel amplification in different applications through the system simulation. Making use of this system platform, fiber-optic transmission systems with suitable limitations can be designed based on the power budget including various sources of power penalties.

Appendix

Supplementary device parameters used in the system simulations:

- RCG Parameters

------RCG-pattern-length-
32
------RCG-power/amplitude-unit-mW/mV-
1.
------RCG-bitshape-{rectangle,gpulse,triangle,rcosine}-
gpulse
------RCG-variance-unit-(%)-
2.
------RCG-duty-cycle-unit-(%)-
100.

-Laser Parameters

------CHOICE--1>internal-or--2>external-modulation-
2
------Bias-current-unit-(A)-
0.060
------Modulation-current-unit-(A)-
0.015
------LD-CHOICE--1>Bulk--2>QW--
1

------LD-length-unit-(μm)-

300

------LD-width-unit-(μm)-

2

------LD-depth-unit-(μm)-

0.2

------group-index-

3.9

------K-Petermann-factor-

1

------Population-inversion-factor-

2

------Cavity-loss-unit-(cm^{-1})-

20

------Linewidth-enhancement-factor-

3

------Carrier-lifetime-unit-($1e^{-9}s$)-

1.0

------Photon-lifetime-unit-($1e^{-12}s$)-

3.0

------Confinement-factor-

0.3

------Gain-coefficient-bulk-unit-($1e^{-16}cm^{2}$)-

3.0

------Gain-coefficient-QW-unit-(cm^{-1})-

1000

------Gain-saturation-factor-unit-($1e^{-17}$)-

2

------Carrier-density-at-transparency-unit-($1e^{18}m^{-3}$)-

1.0

------Gain-width-unit-(nm)-

49.2

------Noise-switch-(1="On", 0="OFF")

0

-Modulator Parameters

------CHOICE--1>EA --2>MZ (one-arm)--3>MZ (two-arm)-

1

------EA-Modulator-length-unit-(μm)-

195.

------EA-Modulator-waveguide-confinement-factor-

0.2

------EA-Modulator-modal-refractive-index-

3.2

------EA-Modulator-bias-voltage-unit-(V)-

0.

------EA-Modulator-modulation-voltage-unit-(V)-

1.5

------MZ-Modulator-arm-length-unit-(μm)-

620.

------MZ-Modulator-length-difference-between-two-arms-unit-(μm)-

0.

------MZ-Modulator-input-Y-branch-power-splitting-ratio-

1.4

------MZ-Modulator-output-Y-branch-power-splitting-ratio-

1.4

------MZ-Modulator-modal-refractive-index-

3.2

------MZ-Modulator (one-arm)-bias-voltage-unit-(V)-

3.

------MZ-Modulator (one-arm)-modulation-voltage-unit-(V)-

2.

------MZ-Modulator (two-arm)-bias-voltage-unit-(V)-

3.0

------MZ-Modulator (two-arm)-modulation-voltage-unit-(V)-

1.6

------Low Pass Filter -EA-Modulator-rising-time-unit-(ps)-

50.

------Low Pass Filter-MZ-Modulator-rising-time-unit-(ps)-

35.

-Optical Fiber Parameters

------Fiber-length-unit-(km)-

60.

------Fiber-attenuation-unit-

0.1

------Fiber-second-order-dispersion-
0.
------Fiber-third-order-dispersion-
-1.117
------Fiber-nonlinear-gamma-dispersion-
0.
------Fiber-number-of-steps-
20

-Photodetector Parameters

------FIB-response time unit-(ps)-
200.
------FIB-gain-unit-
1.
------FIB-responsivity-unit-(A/W)-
0.8

Bibliography

[1] S. Shimada, H. Ishio, ed., *Optical Amplifiers and their Application*. John Wiley & Sons, 1994. ISBN 0-471-94005-4.

[2] M.J. Connelly, *Semiconductor Optical Amplifiers*. Kluwer Academic Publishers, 2002. ISBN 0-7923-7657-9.

[3] J.G.L.Jennen, *Noise and Saturation effects in High-speed Transmission Systems with Semiconductor Optical Amplifiers*. Technische Universiteit Eindhoven, 2000. ISBN 90-386-1760-7.

[4] G. Keiser, *Optical Fiber Communications (3rd Edition)*. McGraw-Hill International Ed., 2000.

[5] G.P. Agrawal, *Fiber-Optical Communication Systems (2nd Edition)*. John Wiley & Sons, 1997. ISBN 0-471-17540-4.

[6] Jongwoon Park, Xun Li, Wei-Ping Huang, "Performance simulation and design optimization of gain-clamped semiconductor optical amplifiers based on distributed bragg reflectors", *IEEE Journal of Quantum Electronics*, vol. 39, pp. 1415-1423, November 2003.

[7] C.Y. To, Xun Li, *Time-Domain Simulation of Optical Amplifiers in Wavelength Division Multiplexed (WDM) Photonics Systems and Networks*. Master thesis, McMaster University, Canada, November 2003.

[8] Xun Li, Wei-Ping Huang, "Simulation of DFB semiconductor lasers incorporating thermal effects", *IEEE Journal of Quantum Electronics*, vol. 31, pp. 1848-1855, October 1995.

[9] W. Li, W.P. Huang, X. Li, J. Hong, "Multiwavelength gain-coupled DFB Laser Cascade: Design modeling and simulation", *IEEE Journal of Quantum Electronics*,

vol. 36, pp. 1110-1116, October 2000.

[10] M.J. Connelly, "Wideband semiconductor optical amplifier steady-state numerical model", *IEEE Journal of Quantum Electronics*, vol. 37, pp. 439-447, March 2001.

[11] M.J. Connelly, "Wideband dynamic numerical model of a tapered buried stripe semiconductor optical amplifier gate", *IEE Proc.-Circuits Devices Syst.*, vol. 149, pp. 173-178, June 2002.

[12] A.A.M. Saleh et al., "Modeling of gain in erbium-doped fiber amplifiers", *IEEE Photonics Technology Letters*, vol. 2, pp. 714-717, October 1990.

[13] Y. Sun et al., "Model for gain dynamics in erbium-doped fibre amplifiers", *Electronics Letters*, vol. 32, pp. 1490-1491, August 1996.

[14] C.R. Giles, E. Desurvire, J.R. Simpson, "Transient gain and crosstalk in erbium-doped fiber amplifiers", *Optics Letter*, vol. 14, pp. 880-882, August 1989.

[15] E. Desurvire, *Erbium Doped Fiber Amplifiers: Design and System Applications*. Artech House, Boston, 1993.

[16] E. Desurvire, "Analysis of transient gain saturation and recovery in erbium-doped fiber amplifiers", *IEEE Photonics Technology Letters*, vol. 1, pp. 196-199, August 1989.

[17] K.Y. Ko et al., "Transient analysis of erbium-doped fiber amplifiers", *IEEE Photonics Technology Letters*, vol. 6, pp. 1436-1438, December 1994.

[18] Y. Sun et al., "Average inversion level, modeling, and physics of erbium-doped fiber amplifiers", *IEEE Journal of Selected Topics in Quantum Electronics*, vol. 3, pp. 991-1007, August 1997.

[19] S.R. Chinn, "Simplified modeling of transients in gain-clamped erbium-doped fiber amplifiers", *IEEE Journal of Lightwave Technology*, vol. 16, pp. 1095-1100, June 1998.

[20] E. Desurvire et al., "Gain saturation effects in high-speed, multichannel

erbium-doped fiber amplifiers at λ=1.53 μm", *IEEE Journal of Lightwave Technology*, vol. 7, pp. 2095-2104, December 1989.

[21] C.H. Henry et al., "Spectral dependence of the change in refractive index due to carrier injection in GaAs lasers", *Journal of Applied Physics*, vol. 52, pp. 4457-4461, July 1981.

[22] N. Schunk, K. Petermann, "Noise analysis of injection-locked semiconductor injection lasers", *IEEE Journal of Quantum Electronics*, vol. QE-22, pp. 642-650, May 1986.

[23] K. Petermann, *Laser Diode Modulation And Noise.* Kluwer Academic Publishers, 1991.

[24] M. Shtaif, G. Eisenstein, "Noise characteristics of nonlinear semiconductor optical amplifiers in the Gaussian limit", *IEEE Journal of Quantum Electronics*, vol. 32, pp. 1801-1809, October 1996.

[25] B.S. Kim, Y. Chung, J.S. Lee, "An efficient split-step time-domain dynamic modeling of DFB/DBR laser diodes", *IEEE Journal of Quantum Electronics*, vol. 36, pp. 787-794, July 2000.

[26] W.H. Press, S.A. Teukolsky, W.T. Vetterling, B.P. Flannery, *Numerical Recipes in C – The Art of Scientific Computing (2nd Edition).* Cambridge University Press, 1992. ISBN 0-521-43108-5.

[27] T. Watanabe et al., "Transmission performance of chirp-controlled signal by using semiconductor optical amplifier", *IEEE Journal of Lightwave Technology*, vol. 18, pp. 1069-1077, August 2000.

[28] A. Bononi, L.A. Rusch, "Doped-fiber amplifier dynamics: A system perspective", *IEEE Journal of Lightwave Technology*, vol. 16, pp. 945-956, May 1998.

[29] I.P. Kaminow, T.L. Koch, ed., *Optical Fiber Telecommunications IIIB.* Academic Press, 1997. ISBN 0-12-395171-2.

[30] Y. Yamamoto, K. Inoue, "Noise in amplifiers", *IEEE Journal of Lightwave*

Technology, vol. 21, pp. 2895-2915, November 2003.

[31] N.A. Olsson, "Lightwave systems with optical amplifiers", *IEEE Journal of Lightwave Technology*, vol. 7, pp. 1071-1082, July 1989.

[32] G. Giuliani, D. D'Alessandro, "Noise analysis of conventional and gain-clamped semiconductor optical amplifiers", *IEEE Journal of Lightwave Technology*, vol. 18, pp. 1256-1263, September 2000.

[33] J. Jennen, H. de Waardt, G. Acket, "Modeling and performance analysis of WDM transmission links employing semiconductor optical amplifiers", *IEEE Journal of Lightwave Technology*, vol. 19, pp. 1116-1124, August 2001.

[34] E. Tangdiongga et al., "Performance analysis of linear optical amplifiers in dynamic WDM systems", *IEEE Photonics Technology Letters*, vol. 14, pp. 1196-1198, August 2002.

[35] D. Marcuse, "Computer model of an injection laser amplifiers", *IEEE Journal of Quantum Electronics*, vol. QE-19, pp. 63-73, January 1983.

[36] D. Marcuse, "Computer simulation of laser photon fluctuations: Theory of single-cavity laser", *IEEE Journal of Quantum Electronics*, vol. QE-20, pp. 1139-1148, October 1984.

[37] C.Y. Jin et al., "Photon iterative numerical technique for steady-state simulation of gain-clamped semiconductor optical amplifiers", *IEE Proc.-Optoelectronics*, vol. 150, pp. 503-507, Decemeber 2003.

[38] C.Y. Jin et al., "Detailed model and investigation of gain saturation and carrier spatial hole burning for a semiconductor optical amplifier with gain clamping by a vertical laser field", *IEEE Journal of Quantum Electronics*, vol. 40, pp. 513-518, May 2004.

[39] T. Yamatoya, F. Koyama, "Optical preamplifier using optical modulation of amplified spontaneous emission in saturated semiconductor optical amplifier", *IEEE Journal of Lightwave Technology*, vol. 22, pp. 1290-1295, May 2004.

[40] M. Settembre et al., "Cascaded optical communication systems with in-line

semiconductor optical amplifiers", *IEEE Journal of Lightwave Technology*, vol. 15, pp. 962-967, June 1997.

[41] L.H. Spiekman, "8 x 10Gb/s DWDM transmission over 240 km of standard fiber using cascade of semiconductor optical amplifiers", *IEEE Photonics Technology Letters*, vol. 12, pp. 1082-1084, August 2000.

[42] L.M. Zhang, J.E. Carroll, "Semiconductor 1.55 μm laser source with gigabit/second integrated electroabsorptive modulator", *IEEE Journal of Quantum Electronics*, vol. 30, pp. 2573-2577, November 1994.

[43] G.P Agrawal, N.A Olsson, "Self-phase modulation and spectral broadening of optical pulses in semiconductor laser amplifiers", *IEEE Journal of Quantum Electronics*, vol. 25, pp. 2297-2306, November 1989.

[44] M. Shtaif, B. Tromborg, G. Eisenstein, "Noise spectra of semiconductor optical amplifiers: Relation between semiclassical and quantum descriptions", *IEEE Journal of Quantum Electronics*, vol. 34, pp. 869-878, May 1998.

[45] S. Donati, G. Giuliani, "Noise in an optical amplifier: Formulation of a new semiclassical model", *IEEE Journal of Quantum Electronics*, vol. 33, pp. 1481-1488, September 1997.

[46] J. Wang, K. Petermann, "Noise analysis of semiconductor lasers within the coherence collapse regime", *IEEE Journal of Quantum Electronics*, vol. 27, pp. 3-9, January 1991.

[47] M. Ahmed, M. Yamada, M. Saito, "Numerical modeling of intensity and phase noise in semiconductor lasers", *IEEE Journal of Quantum Electronics*, vol. 37, pp. 1600-1610, December 2001.

[48] L.M. Zhang et al., "Dynamic analysis of radiation and side-mode suppression in a second-order DFB laser using time-domain large-signal traveling wave model", *IEEE Journal of Quantum Electronics*, vol. 30, pp. 1389-1395, June 1994.

[49] L.M Zhang et al., "Large-signal dynamic model of the DFB laser", *IEEE Journal of Quantum Electronics*, vol. 28, pp. 604-611, March 1992.

[50] A. Mecozzi, J. Mork, "Saturation effects in nondegenerate four-wave mixing between short optical pulses in semiconductor laser amplifiers", *IEEE Journal of Selected Topics in Quantum Electronics*, vol. 3, pp. 1190-1205, October 1997.

[51] B. Thedrez, C.H. Lee, "A reassessment of standard rate equations for low facet reflectivity semiconductor lasers using traveling wave rate equations", *IEEE Journal of Quantum Electronics*, vol. 28, pp. 2706-2713, December 1992.

[52] P. Vankwikelberge et al., "CLADISS – A longitudinal multimode model for the analysis of the static, dynamic, and stochastic behavior of diode lasers with distributed feedback", *IEEE Journal of Quantum Electronics*, vol. 26, pp. 1728-1741, October 1990.

[53] D. Cassioli et al., "A time-domain computer simulator of the nonlinear response of semiconductor optical amplifiers", *IEEE Journal of Quantum Electronics*, vol. 36, pp. 1072-1080, September 2000.

[54] A.K. Srivastava et al., "EDFA transient response to channel loss in WDM transmission system", *IEEE Journal of Quantum Electronics*, vol. 9, pp. 386-388, March 1997.

[55] Y. Sun et al., "Fast power transients in WDM optical networks with cascaded EDFAs", *Electronics Letters*, vol. 33, pp. 313-314, February 1997.

[56] S. Reichel, R. Zengerle, "Effects of nonlinear dispersion in EDFA's on optical communiation systems", *IEEE Journal of Lightwave Technology*, vol. 17, pp. 1152-1157, July 1999.

[57] M. Janos, S.C. Guy, "Signal-induced refractive index changes in erbium-doped fiber amplifiers", *IEEE Journal of Lightwave Technology*, vol. 16, pp. 542-548, April 1998.

[58] S. Reichel et al., "Simulation of phase modulation in EDFA's using an extended model", *IEEE Photonics Technology Letters*, vol. 10, pp. 1724-1726, December 1998.

[59] A.W.T. Wu, A.J. Lowery, "Efficient multiwavelength dynamic model for erbium-doped fiber amplifier", *IEEE Journal of Quantum Electronics*, vol. 34, pp. 1325-1331, August 1998.

[60] C.R. Giles, E. Desurvire, "Modeling erbium-doped fiber amplifiers", *IEEE Journal of Lightwave Technology*, vol. 9, pp. 271-283, February 1991.

[61] C.R. Giles, E. Desurvire, "Propagation of signal and noise concatenated erbium-doped fiber optical amplifiers", *IEEE Journal of Lightwave Technology*, vol. 9, pp. 147-154, February 1991.

[62] Z. Zhang, Xun Li, *Simulation of Erbium-Doped Fiber Amplifier Based on a Novel Dynamic Model.* Master thesis, McMaster University, Canada, 2002.

[63] Y. Kim et al., "Analysis of frequency chirping and extinction ratio of optical phase conjugate signals by four-wave mixing in SOA's", *IEEE Journal of Selected Topics in Quantum Electronics*, vol. 5, pp. 873-879, May/June 1999.

[64] T. Watanabe et al., "Chirp control of an optical signal using phase modulation in a semiconductor optical amplifier", *IEEE Photonics Technology Letters*, vol. 10, pp. 1027-1029, July 1998.

[65] M. Potenza, "Optical fiber amplifiers for telecommunication systems", *IEEE Communications Magazine*, pp. 96-102, August 1996.

[66] A. Papoulis, S.U. Pillai, *Probabilty, Random Variables and Stochastics Processes (4th Edition).* McGraw-Hill International Ed., 2002. ISBN 0-07-112256-7.

[67] G.P. Agrawal, N.K. Dutta, *Semiconductor Lasers (2nd Edition).* Van Nostrand Reinhold, New York, 1993. ISBN 0-442-01102-4.

[68] Y. Sun et al., "Error-free transmission of 32 x 2.5Gbit/s DWDM channels over 125km using cascaded in-line semiconductor optical amplifiers", *Electronics Letters*, vol. 35, pp. 1863-1865, October 1999.

[69] S. Reichel et al., "Simulation and experiment verification of a 10-Gb/s NRZ field trial at 1.3μm using semiconductor optical amplifiers", *IEEE Photonics Technology Letters*, vol. 10, pp. 1498-1500, October 1998.

[70] J. Sun, G. Morthier, R. Baets, "Numerical and theoretical study of the crosstalk in gain-clamped semiconductor optical amplifiers", *IEEE Journal of Selected Topics in*

Quantum Electronics, vol. 3, pp. 1162-1167, October 1997.

[71] J. Sun, "Theoretical study on cross-gain modulation wavelength conversion with converted signal fedback", *IEE Proc.-Optoelectronics*, vol. 150, pp. 497-502, December 2003.

[72] L. Schares et al., "Phase dynamics of semiconductor optical amplifiers at 10-40 GHz", *IEEE Journal of Quantum Electronics*, vol. 39, pp. 1394-1408, November 2003.

[73] D.R. Zimmerman, L.H. Spiekman, "Amplifiers for the masses: EDFA, EDWA, and SOA amplets for metro and access applications", *IEEE Journal of Lightwave Technology*, vol. 22, pp. 63-70, January 2004.

[74] H. Ono, M. Shimizu, "Analysis of gain dynamics of erbium-doped fiber amplifiers for wavelength-division-multiplexing networks", *IEEE Journal of Quantum Electronics*, vol. 39, pp. 541-547, April 2003.

[75] I. Nusinsky, A.A. Hardy, "Multichannel amplification in strongly pumped EDFAs", *IEEE Journal of Lightwave Technology*, vol. 22, pp. 1946-1952, August 2004.